Analysis of Nacelle Transonic Interference Test Data

NASA CR-159224 Section 4.0

Advanced Concepts Studies For Supersonic Vehicles
May 1980

R. M. Kulfan

CONTENTS

FIGURES

TABLES

ABBREVIATIONS AND SYMBOLS

A_C	nacelle capture area
A_I	nacelle inlet area
C_D	drag coefficient
C_{D_F}	friction drag coefficient
C_{D_L}	drag-due-to-lift coefficient
C_{D_N}	nacelle drag
C_{D_0}	drag at zero lift
C_{D_W}	volume wave drag coefficient
C_L	lift coefficient
$\mathbb{C}_L$	centerline
C_{L_α}	lift curve slope, per radian
C_m	pitching moment about 0.62 of the wing root chord
C_{m_0}	pitching moment at zero lift
C_p	pressure coefficient
deg	degree
D_I	inlet diameter
L	nacelle length, lift
LE	leading edge
L_S	shock standoff distance
M	Mach number
MAX	maximum
MFR	mass-flow ratio
M_l	local Mach number
N	exponent in capture streamtube equation

q	dynamic pressure
r	radius
ref	reference
R_I	nacelle inlet radius
R_S	capture streamtube radius
S_R	reference wing area
TE	trailing edge
WB	wing-body
X	axial distance from nacelle inlet
X_{STA}	body station
α	angle of attack
α_{L0}	angle of attack at zero lift
β	$\sqrt{M^2 - 1}$
Δ	increment
ΔC_p	nacelle interference pressure coefficient in the wing lower surface
ΔS	nacelle area growth under the wing
η	fraction of semispan factor
π	pi

SUBSCRIPTS

∞	freestream value
o	zero lift value
loc	local value
C_p	value for specified C_p
INT	interference
NAC	nacelle

4.0 ANALYSIS OF NACELLE TRANSONIC INTERFERENCE TEST DATA

4.1 TASK STATEMENT

The objective of this task was to assess the accuracy of theoretical predictions of engine-airframe aerodynamic interference effects at low supersonic Mach numbers. Theoretical analyses were to be made of data (ref. 4-1) that had been obtained in an extensive NASA wind-tunnel test of aerodynamic penalties associated with propulsion system installation and operation at subsonic through supersonic speeds. In particular, effects of nacelle inlet spillage were to be considered.

4.2 STUDY APPROACH

Mutual interference between engine nacelles and the airframe can have an important effect on the aerodynamic efficiency of a supersonic aircraft. A number of systematic analytic studies have been made to obtain an understanding of the design considerations necessary to optimize the favorable aerodynamic interference effects (refs. 4-2 through 4-6). The validation of the necessary analytic design tools by means of test-theory comparisons is rather limited. This is particularly true for the low supersonic speed regime. Additionally, engine spillage effects on aerodynamic interference are relatively unknown.

NASA conducted an extensive wind-tunnel test program to evaluate aerodynamic performance penalties associated with the propulsion system installation and operation at subsonic through low supersonic speeds. A parallel objective of this test program was to provide an experimental data base of detailed force and pressure measurements for use in systematic evaluations of analytical prediction methods. The results of the NASA experimental test program are reported in References 4-1, -7, and -8.

A limited study was made to assess the accuracy of analytic methods for predicting transonic engine-airframe interference effects by theoretical analyses of the NASA test data. Theoretical predictions were made of the aerodynamic characteristics of the NASA wind-tunnel test configuration for a number of different nacelle locations. Comparisons were then made between predictions and the corresponding experimental data.

The test-versus-theory comparisons include:

- isolated wing-body lift, drag, and pitching moment
- isolated nacelle drag and pressure distributions
- mutual nacelle interference drag for various nacelle arrangements
- nacelle interference shock-wave patterns and pressure distributions on the wing lower surface
- nacelle interference effects on wing-body lift, drag, and pitching moments
- total installed nacelle interference effects on lift, drag, and pitching moments.

The study variables include Mach number, angle of attack, nacelle location, and nacelle spillage.

4.3 SUMMARY

To achieve the task objective, a large number of test-versus-theory comparisons were made. The results indicate that the accuracy of the theoretical predictions was dependent upon the configuration arrangement. In general, the predictions of aerodynamic interference due to the nacelles agreed quite well with the test data when the nacelles were located aft near the wing trailing edge. The agreement between the theoretical predictions and test data deteriorated for the more forward nacelle locations. There is evidence that the discrepancy between test and theory for the more forward nacelle locations could be attributed to two factors:

- shock-induced separation on the wing lower surface
- nacelle bow shocks moving in front of the wing leading edge and thereby influencing the wing upper surface.

Neither of these factors were included in the theoretical calculations.

The normal shock spillage effect predictions did not agree as well with the test data as did those without spillage. It is not clear if the inaccuracy in the predictions is due to the modeling of the inlet streamtube or to the fundamental approach of representing what is, in reality, a mixed subsonic-supersonic flow field by an equivalent solid-body shape (for the inlet streamtube) in a totally supersonic analysis.

4.4 CONCLUSIONS

The results of the study indicate that satisfactory methods are available to predict the interference effects of installed engine nacelles at Mach 1.15 and 1.4 without spillage for aft-nacelle configurations typical of efficient supersonic cruise airplanes. The agreement between test and theory deteriorated somewhat for more forward nacelle locations. The normal shock spillage predictions did not agree as well with the test data as those without spillage. Some specific study conclusions are summarized below.

"No Spillage" Conclusions

- Far-field and near-field methods adequately predict wing-body aerodynamic characteristics. Near-field predictions of wing-body drag at zero lift were slightly high.
- Far-field and near-field predictions of the isolated nacelle drag are good at Mach 1.4. The drag predictions at Mach 1.15 are higher than the test results because of an overestimate of the nacelle boattail pressures.
- Far-field predictions of nacelle mutual interference indicate correct trends, but are not in as good agreement with the test data as are the near-field predictions.
- The "glance" method of nacelle pressure field superposition is more accurate than the "wrap" method.
- The locations of nacelle shocks are predicted accurately by the theory.
- Predictions of nacelle interference pressures on the wing are good except in local areas near strong shocks where separation occurs.

- Predictions of Mach number, nacelle location, and angle of attack on nacelle aerodynamic interference are good, but become less accurate as the nacelles are moved forward of the wing leading edge.

- With the nacelles located aft near the wing trailing edge, the favorable interference effects of the nacelle on the wing-body become increasingly large as C_L increases. The net installed drag, both measured and calculated, was less than skin friction drag.

"With Spillage" Conclusions

- The analysis method developed in the study does not properly account for spillage effects on the isolated nacelle pressure distribution near the lip. Consequently, the method overpredicts the drag of the isolated nacelle with spillage.

- The method predicts the forward movement of the nacelle bow shocks on the wing due to spillage.

- The method adequately predicted spillage interference effects on lift and pitching moment at zero angle of attack.

- The method adequately predicts the effect of spillage on wing-body interference. However, the predicted effect of spillage on mutual nacelle interference did not agree very well with the test data.

These results indicate that satisfactory methods are available to predict interference lift, drag, pitching moment, and pressure distributions of installed engine nacelles at Mach 1.15 and 1.4 without spillage for aft-nacelle configurations typical of efficient supersonic cruise airplanes.

4.5 RECOMMENDATIONS

Recommendations for additional efforts in evaluating the accuracy of theoretical methods for predicting engine-airframe interference effects are given below in four general categories:

- additional theoretical methods evaluations, particularly at low transonic speeds (Mach less than 1.0)

- examining and defining limitations of theoretical predictions (without spillage)

- exploring alternate methods to predict normal shock spillage interference effects

- theoretical and experimental studies of oblique shock spillage effects.

Additional Theoretical Methods Evaluations—The NASA experimental nacelle interference data were obtained at high subsonic through low supersonic speeds. The current efforts of the Contractor included evaluation of methods for predicting nacelle interference at low supersonic speeds. Additional efforts should include:

- evaluating transonic methods of predicting nacelle interference by comparison with the high subsonic data

- evaluating alternate supersonic prediction methods

- making the NASA test data more readily available in the form of accessible data tapes and/or tabular form for general use.

Limitations of Theoretical Methods (No Spillage)—Results of the study indicated that the accuracy of the theoretical predictions of nacelle-airframe interference without spillage was dependent upon the configuration arrangement.

Additional efforts should include:

- Examining the effect of the nacelle on the wing upper surface when the nacelle bow shocks fall forward of the leading edge. This could lead to improved predictions when the nacelles are located in a forward position.

- Identifying specific conditions, such as allowable shock strength in regions of wing influenced by the nacelles, local Mach number, etc., that define the limitations of the theoretical predictions.

Alternate Normal Shock Spillage Predictions—There have been no predictions of normal shock spillage interference effects on the NASA model prior to this study. It is not clear if the inaccuracy of the spillage effect predictions in this study is due to the theoretical streamtube shapes or to the fundamental approach of representing what is, in reality, a mixed subsonic–supersonic flow field with an equivalent solid-body shape (for the inlet streamtube) in a totally supersonic analysis.

Additional efforts should include:

- Examining the fundamental approach used for normal shock spillage calculations to determine if the method used in this study, or an alternate method, can be used for reliable spillage effect predictions.

- Using transonic flow predictions of the flow characteristics about an isolated spilling nacelle to define a more appropriate "equivalent" solid-body shape for the interference predictions.

Theoretical and Experimental Studies of Oblique Shock Spillage—The engines of supersonic aircraft configurations at low supersonic speed typically have oblique shock spillage across the shocks from the inlet spikes. To evaluate predictions of oblique shock spillage interference effects, the following are required:

- obtaining oblique shock experimental spillage data similar to the NASA normal shock data used in this study

- conducting theoretical analyses of the above data.

4.6 DISCUSSION

4.6.1 MODEL GEOMETRY AND TEST CONDITIONS

The NASA experimental program was conducted in the AMES 11- by 11-foot wind tunnel. The basic features of the nacelle-airframe interference model are shown in Figure 4-1.

The wing-body configuration is a 0.024 scale model of the U.S. 1971 SST. The wing-body was sting mounted with a six-component internal strain-gage balance. The left-hand wing had 126 static pressure orifices, 95 on the lower surface and 31 on the upper surface. The orifice locations are shown in Figure 4-2. Two different nacelle geometries were tested. One set of nacelles had sharp inlets, and the second set of nacelles had a slightly blunt inlet lip shape. The investigations of this task concerned only the sharp-lip nacelles.

The tested nacelle shape is a simplified and slightly oversize representation of a typical supersonic nacelle installation, as shown in Figure 4-3. The nacelles were located approximately 1.2 inlet diameters below the wing chord plane. This resulted in a gap between the nacelles and the wing lower surface that does not exist in an actual nacelle/airframe installation.

The four individual nacelles were supported below the wing-body model on individual flow-through stings. The two left-hand side nacelles (looking upstream) were pressure instrumented. The two right-hand side nacelles were mounted individually on separate six-component internal strain-gage balances. The pressure instrumented nacelles had 40 static-pressure orifices, as shown in Figure 4-2.

The six-component force balances used to support the right-hand nacelles were housed in the thickness of each nacelle. A two-shell flow-through balance, located in each nacelle, used four instrumented flexures located 90 deg apart at two axial locations. The nacelle balances measured the aerodynamic forces on the external surface of the nacelle, plus the forces on a small portion of the internal duct near the inlet. The wind-tunnel data corrections included removal of the estimated skin friction drag on this internal duct area.

The nacelle support system provided the flexibility of positioning the nacelles vertically, streamwise, and spanwise, relative to the wing-body combination and to each other. The range of achievable nacelle locations is indicated in Figure 4-1. The support system also provided for independent control and measurement of mass flow through each nacelle by means of a mass-flow control plug and appropriate pressure instrumentation.

The test configurations included:

- isolated wing-body
- isolated nacelle
- four nacelles in various relative positions
- wing-body plus nacelles in various locations.

The test data included:

- wing-body lift (C_L), drag (C_D), and pitching moment (C_m) data
- wing pressure measurements
- lift, drag, and pitching moment measurements of the individual inboard and outboard nacelles
- nacelle surface pressures.

These tested configurations provided the following measurements of isolated and interference data:

- isolated wing-body data: measurements on wing-body without the nacelles present
- isolated nacelle data: measurements on a single nacelle
- mutual nacelle interference: difference in nacelle measurements with and without the other nacelles present
- nacelle interference on wing-body: difference in wing-body measurements with and without the nacelles present
- wing-body interference on the nacelles: difference in nacelle measurements with and without the wing-body present
- total wing-body plus nacelle data: sum of wing-body data plus nacelle data
- spillage interference: difference in measurements on identical configurations with the nacelles spilling according to a specific controlled mass-flow ratio (MFR), and the corresponding data obtained without spillage.

The test conditions included:

- Mach number: 0.90, 0.98, 1.1, 1.15, 1.2, 1.3, 1.4
- angle of attack: α = 0 to 6 deg
- mass-flow ratio: MFR = 0.6 to 1.0

All configurations were tested at the primary Mach numbers of 0.9, 1.15, and 1.4. Some selected configurations were also tested at the remaining Mach numbers. Only a few configurations were tested at angles of attack different than zero. Configurations with spillage were tested only at zero angle of attack.

The model angle of attack was measured relative to a wing reference plane. At zero angle of attack, the model actually experiences significant negative lift.

Staggered and nonstaggered arrangements were tested at six different nacelle stations and three different spanwise locations as shown in Figure 4-4.

The basic force and pressure data are contained in References 4-7 and -8, respectively. Complete descriptions of the wind-tunnel model, test conditions, and available test data are given in Reference 4-1. The summary and incremental data presented in Reference 4-1 were used for the test-versus-theory comparisons in this study. The NASA test data are not accessible in the form of a standard data tape. Consequently, the data used in the test-versus-theory comparisons were extracted from the NASA data report plots using the Contractor's PDP 11 digitizer.

4.6.2 PREDICTION METHODS

At supersonic speeds, the mutual interactions of the wing-body and the nacelles can produce significant interference effects. The nacelle-installed drag is usually defined to include the drag of the isolated nacelles plus the net effects of the nacelle pressure field

acting on the wing-body as well as the effect of the wing-body pressure field acting on the nacelles.

Typically, the nacelle-installed drag, as shown in Figure 4-5, is calculated as the sum of the friction drag of the nacelles, the net wave drag, and the lift interference effects.

The net nacelle wave drag includes

- nacelle pressure drag
- nacelle pressures acting on the wing-body volume or thickness
- the wing-body thickness pressures acting on the nacelles
- mutual nacelle interference.

The mutual nacelle interference consists of the effect of the pressure field of a nacelle acting directly on the other nacelles plus the effect of the pressure field reflecting off the wing surface back onto the nacelles.

The lift interference consists of three items:

- The nacelle pressures reflecting off the wing produce an interference lift, ΔC_L. Because of the interference lift, the wing-body incidence required to produce a specified total lift is reduced, which results in a reduction in the wing-body drag-due-to-lift.

- The nacelle pressures acting on mean lifting surface produce a drag or thrust force.

- The wing lifting pressures produce a buoyancy force on the nacelles.

The net nacelle drag is therefore dependent not only on flight conditions and the shape of the nacelles, but also on the shape and location of adjacent components of the airplane.

The aerodynamic force and moment predictions were made using the system of aerodynamic design and analysis programs described in Reference 4-9. The aerodynamic force coefficients for a specified configuration are built up through superposition.

The drag prediction, as summarized in Table 4-1, includes:

- skin friction drag, C_{D_F}, calculated using flat plate turbulent flow theory

- volume wave drag, C_{D_W}, calculated either by a far-field wave drag program (supersonic area rule) or by a near-field (surface pressure integration) program

- drag-due-to-lift, C_{D_L}, which includes induced drag as well as wave-drag-due-to-lift, calculated by a near-field analysis program.

The near-field force calculations are obtained by integration of the surface pressures (volume or lifting) over each component of the configuration being analyzed. The surface pressures include the isolated component pressures plus the interference pressures acting on each component due to the other components of the configuration.

The nacelle pressure fields imposed on the surface of the wing can be calculated by either the "wrap" or the "glance" methods, summarized in Figure 4-6.

In the "wrap" method, the nacelle pressure fields and accompanying shock waves "wrap" around adjacent nacelles. In application, the pressure field generated by one nacelle is allowed to pass through another nacelle as if it were transparent. This is also the approach inherent in the far-field wave drag calculations. In the "glance" method, the pressure field generated by one nacelle "glances" away from the wing when encountering adjacent nacelles. In application, the nacelle-generated flow field is terminated upon encountering another nacelle. One of the objectives of the study was to determine which of these methods is more nearly correct for the type of configurations analyzed here.

The theoretical methods restrict the influence of the nacelle pressure field to the wing lower surface when the nacelles are mounted below the wing. When the bow shocks of the nacelles move in front of the wing leading edge, the nacelle pressure field will influence the wing upper surface. This effect is not included in the theory.

To calculate spillage effects, the capture streamtube that separates the flow into the inlet from the flow that spills around the inlet is replaced by a solid surface in the mathematical analyses. A simple approach was used in this study to calculate the inlet streamtube shape for spillage behind a normal shock. The method developed by Moeckel (ref. 4-10) was used to calculate both the distance of the normal shock forward of the spilling nacelle and the capture streamtube radius at the normal shock. The shape of the capture streamtube was then represented, as shown in Figure 4-7, by a simple polynomial equation. The calculated streamtube shape grows with zero initial slope at the normal shock to match the inlet radius at the nose of the nacelle.

The presence of the capture streamtube changes the pressure distribution over the nacelle. Relative to a nonspilling nacelle, a large expansion occurs at the lip of the nacelle due to the capture streamtube shape at the inlet. This decreases the pressure near the front of the nacelle, thereby reducing the isolated nacelle drag. The isolated nacelle drag reduction is typically called "lip suction."

The presence of the capture streamtube changes the interference effects associated with the nacelle pressures acting on the wing-body, as well as on the isolated nacelle and the adjacent nacelles. The capture streamtube cannot support a force across its surface. Consequently, in the analyses, only the pressures acting on the nacelle surface can contribute directly to drag on the nacelle. Hence, the wing-body interference acting on the nacelles is unchanged by spillage.

In the sections that follow, test-versus-theory comparisons provide an indication of the accuracy of the theoretical predictions of the various lift, drag, and pitching moment components with and without spillage.

4.6.3 ISOLATED WING-BODY AND NACELLE COMPARISONS

Figures 4-8 through -14 contain comparisons of the predicted aerodynamic characteristics of the isolated wing-body configuration.

Drag predictions at zero lift were made using both the far-field (area-rule) and near-field methods. The drag predictions for this wing-body configuration using the far-field theory wave drag estimates agree very well with the test data. The near-field theory appears to slightly overestimate the wing-body zero-lift wave drag.

The predicted drag polars are shown in Figures 4-9 and -10 for Mach 1.4 and 1.15, respectively. The near-field zero-lift wave drag estimates were used in these predictions. The main difference between the theoretical and experimental drag polars is the overestimated drag at zero lift. The predicted and experimental polar shapes are nearly the same.

The theoretical lift and pitching moment curves are compared with test data in Figures 4-11 and -12. The theoretical lift curves agree very well with the test data.

The zero-lift pitching moment predictions agree fairly well with the test data. The differences in the slopes of the pitching moment curves indicate that theory predicts the aerodynamic center too far aft.

Figures 4-13 and -14 summarize the wing-body lift and pitching moment characteristics from subsonic through low supersonic Mach numbers. These figures also contain test data obtained by the Contractor on the same model prior to the NASA nacelle-airframe interference test program. The subsonic predictions shown in the figures were obtained by the Contractor's in-house aerodynamic influence coefficient method.

The good agreement between the theoretical and experimental drag polars and lift curves indicate that the theory should predict the reductions in wing-body drag-due-to-lift associated with the nacelle interference lift (described in sec. 4.6.2.)

Theoretical predictions of the surface pressure distributions and zero-lift drag of the isolated nacelle are compared with the test data shown in Figure 4-15.

Nacelle wave drag estimates were made using both the far-field and near-field methods. The theoretical predictions agree with the test results at Mach 1.3 and 1.4; however, the near-field estimates are slightly better than the far-field estimates. Theory overestimates the nacelle drag at Mach 1.2 and below.

The nacelle pressure distribution, shown in Figure 4-15 at Mach 1.4, closely matches the test data. At Mach 1.15, theory overestimates the expansion (i.e., negative) pressures on the nacelle boattail, which leads to the overestimation of drag at the lower supersonic Mach numbers. The pressure at the first station at both Mach numbers is less than theory. This is possibly due to nacelles actually spilling a small amount of flow at the test conditions.

4.6.4 MUTUAL NACELLE INTERFERENCE COMPARISONS

Figures 4-16, -17, and -18 contain comparisons of predicted and measured mutual interference drag for various nacelle separation and stagger distances. The measured mutual nacelle interference was obtained as the difference in the drag of the nacelles with and without the other nacelles present.

The near-field theory predictions for the base nacelle spanwise separation agree well with the corresponding test data for Mach 1.4 and 1.15.

The far-field drag predictions shown in Figures 4-16, -17, and -18 indicate correct trends but are not in as good agreement with test data as are the near-field predictions.

4.6.5 NO-SPILLAGE INTERFERENCE COMPARISONS

Theoretical nacelle shock-wave patterns and interference pressures on the wing are compared with test data for one of the aft unstaggered nacelle locations in Figures 4-19 and -20.

The experimental interference pressures were obtained as the difference in the wing lower surface pressures with and without the nacelles present. The interference pressures were calculated by the "wrap" and "glance" methods described in Section 4.6.2.

The predicted nacelle bow-shock locations agree well with the experimental shock locations, as indicated by a sudden "jump" in interference pressures, ΔC_P, from zero to a large positive value.

The interference pressures predicted by the "glance" method agree reasonably well with the experimental data. The experimental bow-shock strength is less than indicated by the test data. This may be the result of a shock boundary-layer interaction softening this initial sudden pressure rise. The additional pressure peaks predicted by the "wrap" method are not evident in the test data in either figure.

Figures 4-21 and -22 contain comparisons of predicted shock-wave patterns and interference pressure fields with test data for a forward unstaggered nacelle location in which the outboard nacelle is near the wing leading edge. In this nacelle arrangement, the wing experiences not only the bow shocks from the nacelles, but also aft shocks. The aft shocks arise from the flow compression at the aft end of the nacelle where the flow-through sting enters the nacelle shell.

Again, the additional pressure peaks predicted by the "wrap" method are not evident in the test data. These results indicate that the "glance" method of nacelle pressure-field superposition is more realistic than the "wrap" method.

The predicted and measured interference pressures for this wing-body forward nacelle arrangement agree quite well except in local areas near the aft shock and at the most outboard station.

In Reference 4-11 it is shown that flow across a glancing shock wave, in which the flow is deflected in the plane of the wing, will separate if the pressure rise across the shock wave exceeds 50%. Furthermore, it is shown that a local negative pressure field on the wing can amplify the pressure rise across a shock wave.

The calculated pressure rises across the nacelle bow shocks (figs. 4-21 and -22) range between 25 to 30%. This should not cause separation—indeed, the experimental bow-shock data give no indication of separation.

The aft shock waves from the nacelle are much stronger because of the large boattail angle at the aft end of the nacelle. Furthermore, the nacelle area reduction along the boattail produces large negative expansion pressures just upstream of the aft shock waves. This local negative pressure field further amplifies the strength of the already strong aft shocks. Consequently, the pressure rise across the aft shocks varies from 60 to 100% across the wing. Thus, boundary-layer separation is most certain to occur in the area of the aft shocks. The differences in the experimental and theoretical pressures near the aft shocks are probably due to shock-induced boundary-layer separation.

These results demonstrate the importance of limiting the strength of nacelle-created shock waves likely to interact with a wing, particularly in the areas of local negative pressures.

Figures 4-23 through 4-26 contain additional test-versus-theory comparisons of nacelle interference pressures on the wing lower surface. In these comparisons, the outboard nacelles are staggered aft of the inboard nacelles. The theoretical interference pressures agree quite well with the test data, except in the area of the strong aft shocks from the inboard nacelles.

In Figures 4-27 through -30, comparisons are made between calculated nacelle contributions to lift, drag, and pitching moment with the corresponding test data. The nacelles for these comparisons were unstaggered and in an aft location.

The drag comparisons include the interference on the wing-body, the wing-body interference on the nacelles, and the total nacelle-installed drag. The drag predictions by the "glance" method agree quite well with the test data. The "wrap" method over-predicts the favorable nacelle interference on the wing-body.

At the higher lift coefficients, the total nacelle-installed drag is reduced to approximately the isolated friction-drag level. This favorable effect is primarily due to the reduction in wing-body drag-due-to-lift associated with the nacelle interference lift.

The theoretical interference lift and pitching moment increments were calculated from the nacelle interference pressure fields acting on the wing lower surface. The experimental lift and pitching moment data indicate that the nacelles also experience a change in lift, and, hence, pitching moment, when located in the pressure field from the wing lower surface. The effect of wing-body pressures on nacelle lift is not considered in the theoretical calculations.

The measured interference lift increment increases with angle of attack. The theoretical interference lift calculations, shown in Figures 4-28 and -30, were made at a constant local Mach number equal to the freestream Mach number. Slender-body theory estimates were subsequently made to explore the effect of variations in local Mach number on interference lift. The results of these slender-body theory estimates are shown in Figure 4-31. A negative pressure field in the area of the nacelles at low α, corresponding to a local Mach number greater than freestream, reduces the interference lift. Conversely, a positive pressure field or high α, or lower local Mach number, enhances the interference lift. The calculated effects of local pressure field on interference lift are consistent with the experimental results shown in Figures 4-28 and -30. The effect of the local pressure field on the interference lift is seen to be greatest at the very low supersonic Mach numbers.

Figures 4-32 through -35 contain test-versus-theory comparisons of nacelle-installed drag, interference lift, and pitching moment for an unstaggered nacelle arrangement with the nacelle inlets near the wing leading edge. Theory and test data indicate that the nacelle interference effects for this forward location are highly unfavorable. The installed drag increases with angle of attack and approximately doubles the isolated nacelle drag level.

The theoretical predictions differ significantly from the test data. This difference is believed to be due to two effects: (1) shock-induced separation associated with the strong nacelle aft shocks, and (2) the influence of the nacelle pressure field affecting the upper surface of the wing.

Figure 4-36 summarizes the powerful effect of nacelle interference on the total wing-body-nacelle maximum lift/drag ratio. The lift/drag ratio of the isolated wing-body is approximately 8.7 at Mach 1.4. An increase in drag equal to the drag of four isolated nacelles would result in a 16% reduction in the lift/drag ratio to a value of 7.3.

The measured lift/drag ratio for the nacelles in the aft location is 8.0. Favorable interference for this location reduced the installed nacelle penalty by one half, relative to the isolated nacelle drag level.

Moving the nacelles to the forward location nearly doubled the nacelle installation penalty. The lift/drag ratio for this arrangement is approximately 6.3, which is a 28% reduction in lift/drag ratio, relative to the wing-body levels.

Figures 4-37 through 4-48 show the effect of nacelle location on aerodynamic interference for unstaggered and staggered nacelle arrangements. The test data and corresponding theoretical predictions are for a fixed reference angle of attack of zero degrees.

Nacelle location is seen to have a powerful effect on the nacelle interference. At the aft nacelle locations, both the interference of the nacelles on the wing-body and the wing-body on the nacelles are favorable. The nacelles in the aft locations produce a substantial level of favorable interference. As the nacelles are moved forward, both of these interference components become unfavorable, which results in considerable unfavorable net interference. The predicted interference effects agree reasonably well with the test data, but become less accurate at the more forward locations.

4.6.6 SPILLAGE EFFECTS

The results that have been presented thus far correspond to engine operation without spillage (i.e., mass-flow ratio = 1.0). The effects of nacelle spillage (mass-flow ratios as low as 0.7) on the interference forces were also investigated in the NASA nacelle-airframe interference test program. Experimental measurements, however, were only obtained at zero angle of attack. As previously mentioned, the wing-body produces considerable negative lift at this attitude.

The mass flow through each nacelle was varied by a control plug in the corresponding flow-through sting. At supersonic speeds a normal shock forms in front of the nacelle and moves progressively upstream as the mass-flow ratio through the nacelle is reduced.

Streamtube shapes calculated by the method described in Section 4.6.2 are shown in Figures 4-49 and -50 for a range of mass-flow ratios at Mach 1.4 and 1.15, respectively. Figures 4-51 and-52 contain comparisons of predicted and measured isolated nacelle pressure distributions for different amounts of spillage. Reductions in mass-flow ratio cause a decrease in local pressures on the forward section of the nacelle. The experimental pressure reduction is greater than predicted by the theory, particularly at the lowest mass-flow ratio (i.e., greatest spillage). This is probably because the theoretical analysis treats the capture streamtube as a solid shape in a supersonic flow field, whereas the actual nacelle experiences a complicated mixed subsonic-supersonic flow field.

The experimental data in Figure 4-53 show large reductions in isolated nacelle drag associated with the reduced nose pressures.

Slender-body theory estimates of the effect of spillage on interference lift are shown in Figure 4-54. The slender-body theory calculations of interference lift depend only on the net area change of the capture streamtube and not on the shape. The trends predicted by the slender-body theory estimates agree well with the test data.

Calculated shock-wave patterns and nacelle pressure distributions on the wing are compared with test data for the nacelles with and without spillage at Mach 1.4 and 1.15 in Figures 4-55 and -56, respectively. These calculations were made with the streamtube geometries shown in Figures 4-49 and -50.

The predicted effect of spillage on nacelle bow-shock locations agrees with the test data. The predicted effects of spillage on the interference pressures on the wing are in fair agreement with the test results. The corresponding interference lift and pitching moment data are shown in Figure 4-57. Spillage is seen to have a rather large effect on the interference lift.

Figures 4-58 and -59 contain comparisons of calculated nacelle interference drag with test data for different mass-flow ratios (i.e., amounts of spillage). The drag of the isolated nacelle, measured at the average mass flow for the nacelles at each nominal test condition, was removed from the corresponding measured total wing-body nacelle drag. Similarly, the theoretical interference drag predictions do not include the calculated isolated nacelle drag.

The effect of spillage on the nacelle interference acting on the wing-body appears to be correctly predicted by the theory at both Mach 1.4 and 1.15.

The effect of spillage on the interference on the nacelles is different from that predicted by theory. Consequently, the theoretical effect of spillage on the total nacelle-installed aerodynamic interference drag does not agree very well with the test data.

In the theoretical calculations, the effect of spillage on the interference on the nacelles is due to a change in mutual nacelle interference, which, in turn, is due to the effect of the inlet streamtubes on the nacelle pressure fields acting on the adjacent nacelles.

It is not yet clear if the inaccuracy in the predictions is due to the theoretical streamtube shapes or due to the fundamental approach of representing what is in reality a mixed subsonic-supersonic flow field by an equivalent solid body shape (for the inlet streamtube) in a totally supersonic flow field.

4.7 REFERENCES

4-1 Bencze, D. P.; NASA TMX-3321; Experimental Evaluation of Nacelle-Airframe Interference Forces and Pressures at Mach Numbers of 0.9 to 1.4; March 1977.

4-2 Swan, W. C.; AGARDograph 103; Aerodynamics of Powerplant Installation; Part II; October 1965.

4-3 Nichols, M. R.; NASA TND-3390; Aerodynamics of Airframe-Engine Integration of Supersonic Aircraft; 1966.

4-4 Sigalla, A. and Hallstaff, T. H.; Aerodynamics of Powerplant Installation on Supersonic Aircraft, *Journal of Aircraft*, pp. 273-277, July-August 1967.

4-5 Kane, E. J. and Middleton, W. D.; Considerations of Aerodynamic Interference in Supersonic Airplane Design; AGARD Conference on Aerodynamic Interference, Proceedings No. 71, Paper 3; September 1970.

4-6 Bencze, D. P.; AIAA Paper No. 72-1113; Nacelle-Airframe Interference at Low Supersonic Mach Numbers; November 1972.

4-7 Bencze, D. P.; NASA TMX-62, 489; Wind Tunnel Investigation of Nacelle-Airframe Interference at Mach Numbers of 0.90 to 1.4; 1976.

4-8 Bencze, D. P.; NASA TMX-73, 149 and 73, 088; Wind Tunnel Investigation of Nacelle--Airframe Interference at Mach Numbers of 0.9 to 1.4; 1976.

4-9 Middleton, W. D., Lundry, J. L., and Coleman, R. G.; NASA CR-2716; A Computational System for Aerodynamic Design and Analysis of Supersonic Aircraft, Part 2--User's Manual; August 1976.

4-10 Moeckel, W. E.; NASA TN 1921; Approximate Method for Predicting Form and Location of Detached Shock Waves Ahead of Plane or Axially Symmetric Bodies; June 1949.

4-11 Kulfan, R. M. and Sigalla, A.; Real Flow Limitations in Supersonic Airplane Design; *Journal of Aircraft*, Vol. 16, No. 10, pp. 645-658; October 1979.

Table 4-1. Drag Prediction Methods

Drag component	Method[a]	Nacelle pressure field representation				
		Inlet Mach number		Theory	Pressure field superposition	
		M_∞	M_I		"Wrap"	"Glance"
C_{D_F} – friction drag	• Sommer and Short T* method	●	X	———	—	—
C_{D_W} – volume wave drag	• Far-field theory (area rule) program	●	–	Linear	●	–
	• Near-field theory program	●	–	Whitham	●	●
C_{D_L} – drag due to lift	• Lift analysis program	●	X	Whitham	●	●

[a]Middleton/Carlson—supersonic aerodynamic design and analysis system

X—Capability

●—Used in this study

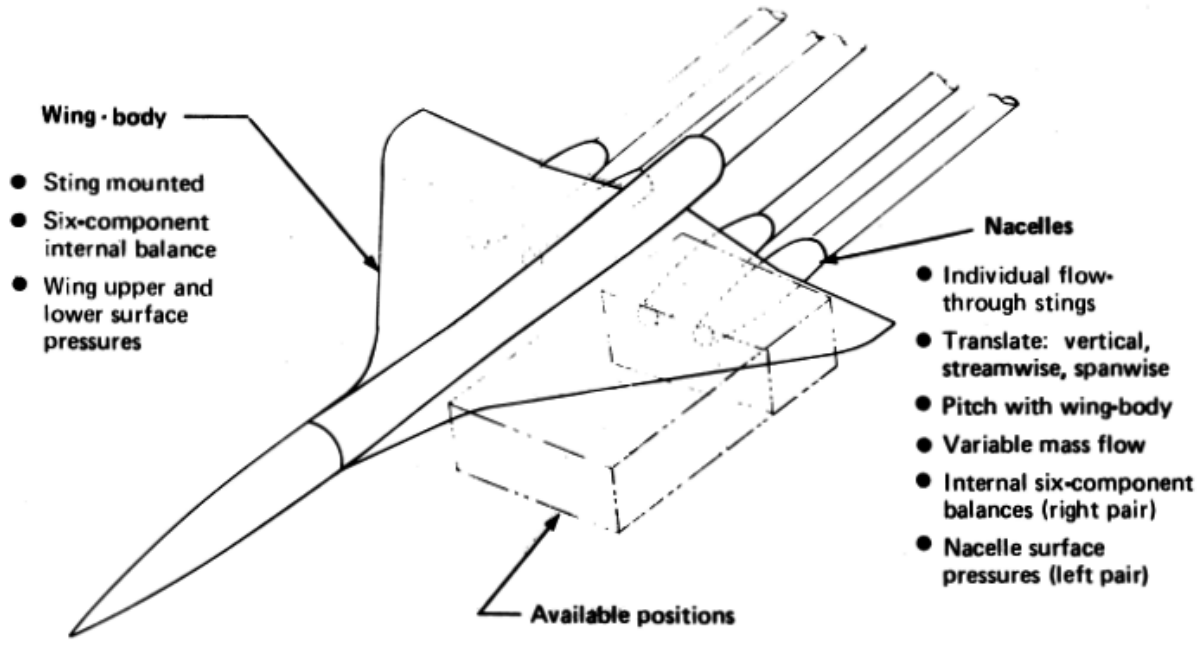

Figure 4-1. NASA-Ames Nacelle/Airframe Interference Model Features

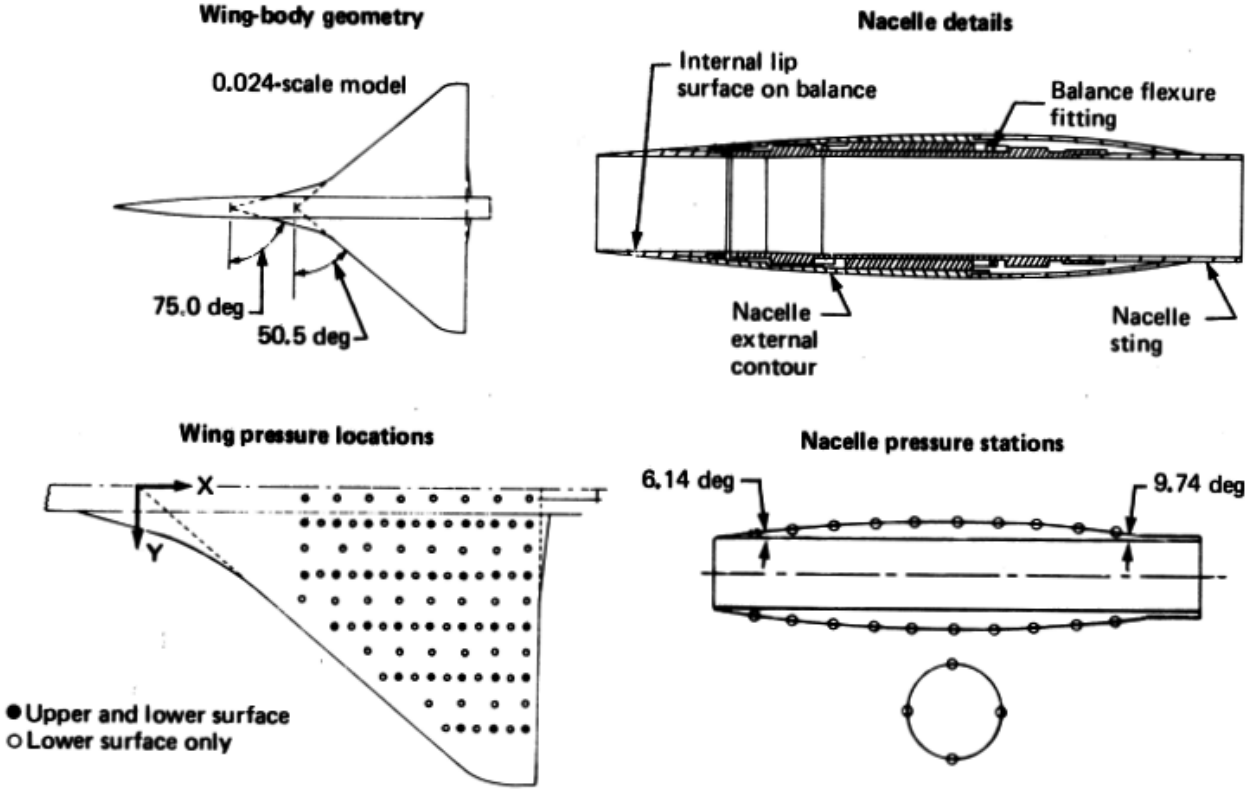

Figure 4-2. Wind Tunnel Model Details

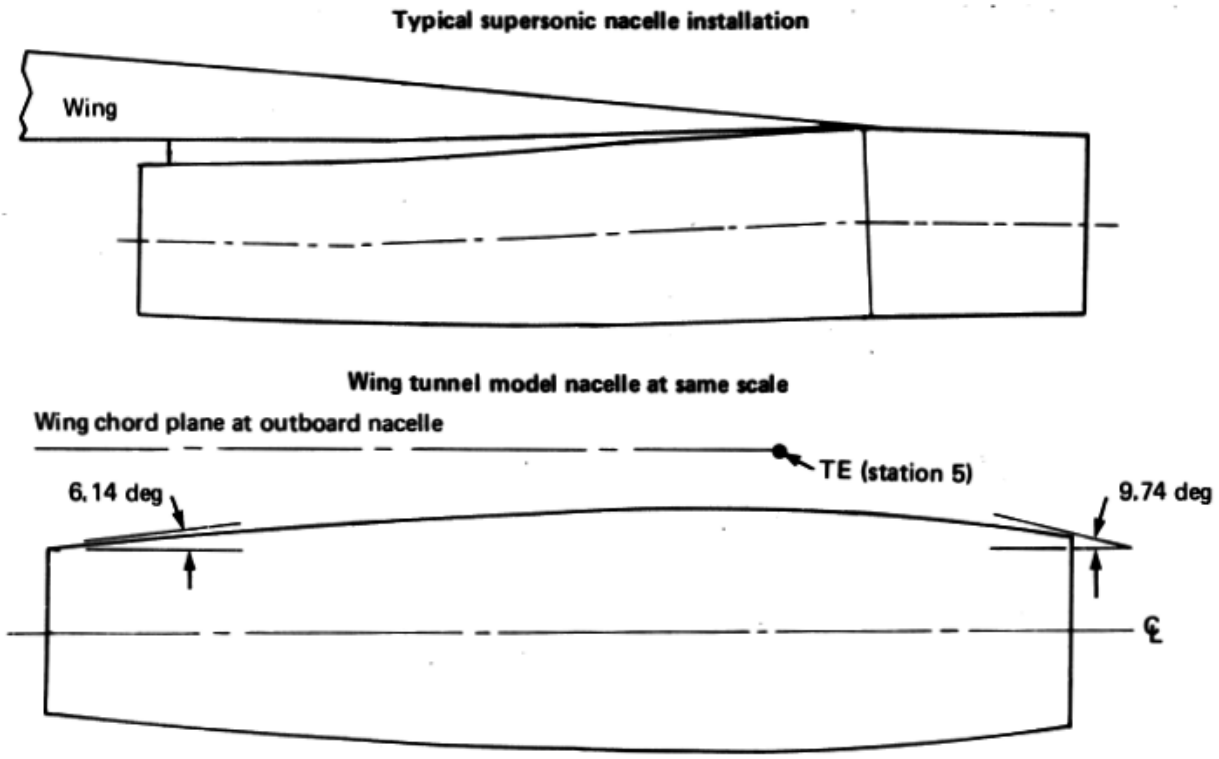

Figure 4-3. Nacelle Geometry Comparison

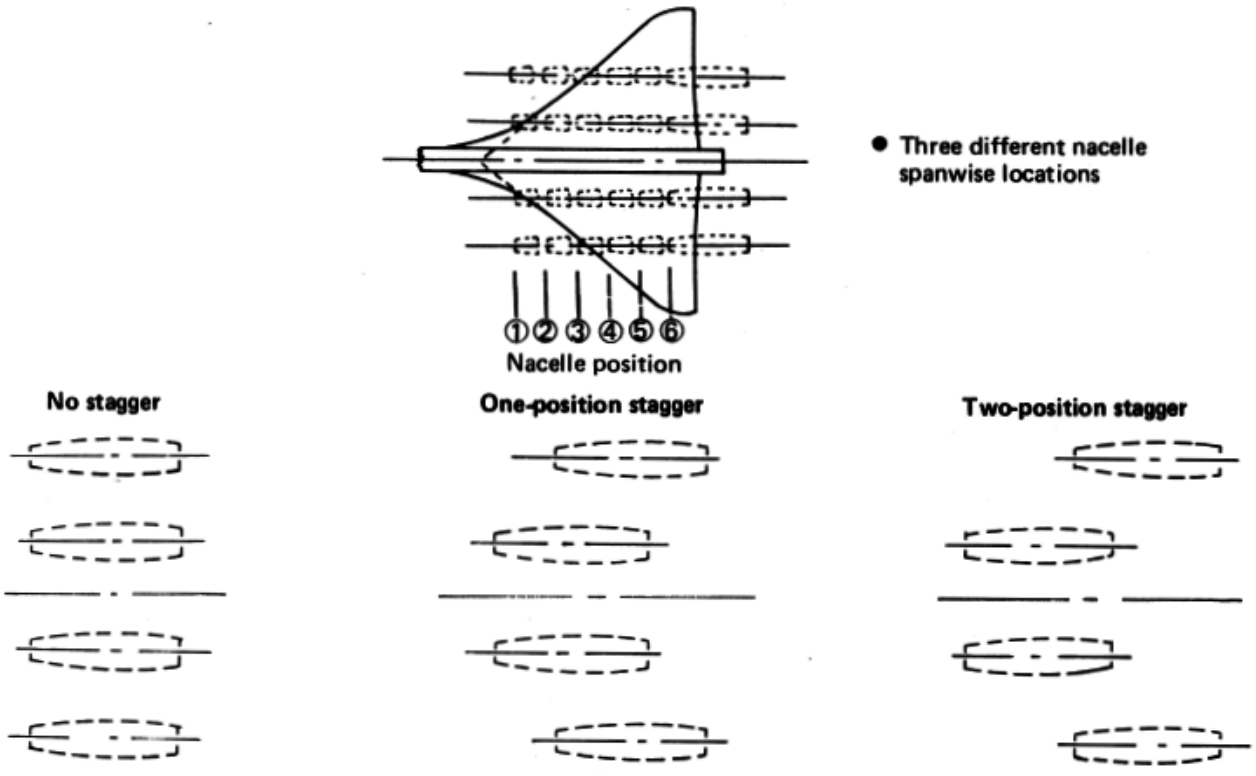

Figure 4-4. Tested Nacelle Locations

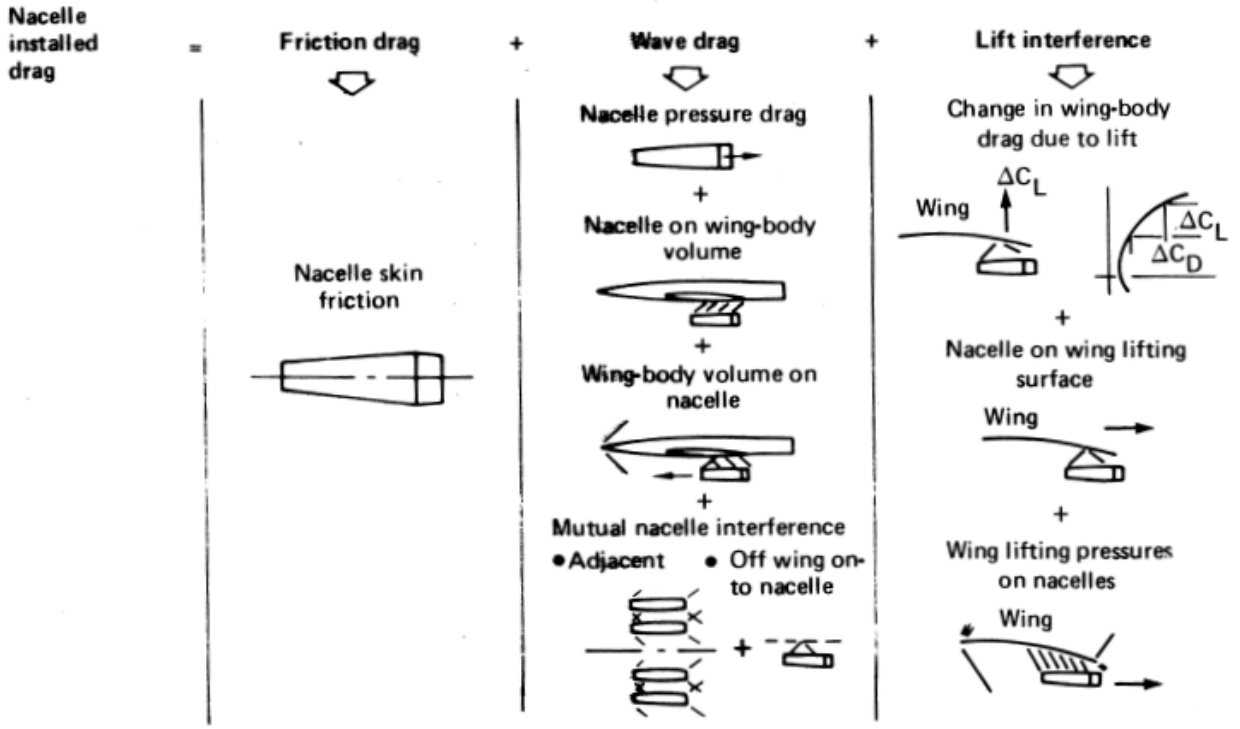

Figure 4-5. Nacelle Installed Drag Components—No Spillage

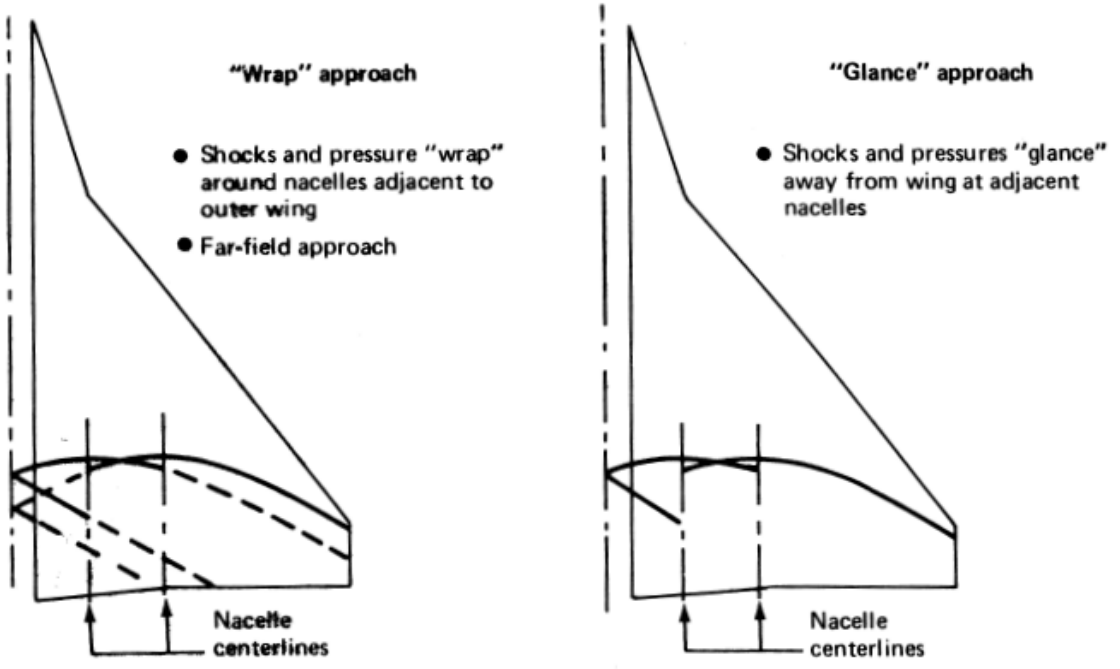

Figure 4-6. "Glance" and "Wrap" Pressure Fields Superposition

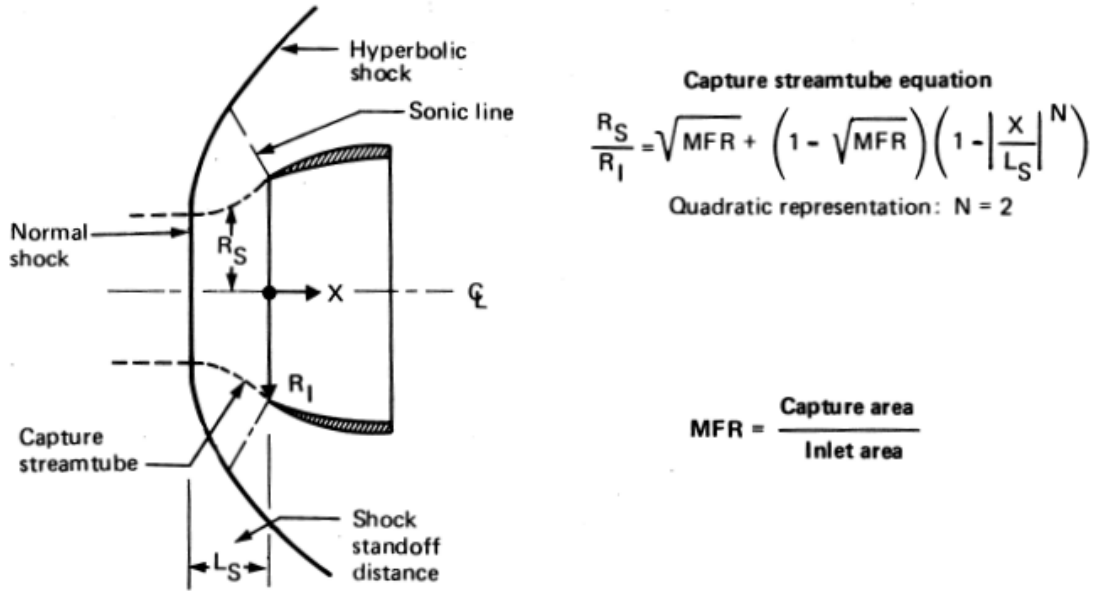

Figure 4-7. Spillage Streamtube Representation

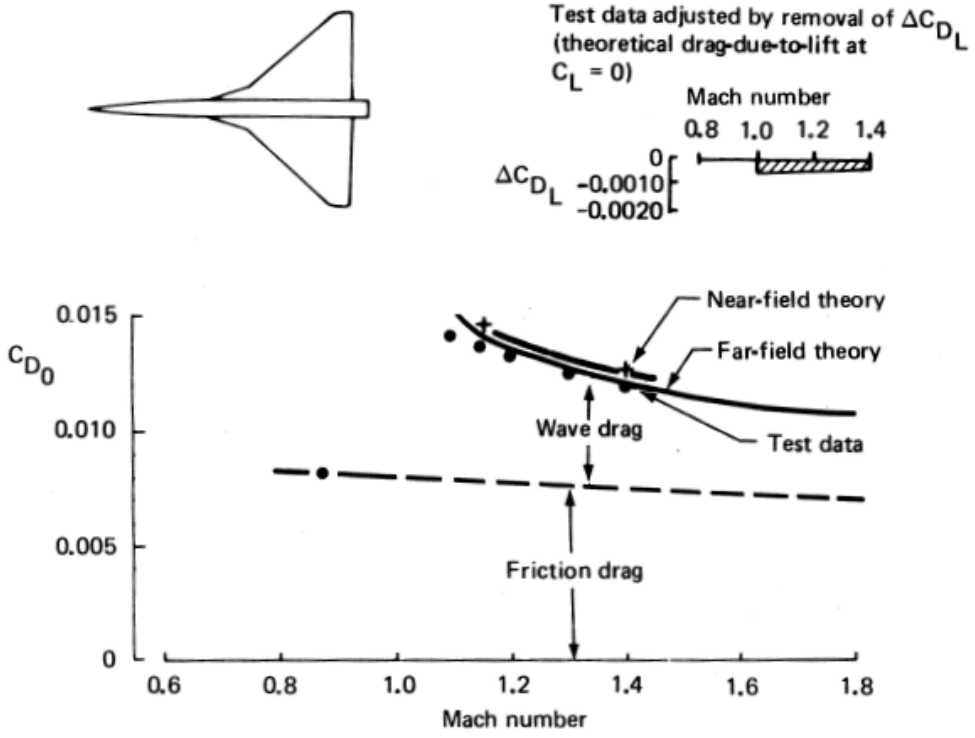

Figure 4-8. Wing + Body Drag Comparisons at Zero Lift

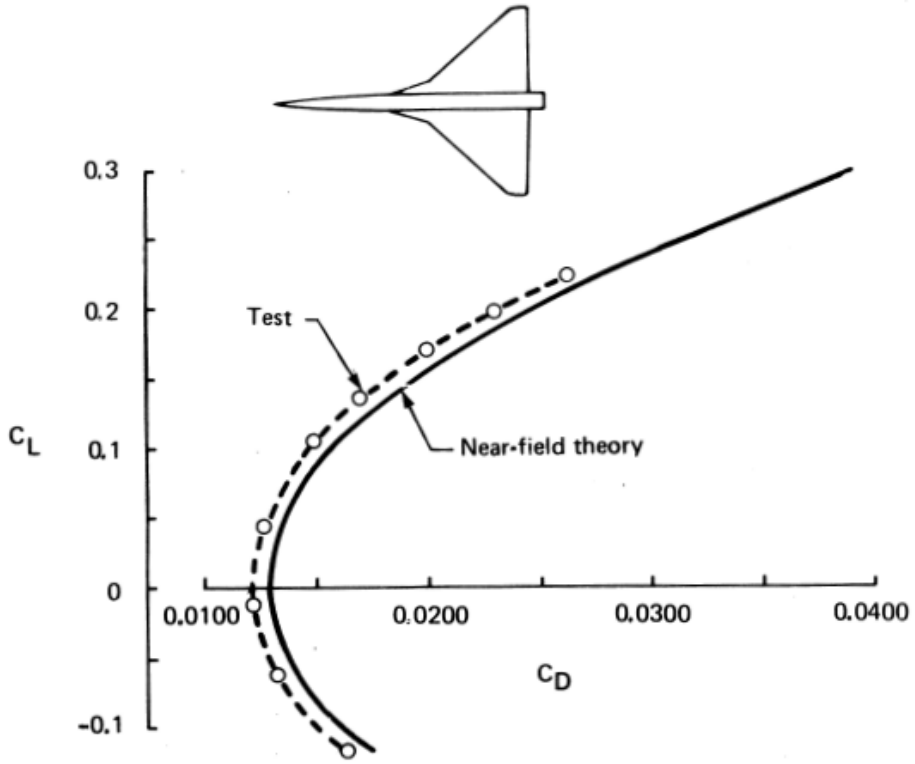

Figure 4-9. Wing + Body Drag Polar, Mach 1.4

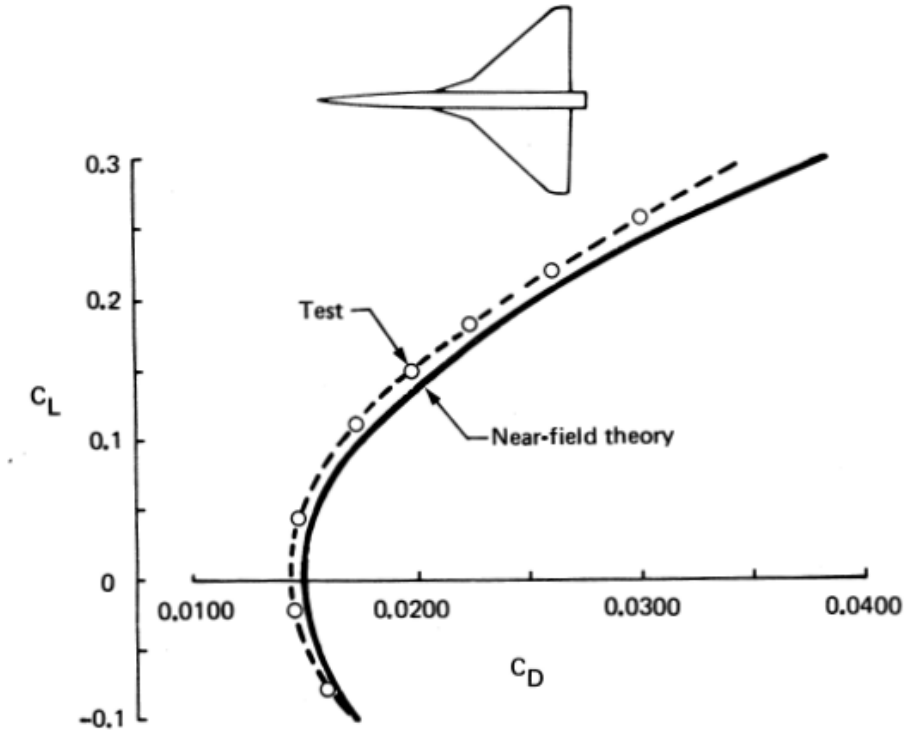

Figure 4-10. Wing + Body Drag Polar, Mach 1.15

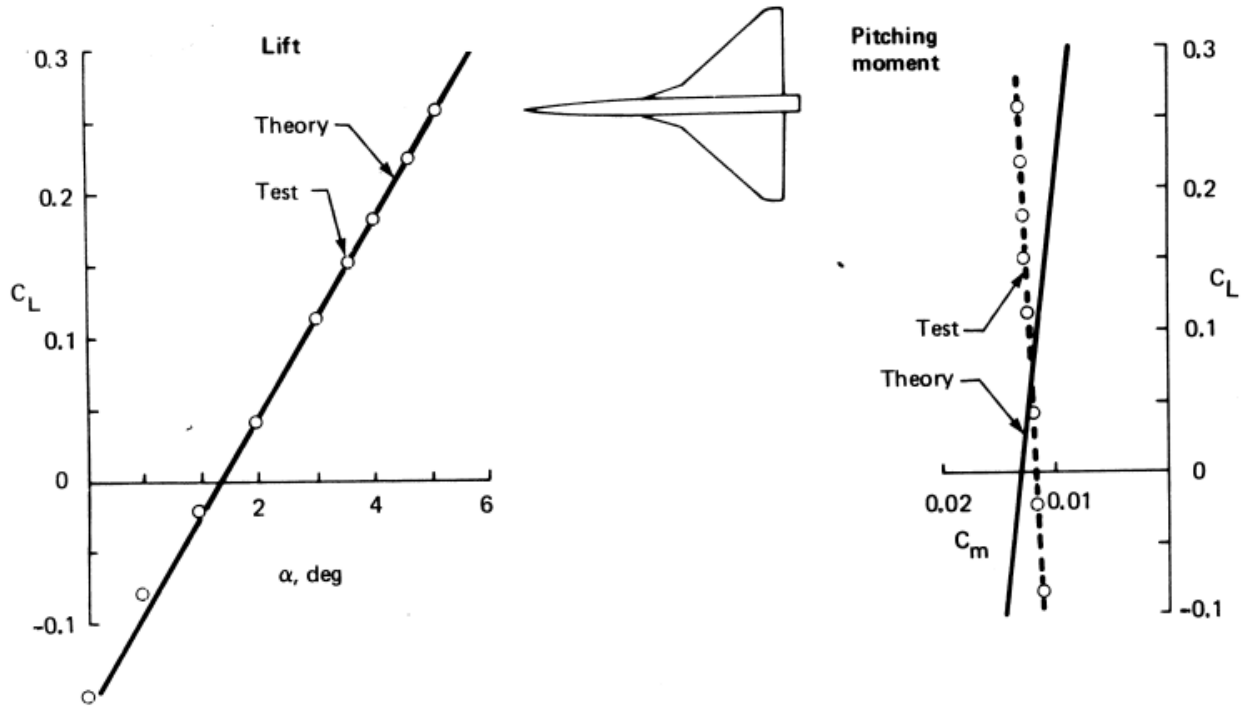

Figure 4-11. Wing + Body Lift and Pitching Moment Curves, Mach 1.4

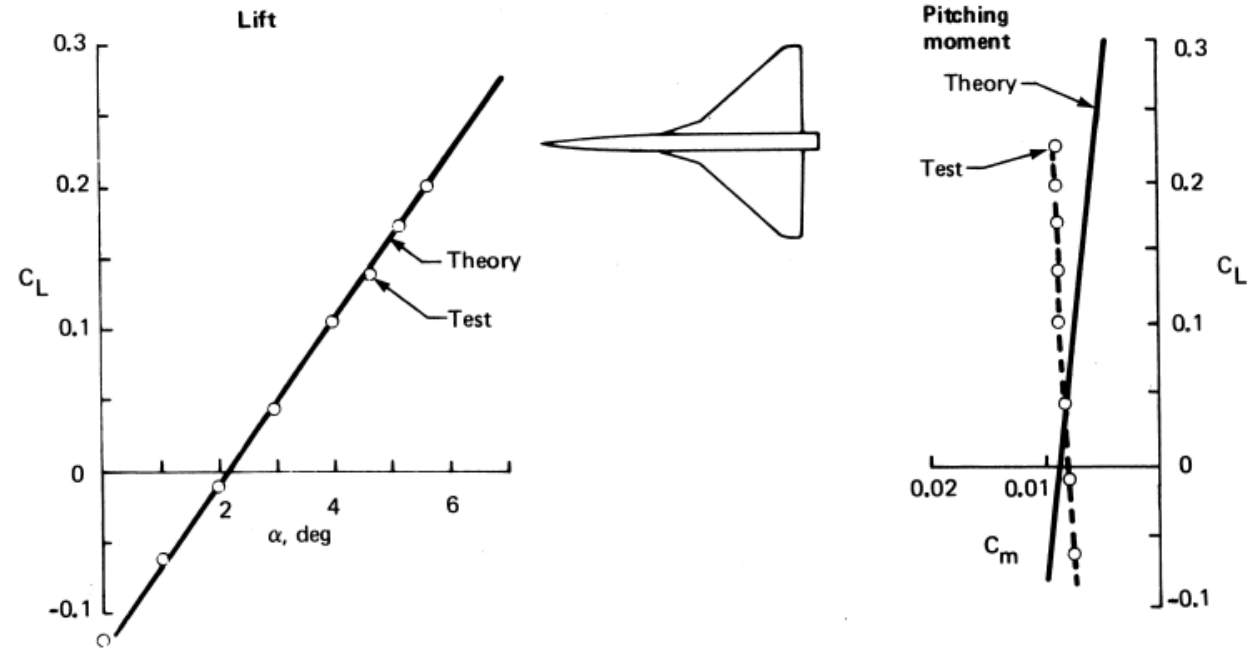

Figure 4-12. Wing + Body Lift and Pitching Moment Curves, Mach 1.15

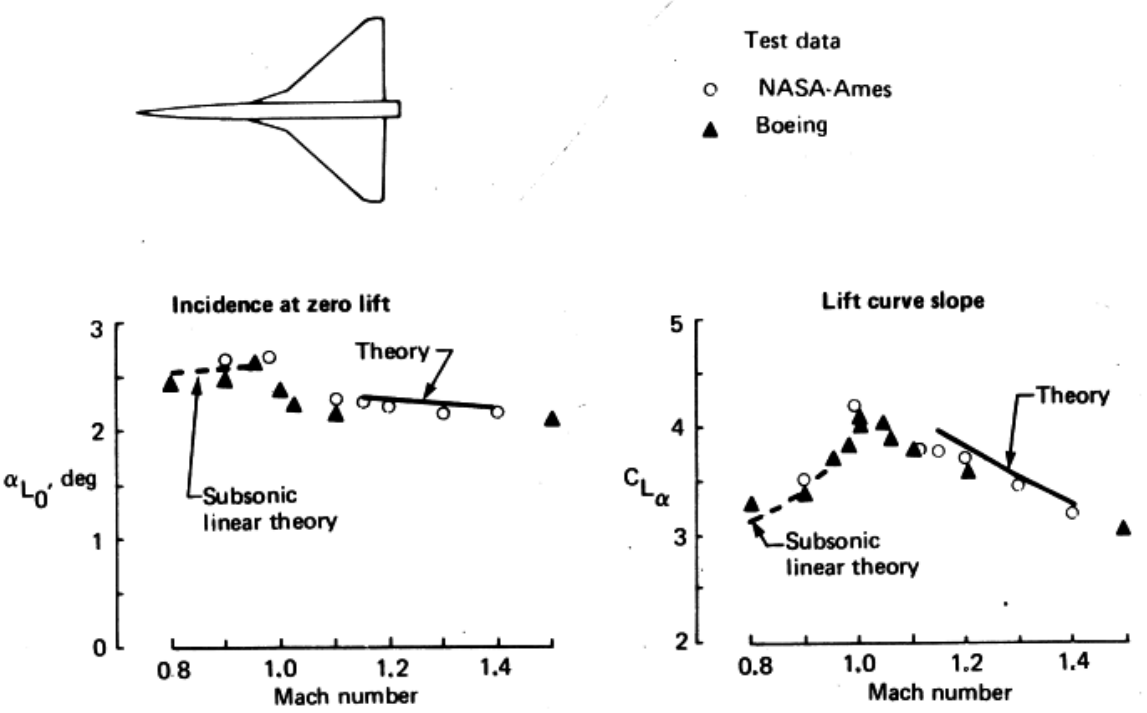

Figure 4-13. Wing + Body Lift Characteristics

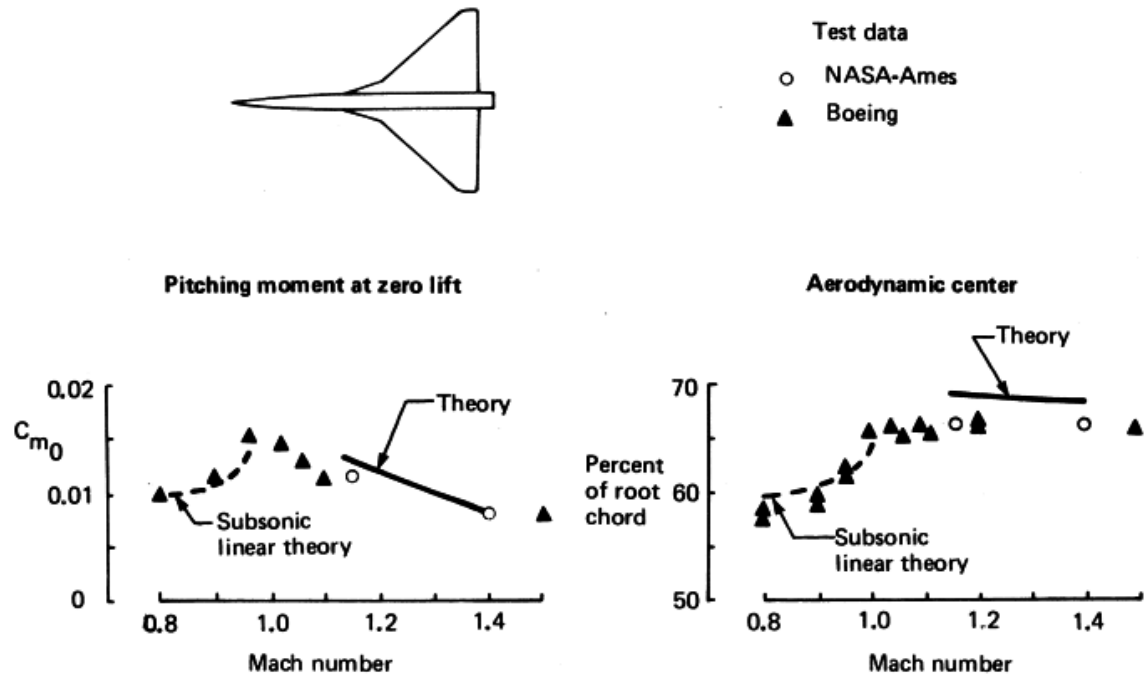

Figure 4-14. Wing + Body Pitching Moment Characteristics

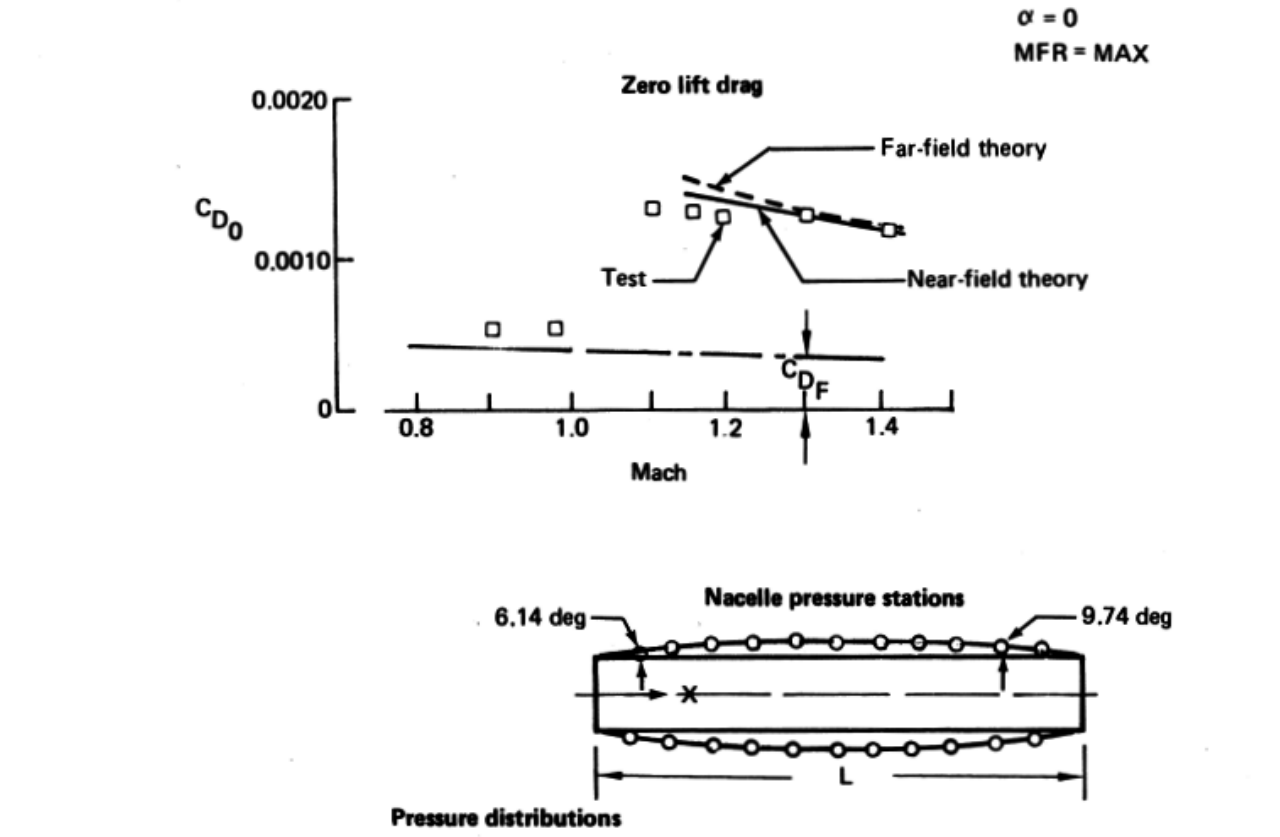

Figure 4-15. Isolated Nacelle Comparisons

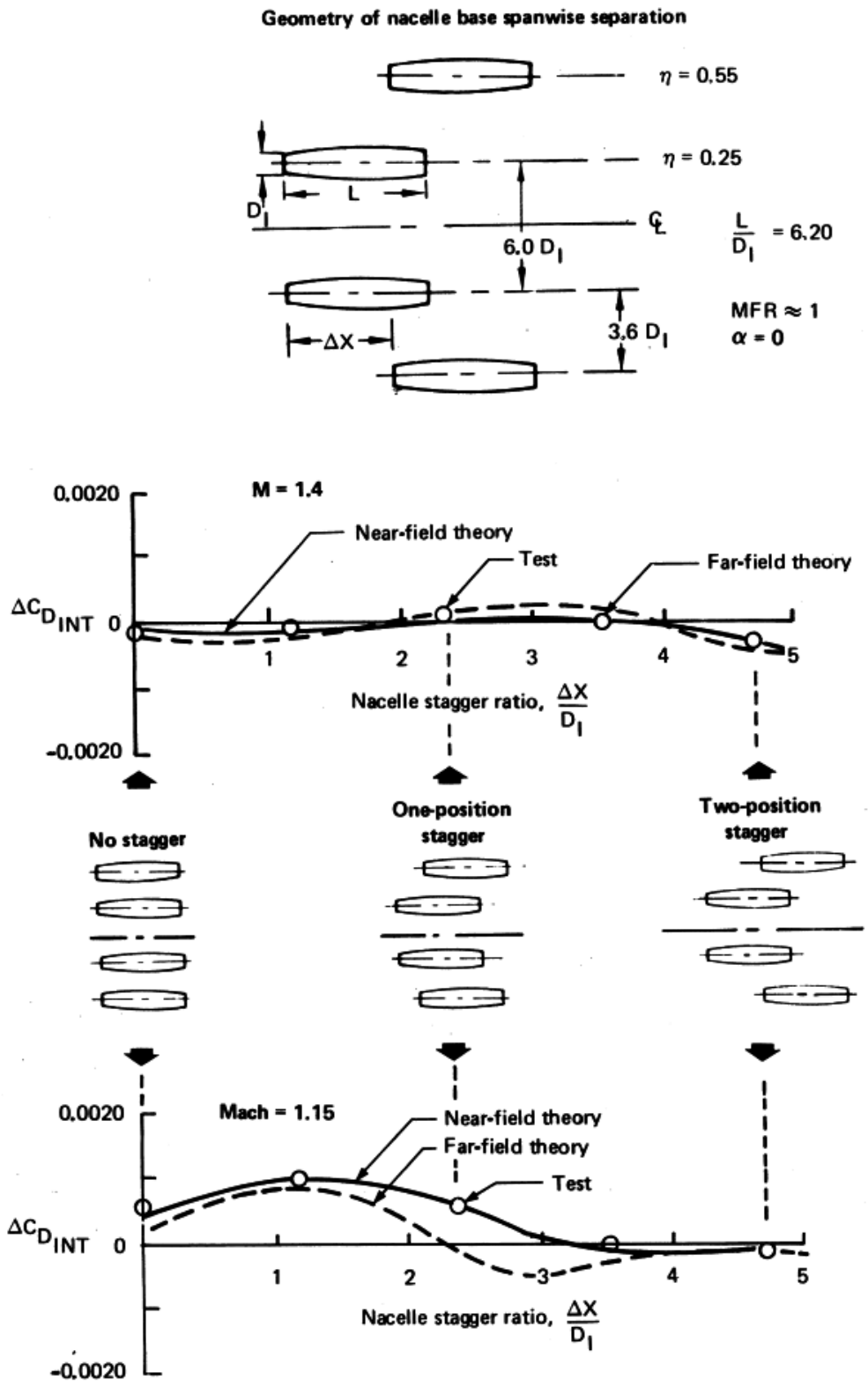

Figure 4-16. Nacelle Mutual Interference for Base Separation

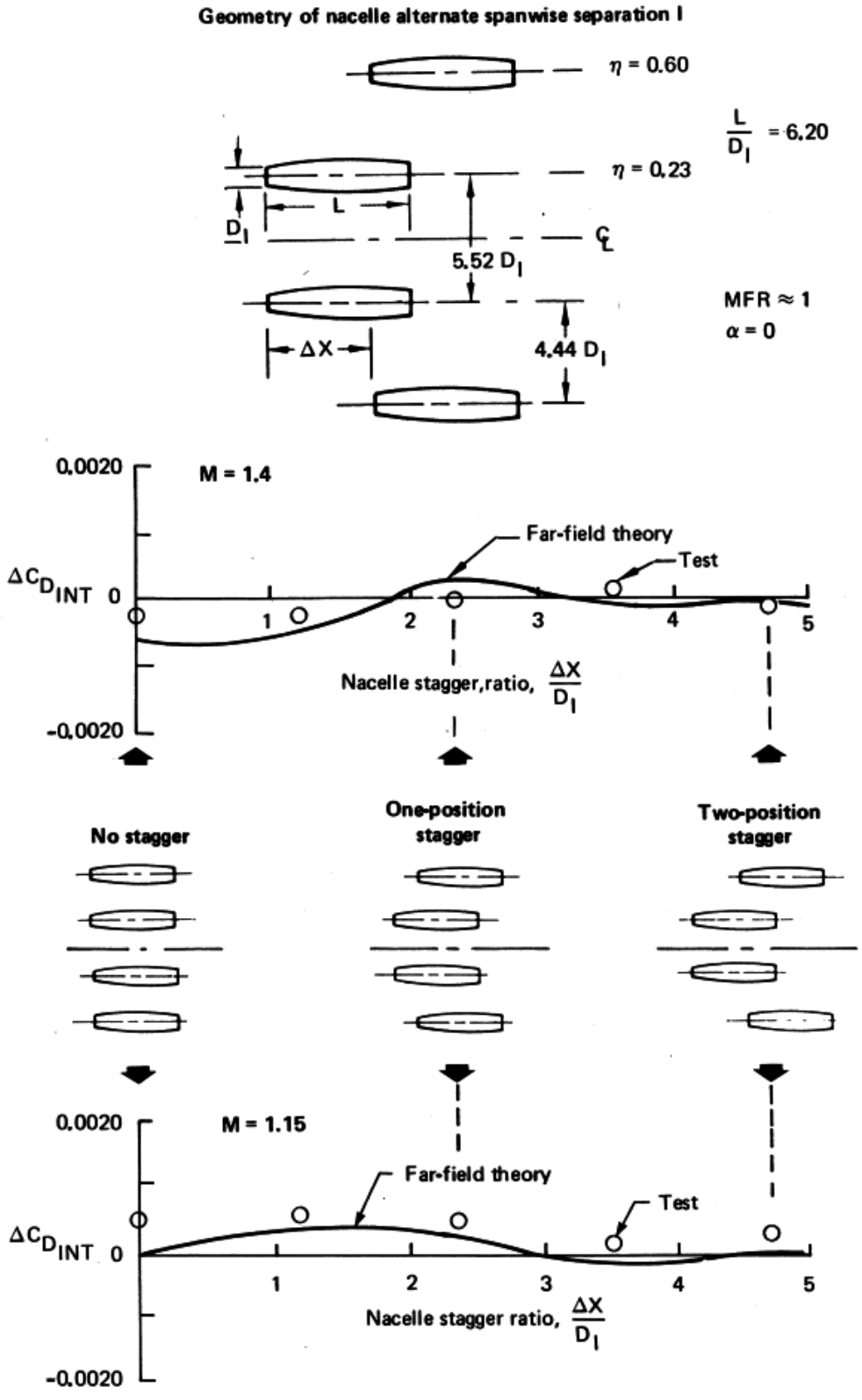

Figure 4-17. Nacelle Mutual Interference for Alternate Separation I

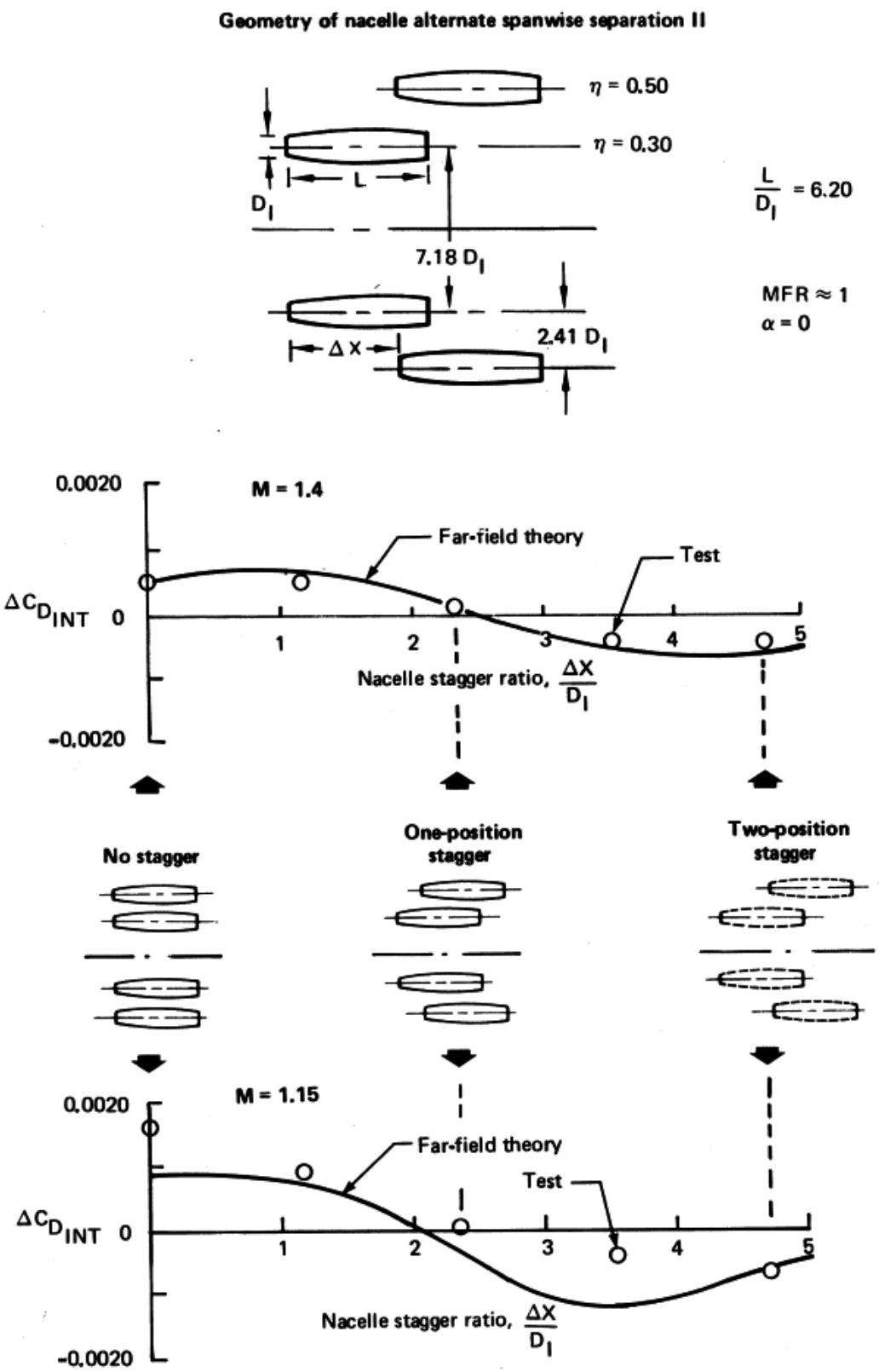

Figure 4-18. Nacelle Mutual Interference for Alternate Separation II

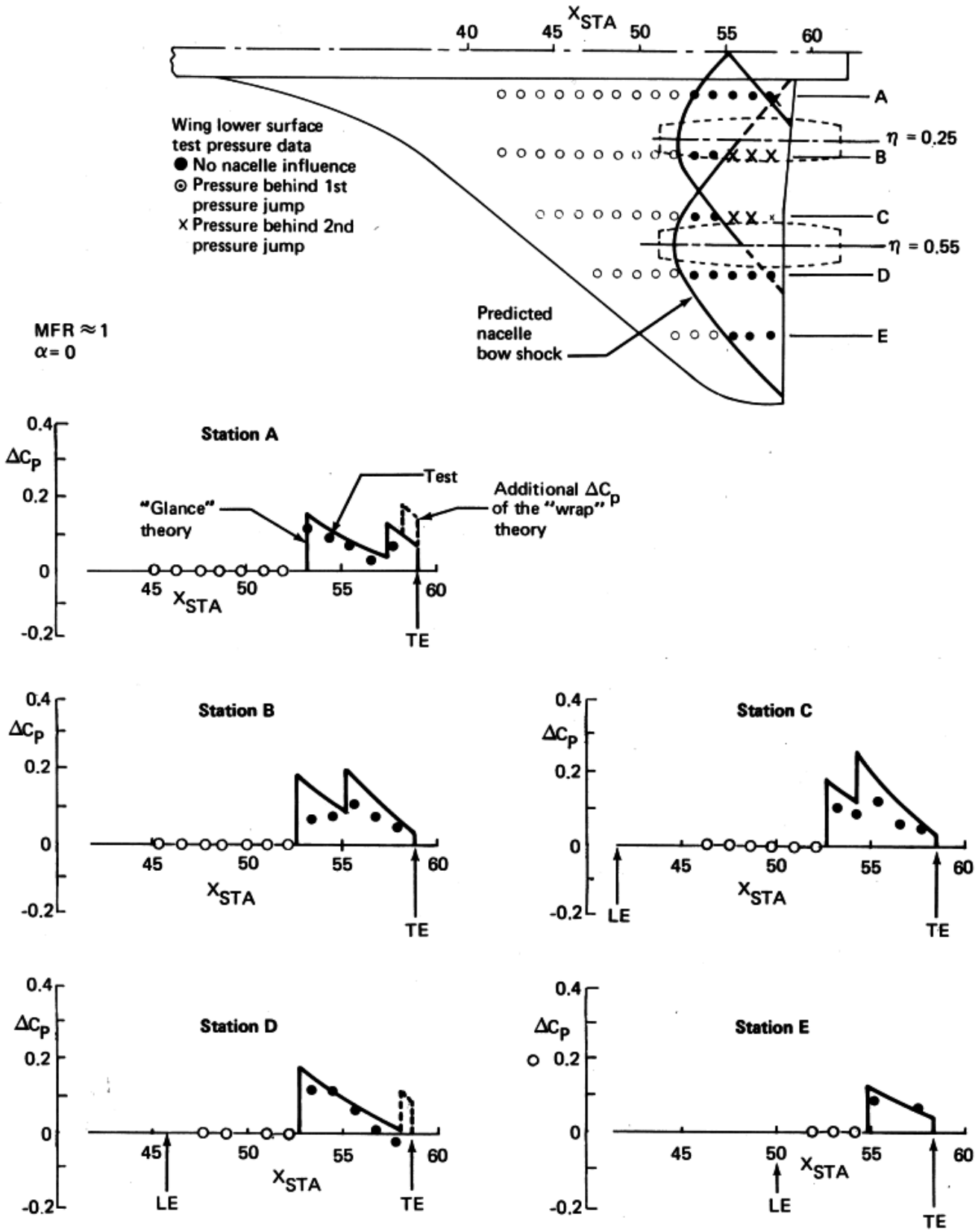

Figure 4-19. Nacelle Interference Pressure Field, M = 1.4, No Stagger, Aft Location

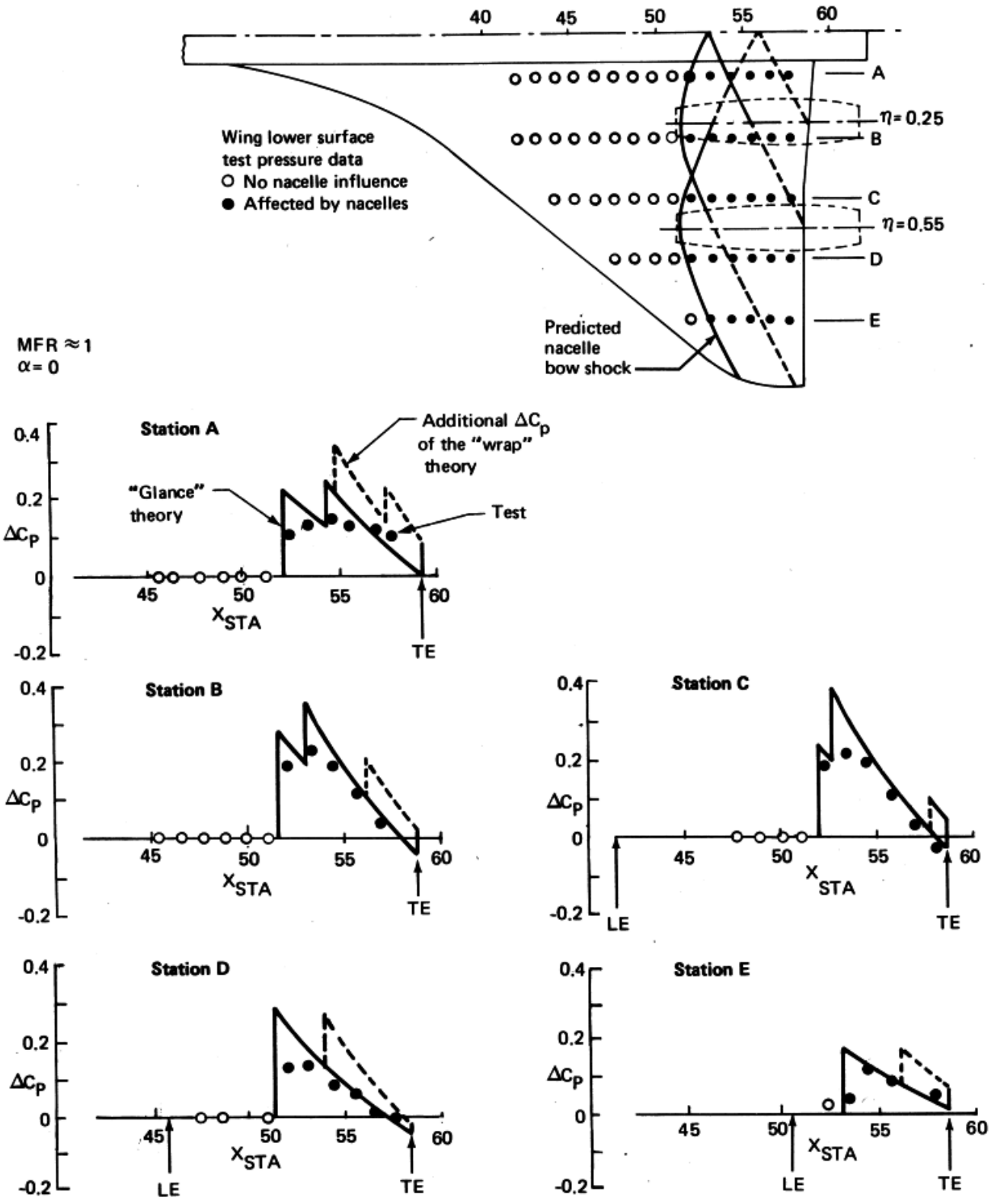

Figure 4-20. Nacelle Interference Pressure Field, M = 1.15, No Stagger, Aft Location

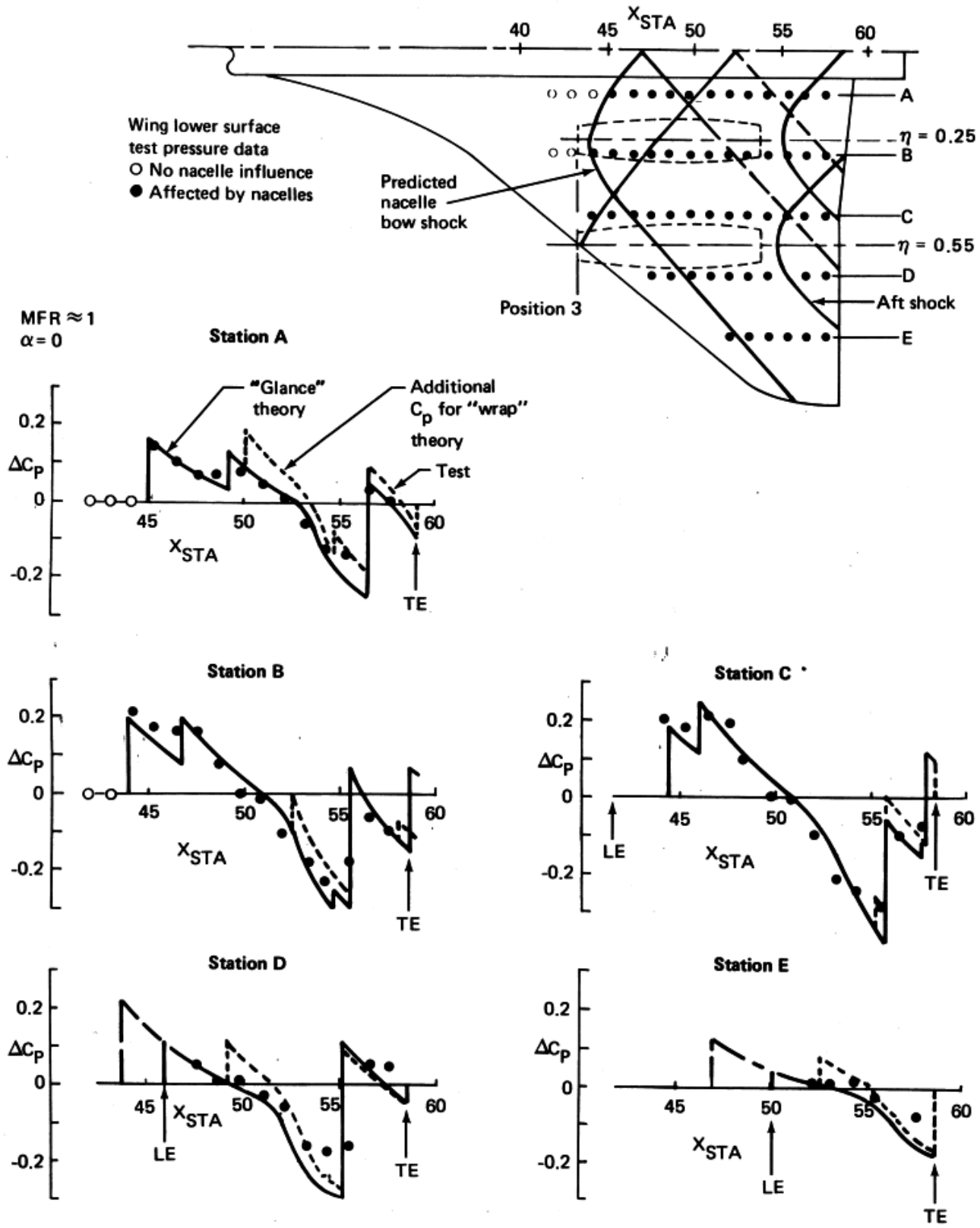

Figure 4-21. Nacelle Interference Pressure Field, M = 1.4, No Stagger Forward Location

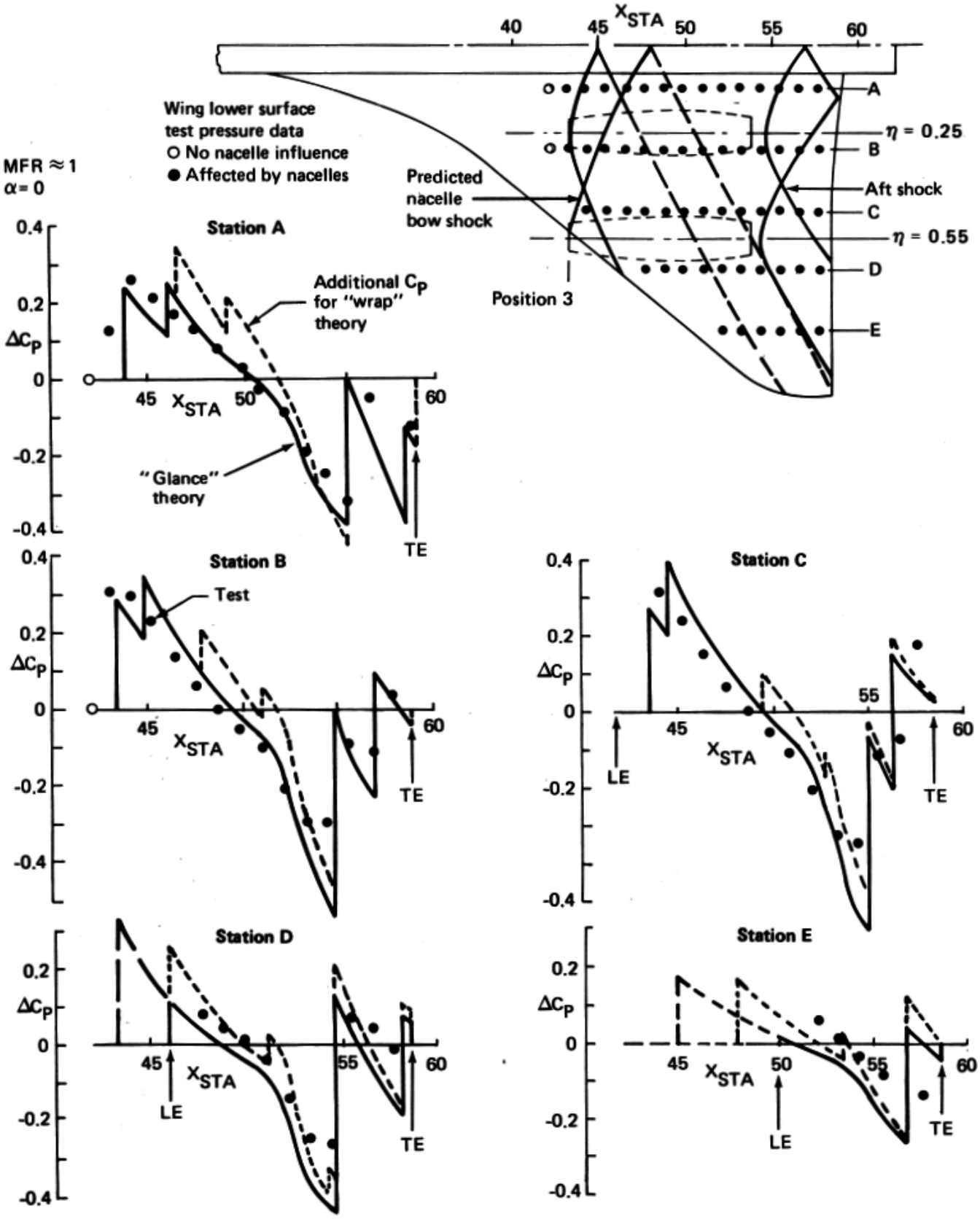

Figure 4-22. Nacelle Interference Pressure Field, M = 1.15, No Stagger, Forward Location

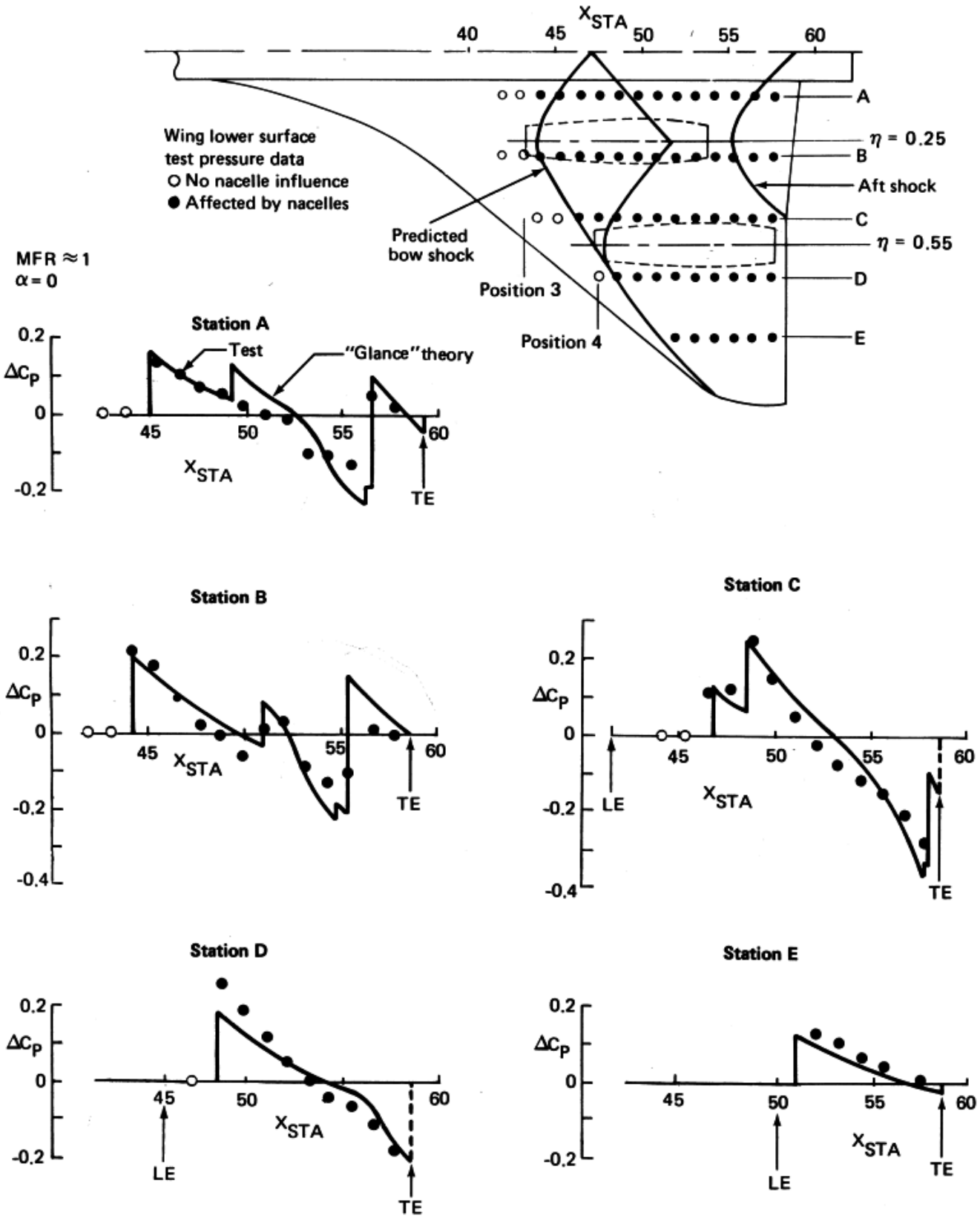

Figure 4-23. Nacelle Interference Pressure Field, M = 1.4, One-Position Stagger

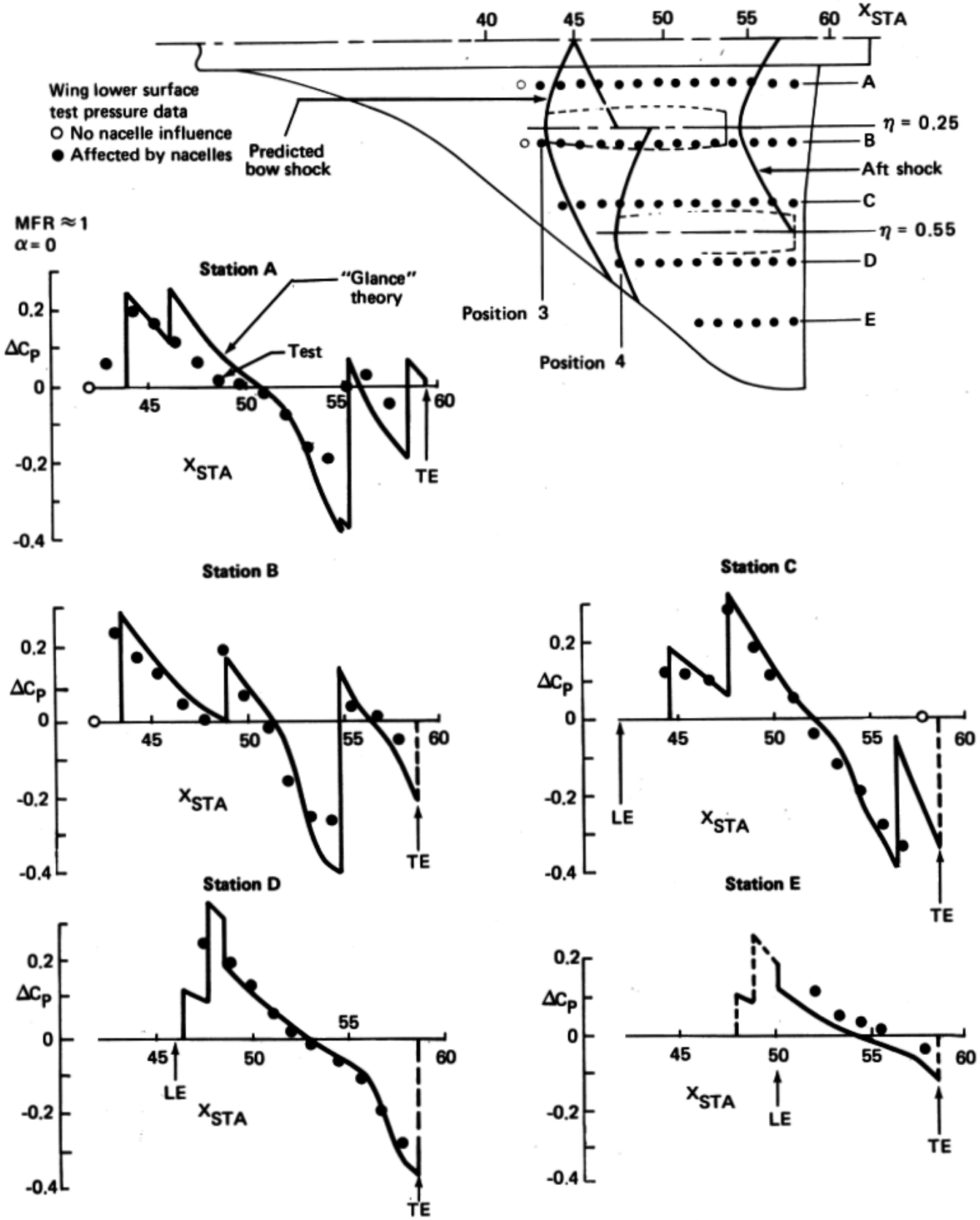

Figure 4-24. Nacelle Interference Pressure Field, M = 1.15, One-Position Stagger

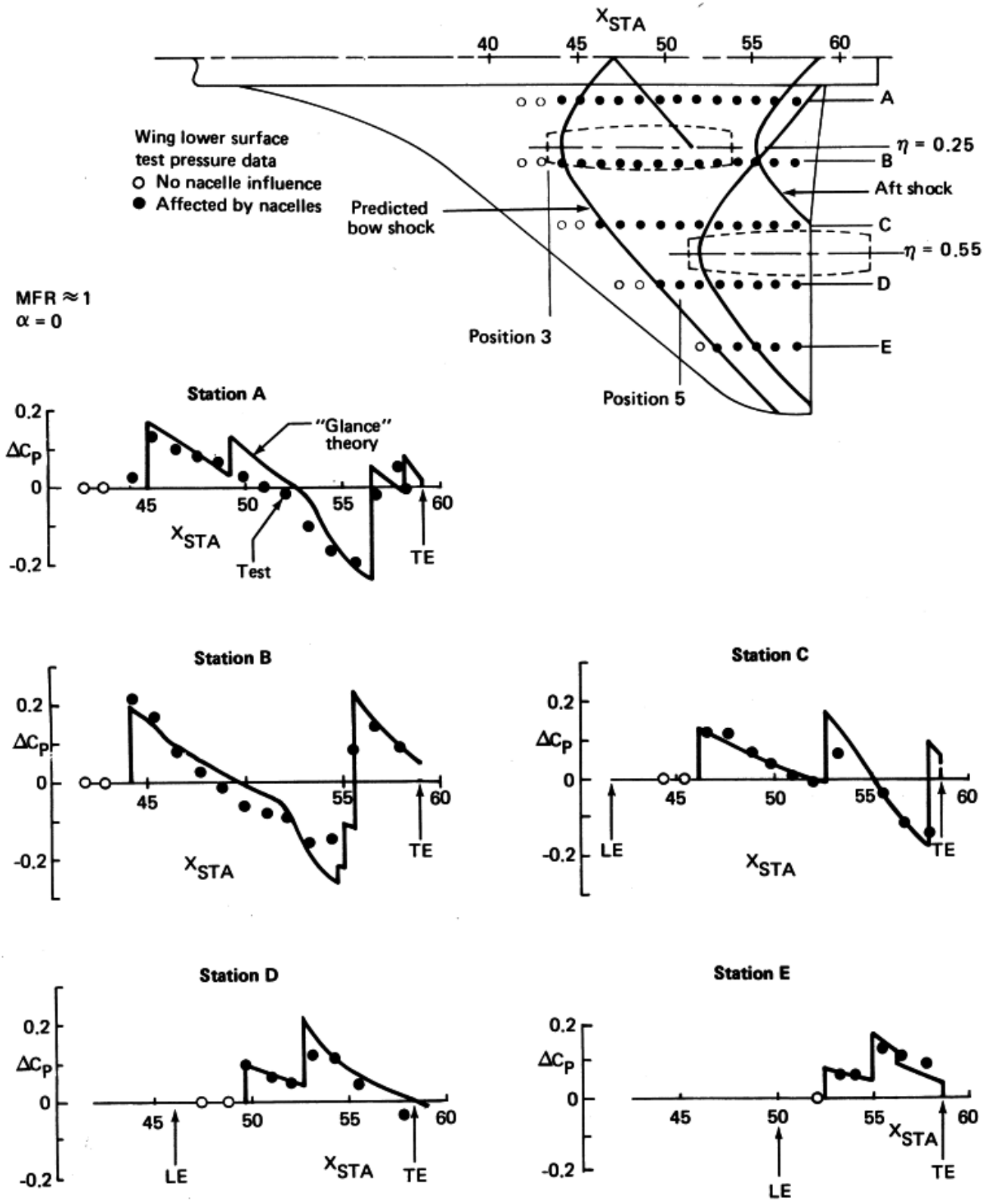

Figure 4-25. Nacelle Interference Pressure Field, M = 1.4, Two-Position Stagger

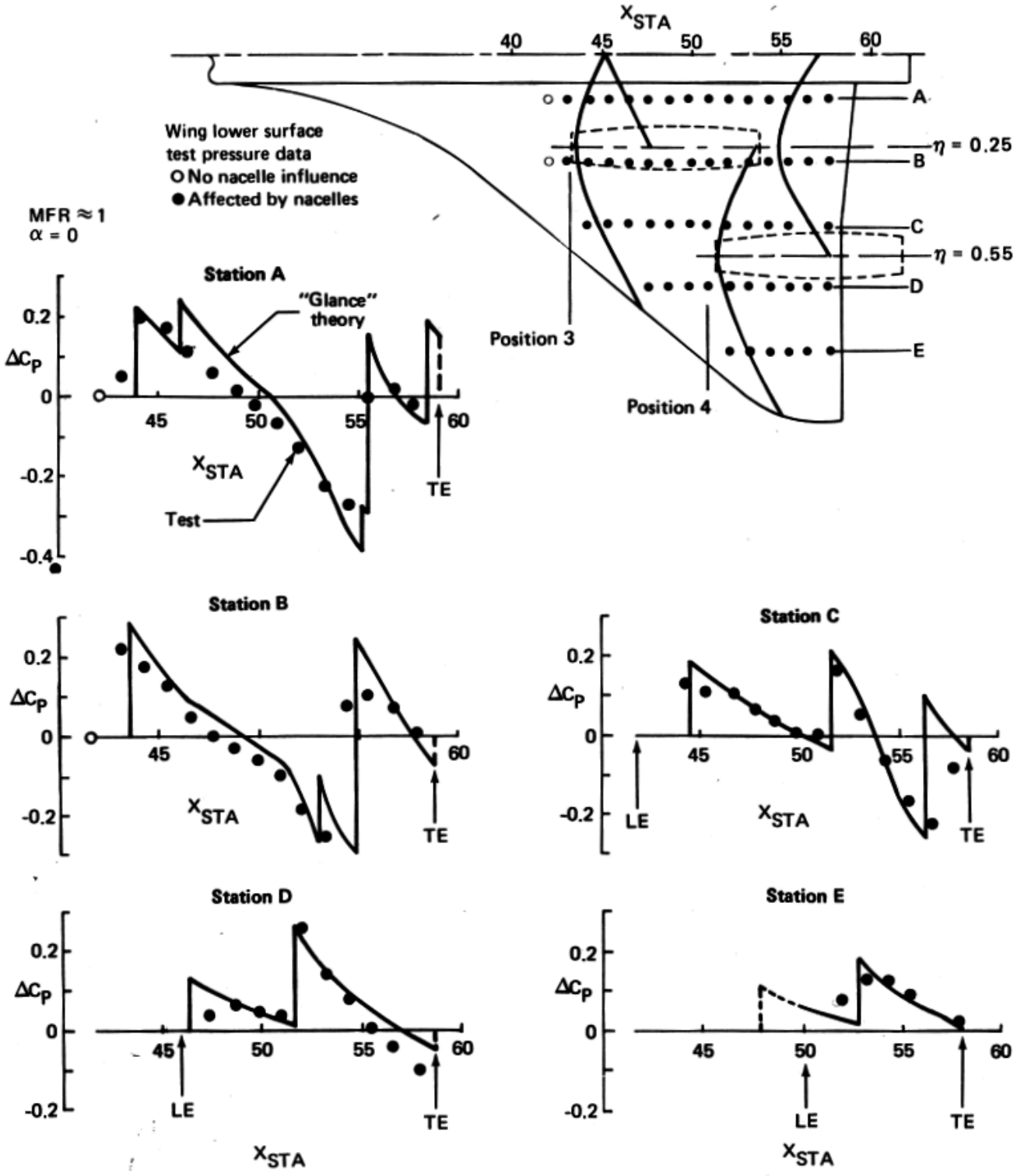

Figure 4-26. Nacelle Interference Pressure Field, M = 1.15, Two-Position Stagger

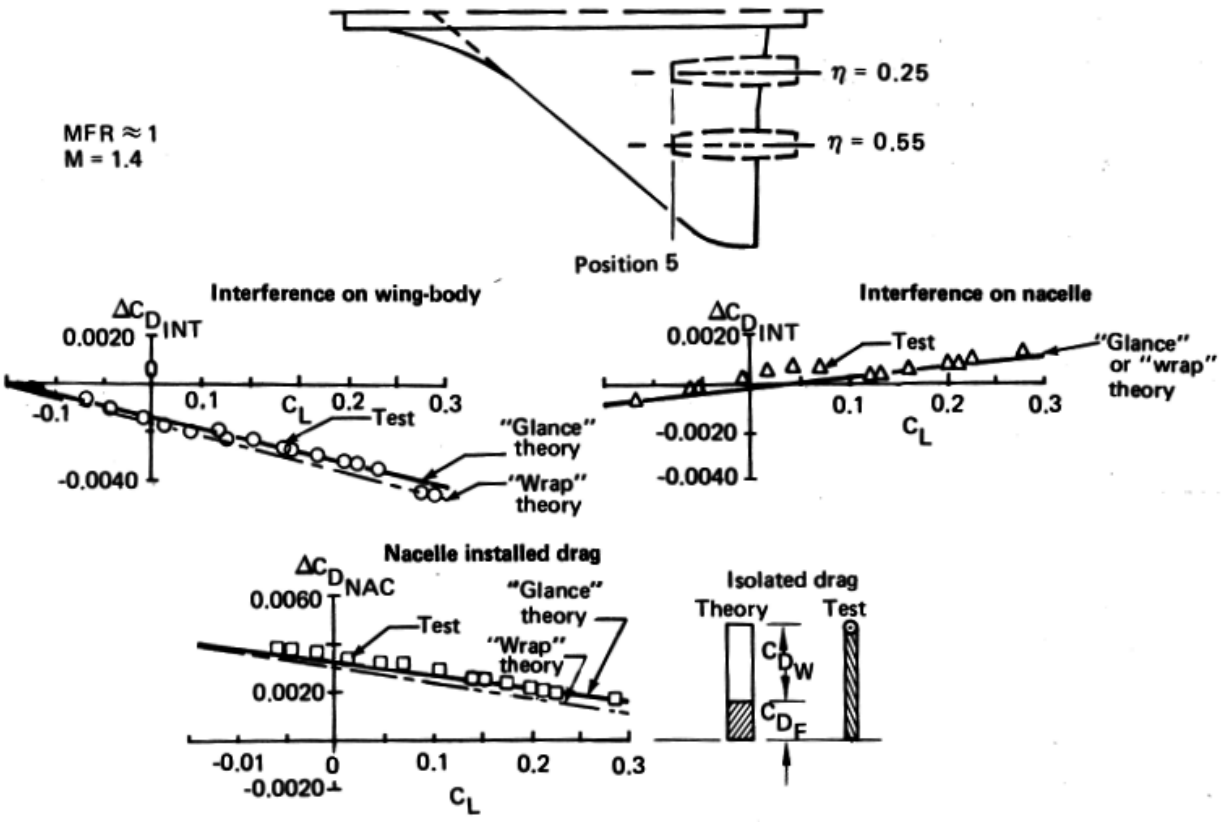

Figure 4-27. Interference Drag, M = 1.4, No Stagger, Aft Location

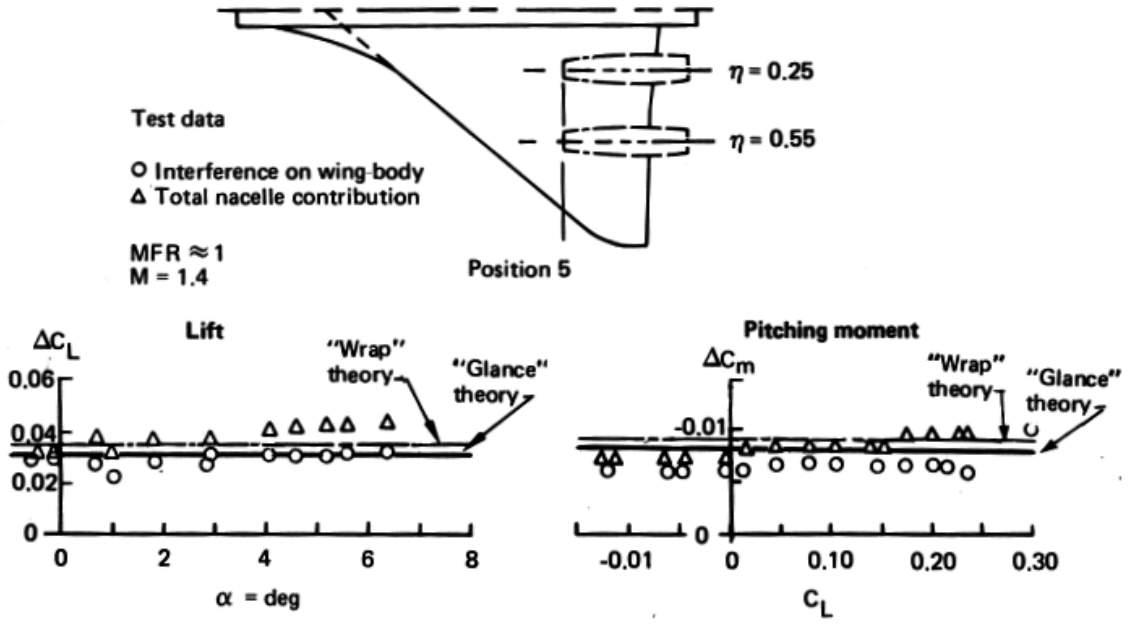

Figure 4-28. Interference Lift and Pitching Moment, M = 1.4, No Stagger, Aft Location

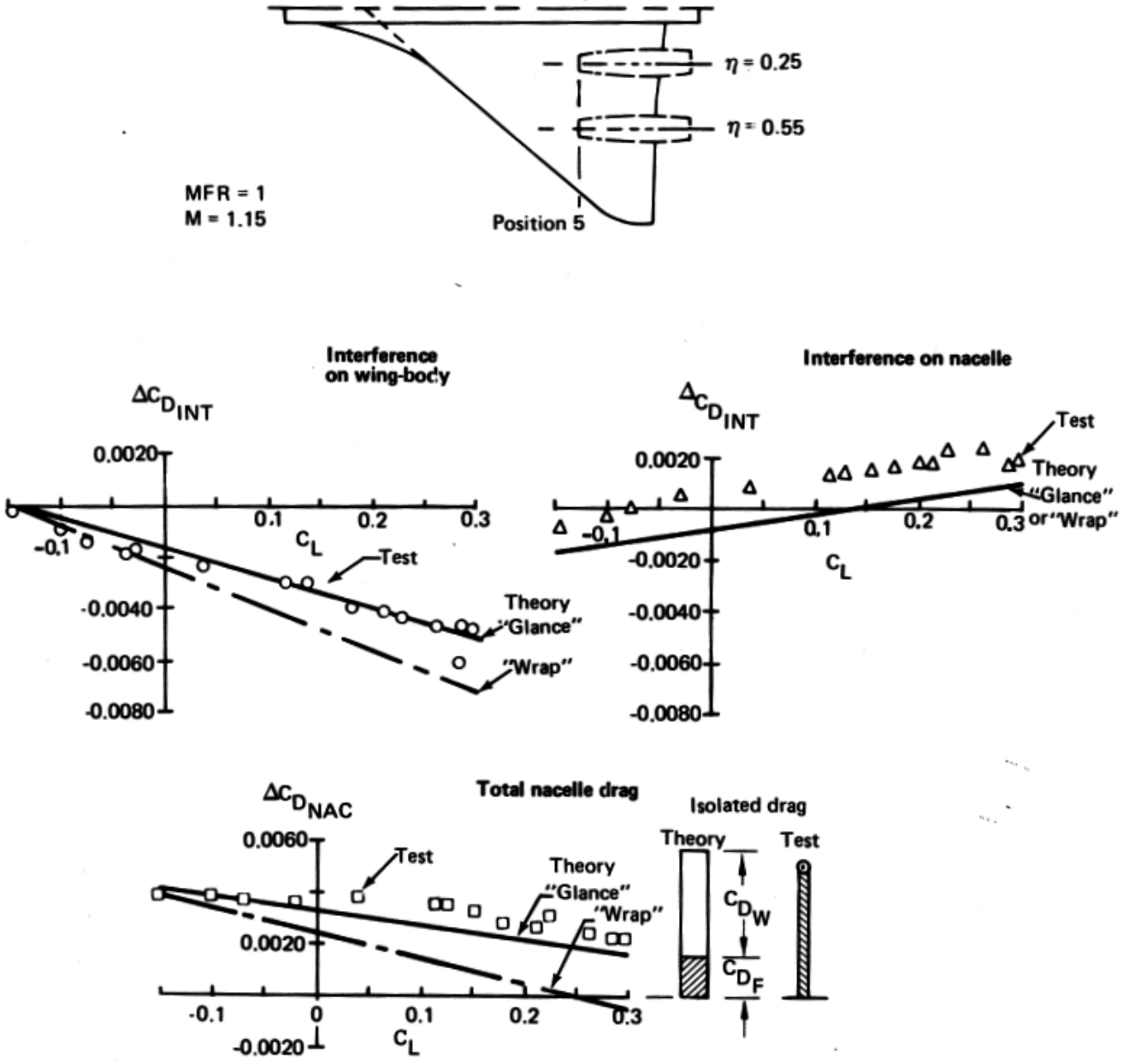

Figure 4-29. Interference Drag, M = 1.15, No Stagger, Aft Location

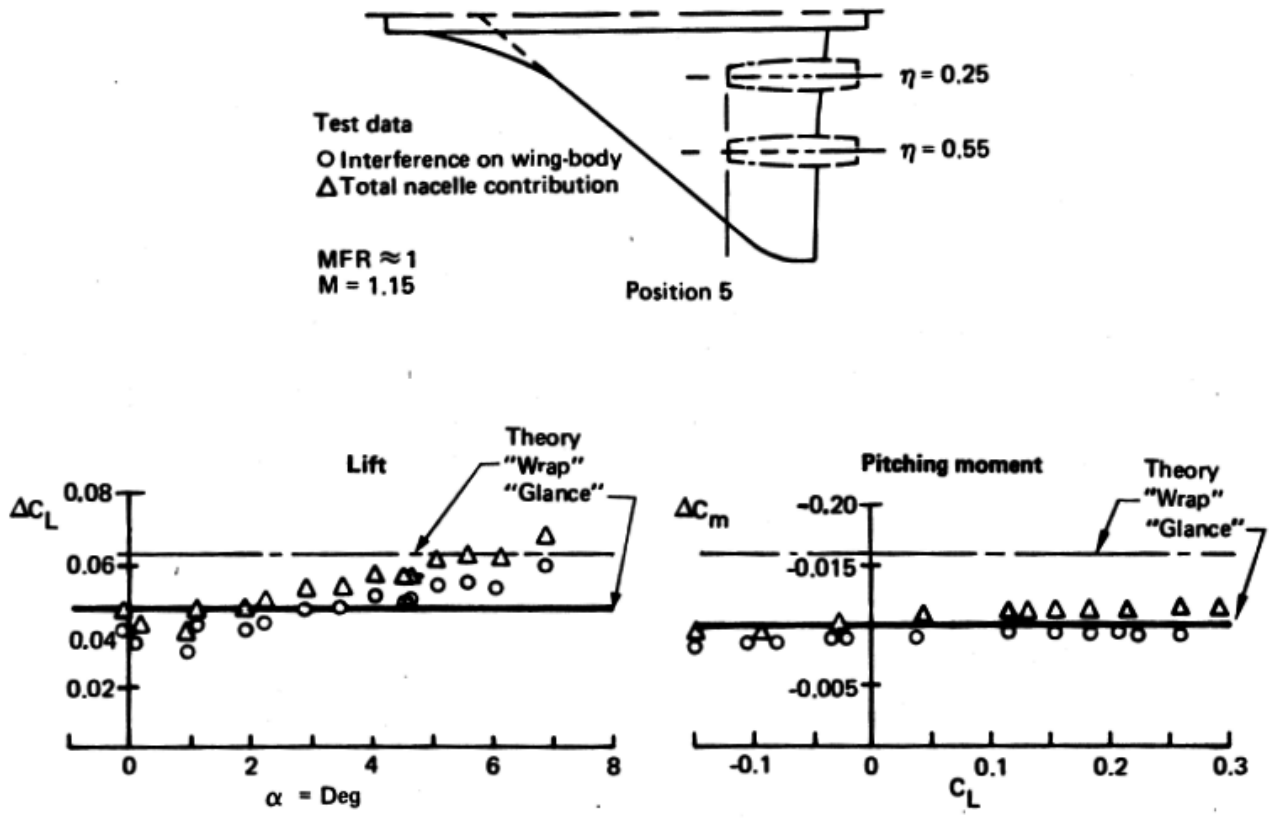

Figure 4-30. .Interference Lift and Pitching Moment, M = 1.15, No Stagger, Aft Location

$$\Delta C_L = \frac{L}{qS_R} = \frac{2\Delta S}{\beta S_R}$$

$$\frac{\Delta C_{L_\ell}}{\Delta C_{L_\infty}} = \frac{\beta_\infty q_\ell}{\beta_\ell q_\infty} = \left[0.7\, C_p\, M_\infty{}^2 + 1\right]\left(\frac{M_\ell}{M_\infty}\right)^2\left(\frac{\beta_\infty}{\beta_\ell}\right)$$

$$M_\ell = \sqrt{5\left[\frac{1 + 0.2\, M_\infty{}^2}{\left\{0.7\, C_p\, M_\infty{}^2 + 1\right\}^{1/3.5}} - 1\right]}$$

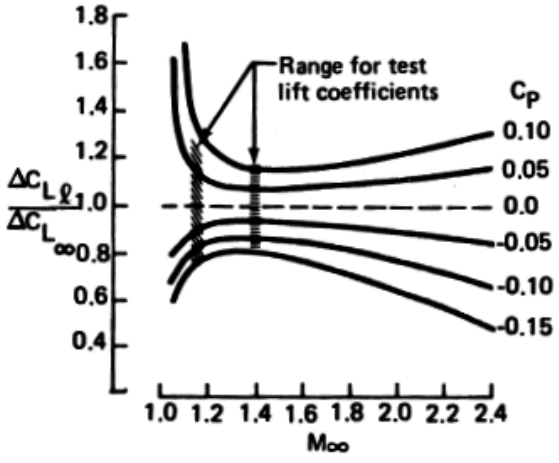

Figure 4-31. Effect of Local Pressure Field on Interference Lift

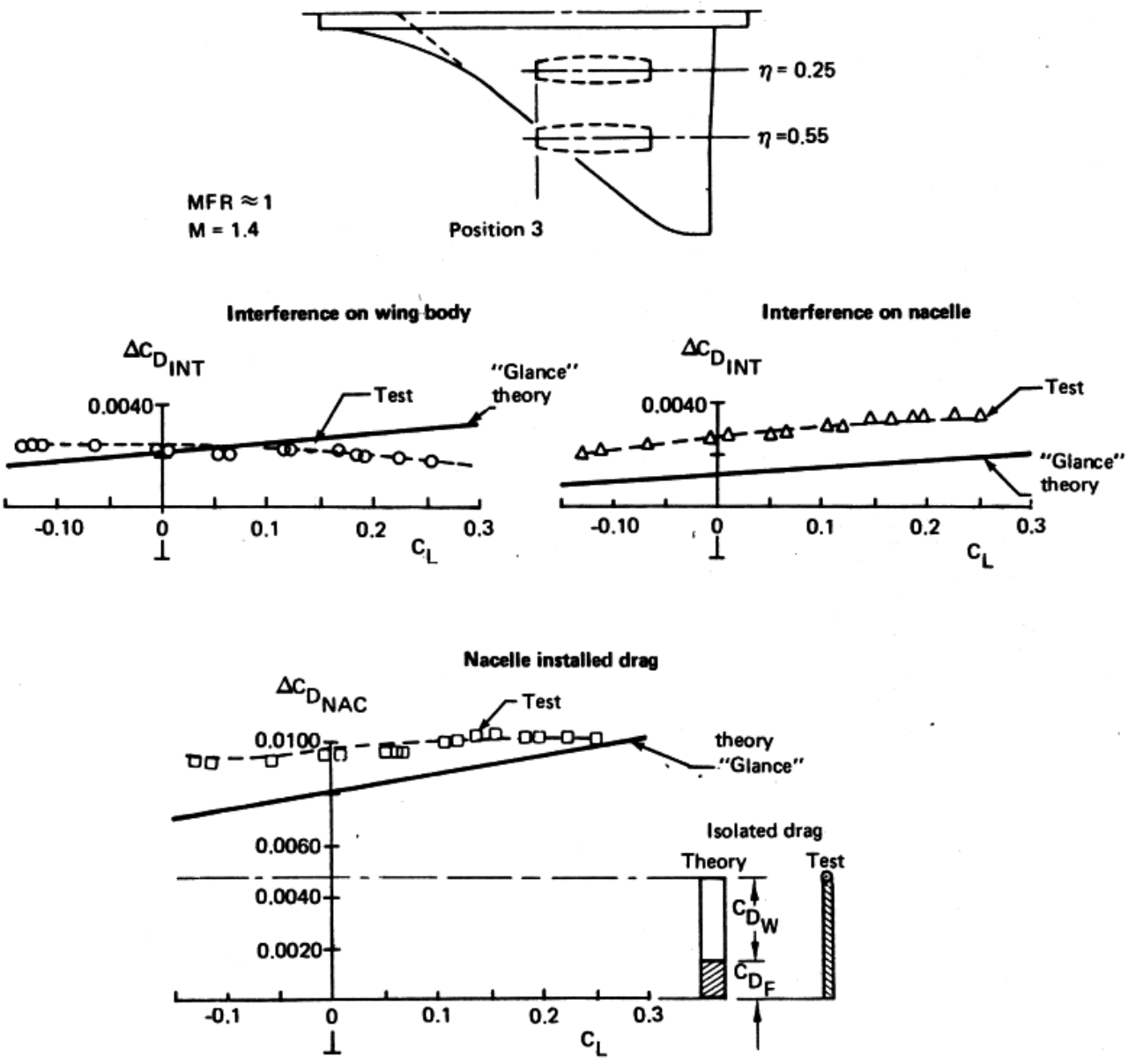

Figure 4-32. Interference Drag; M = 1.4, No Stagger, Forward Location

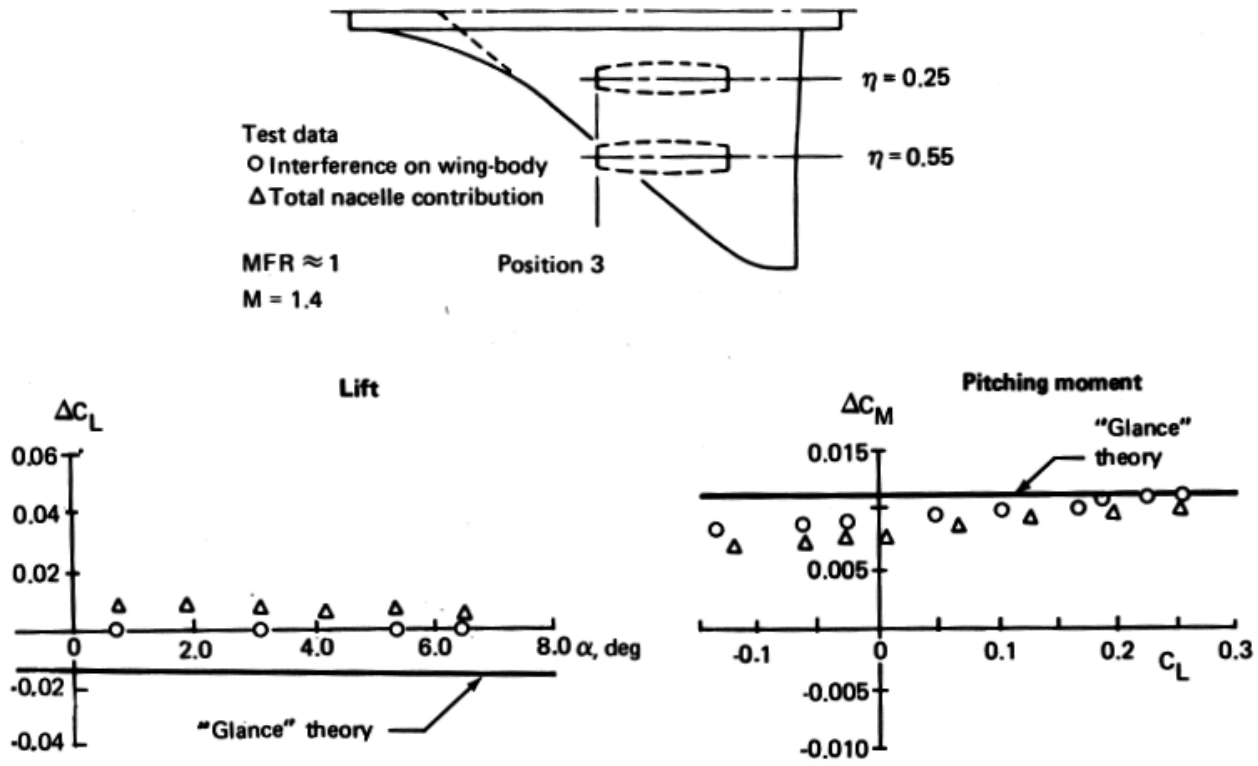

Figure 4-33. Interference Lift and Pitching Moment, M = 1.4, No Stagger, Forward Location

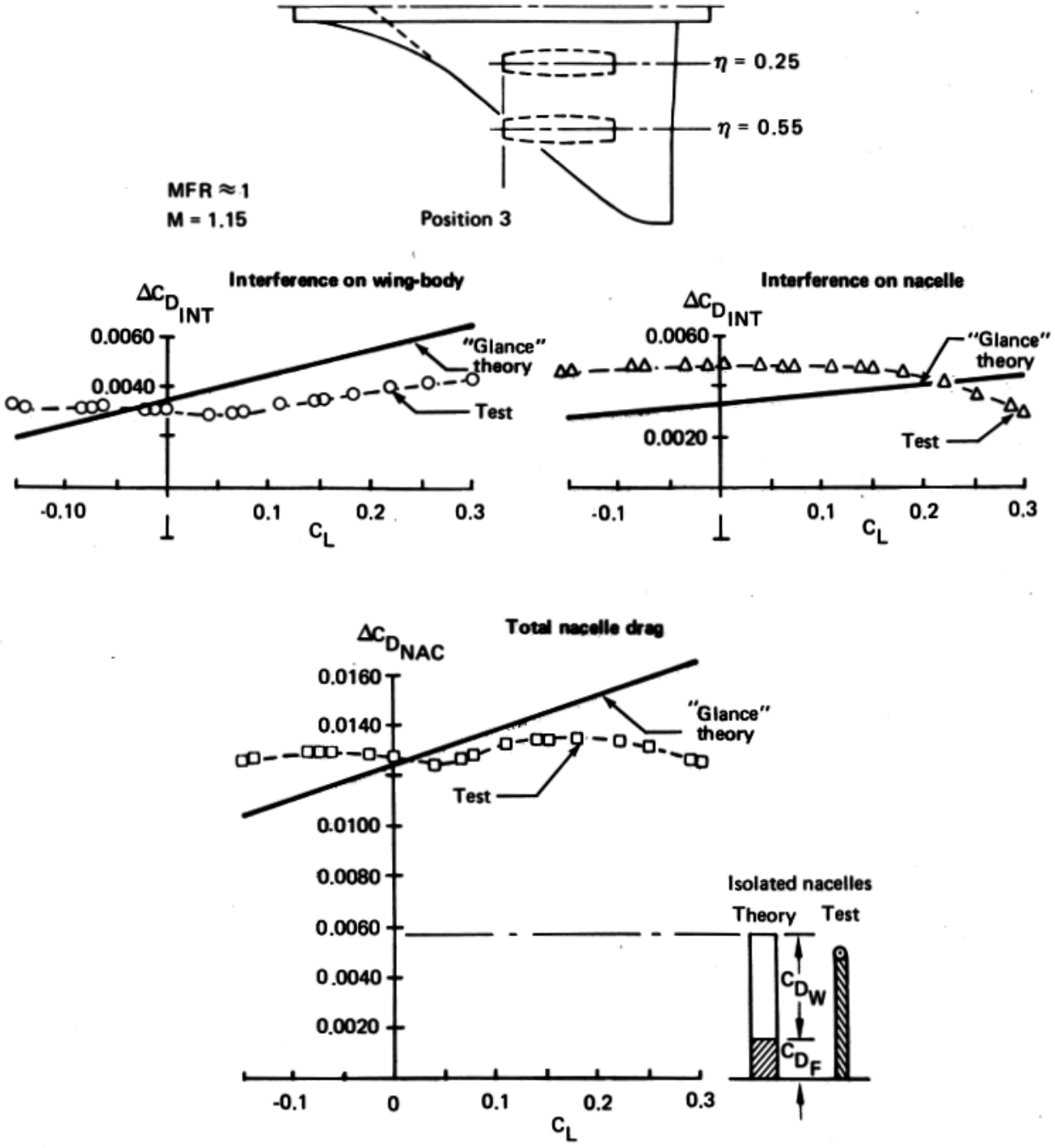

Figure 4-34. Interference Drag, M = 1.15, No Stagger, Forward Location

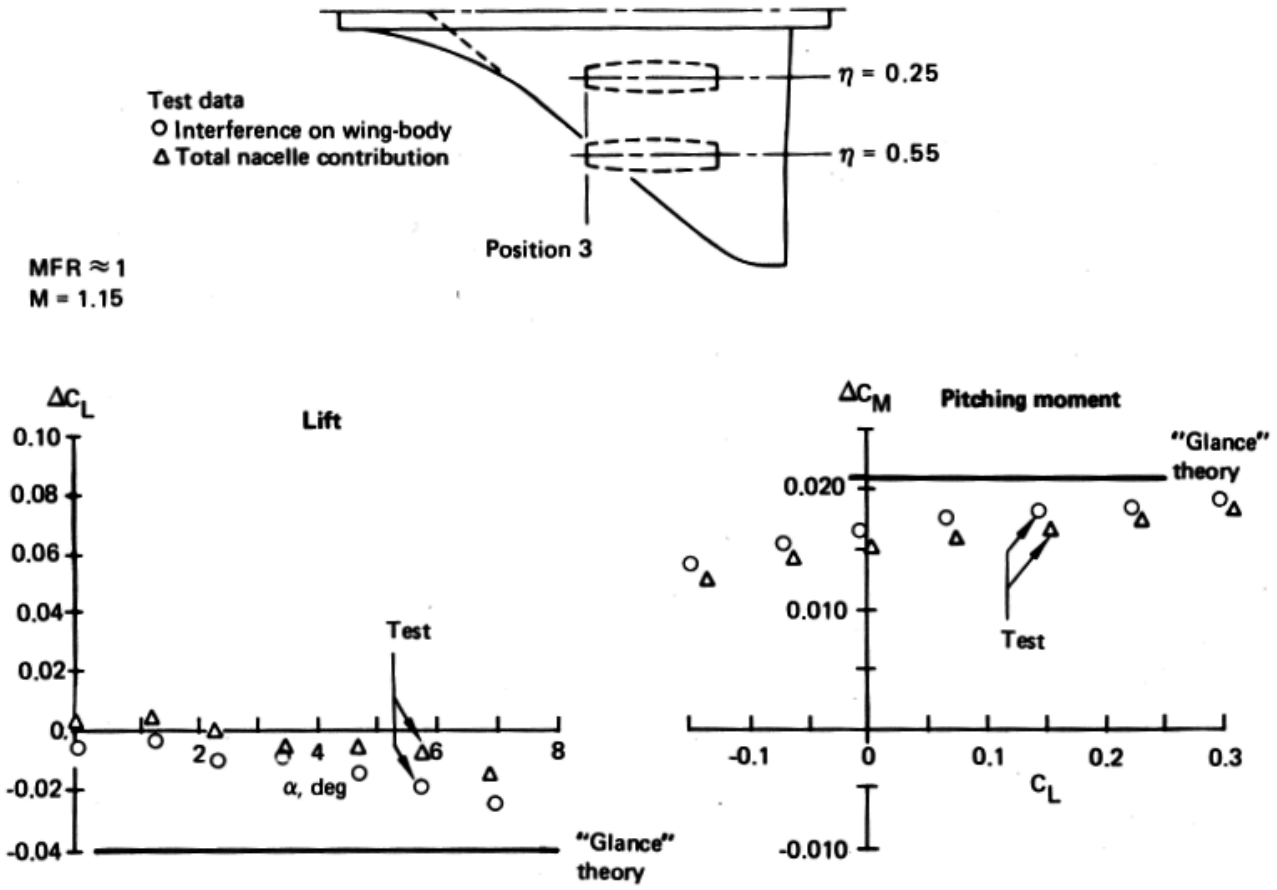

Figure 4-35. Interference Lift and Pitching Moment, M = 1.15, No Stagger, Forward Location

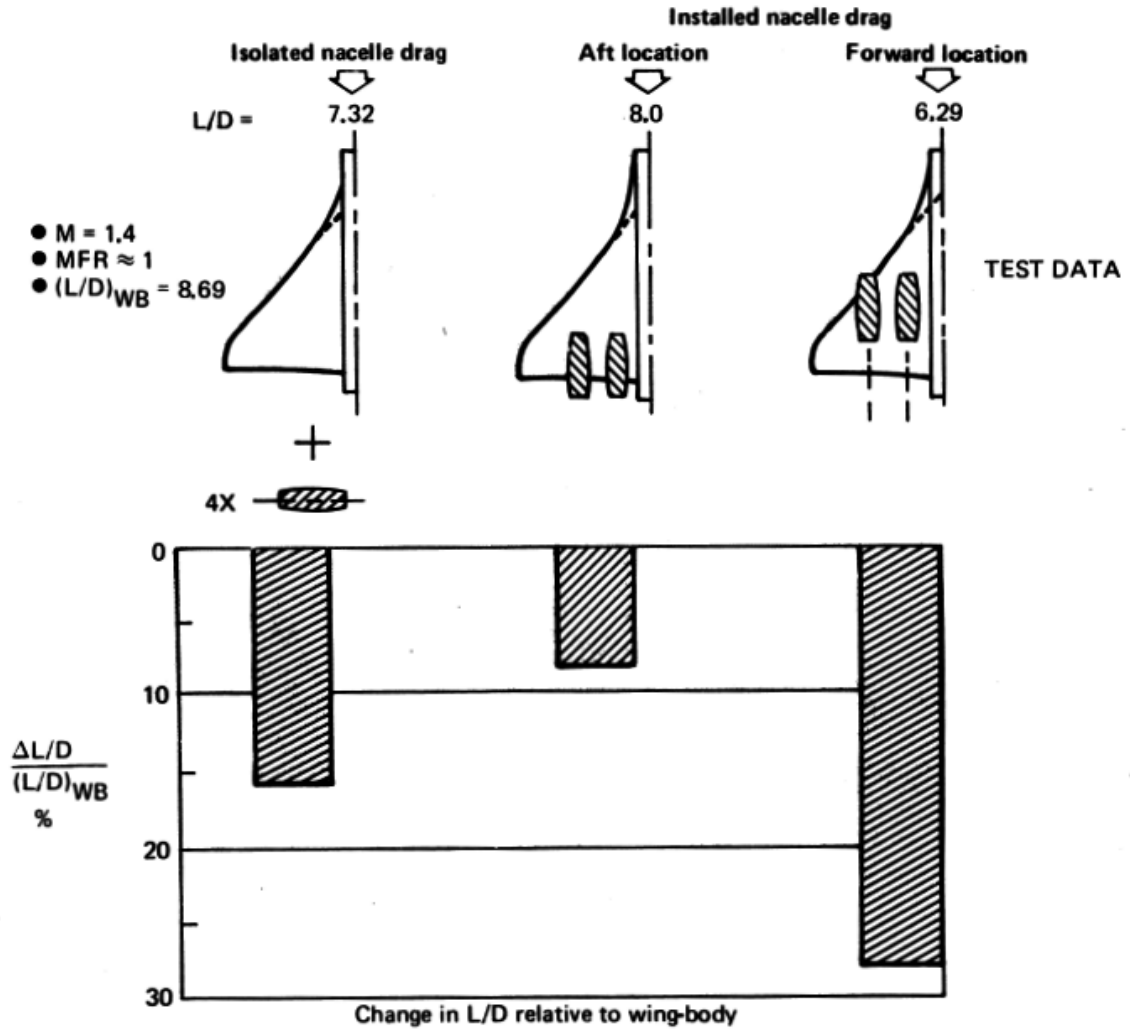

Figure 4-36. Effect of Nacelle Interference on Lift/Drag Ratio

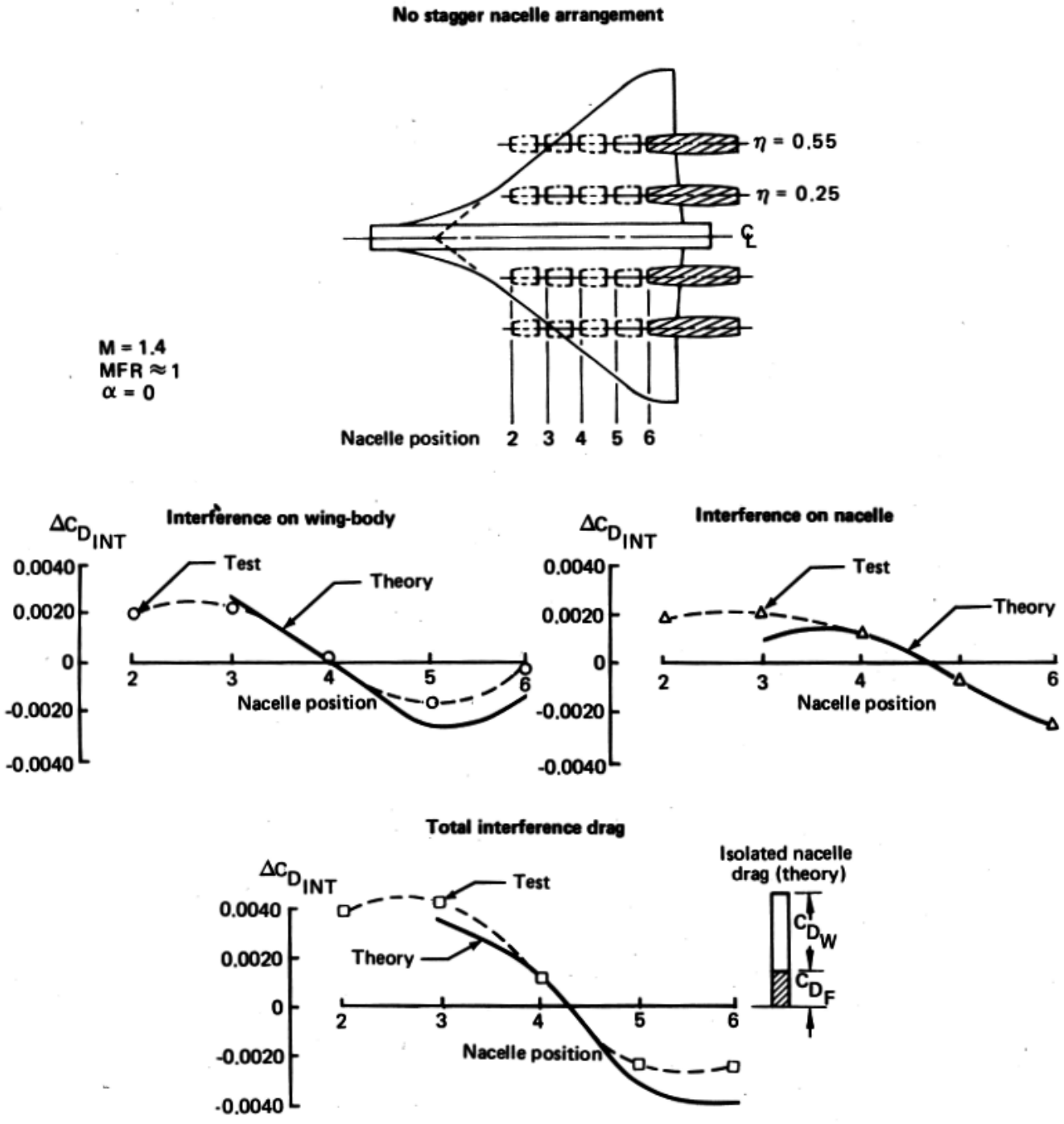

Figure 4-37. Effect of Nacelle Location on Interference Drag, No Stagger, M = 1.4

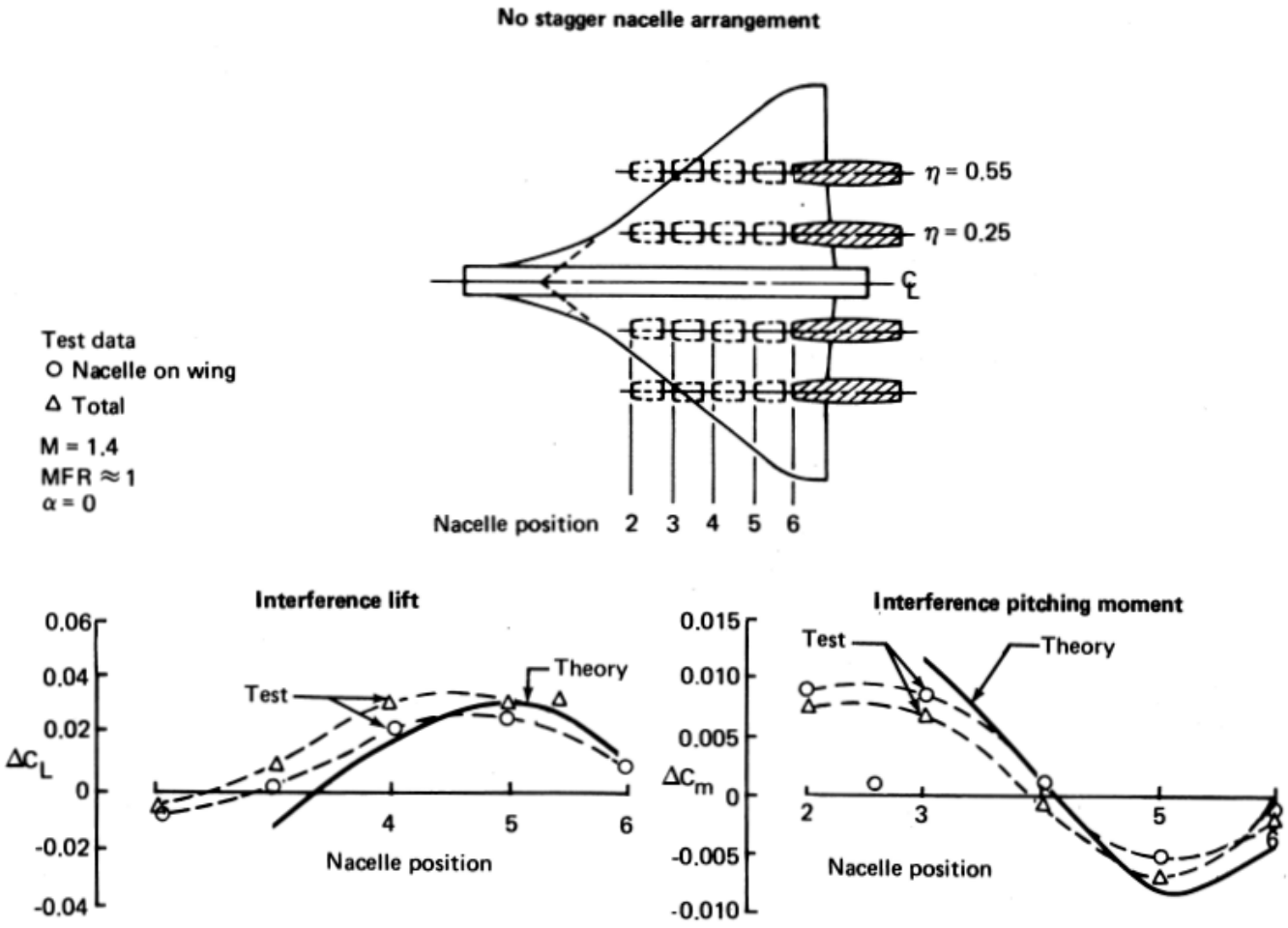

Figure 4-38. Effect of Nacelle Location on Interference Lift and Pitching Moment, No Stagger, M = 1.4

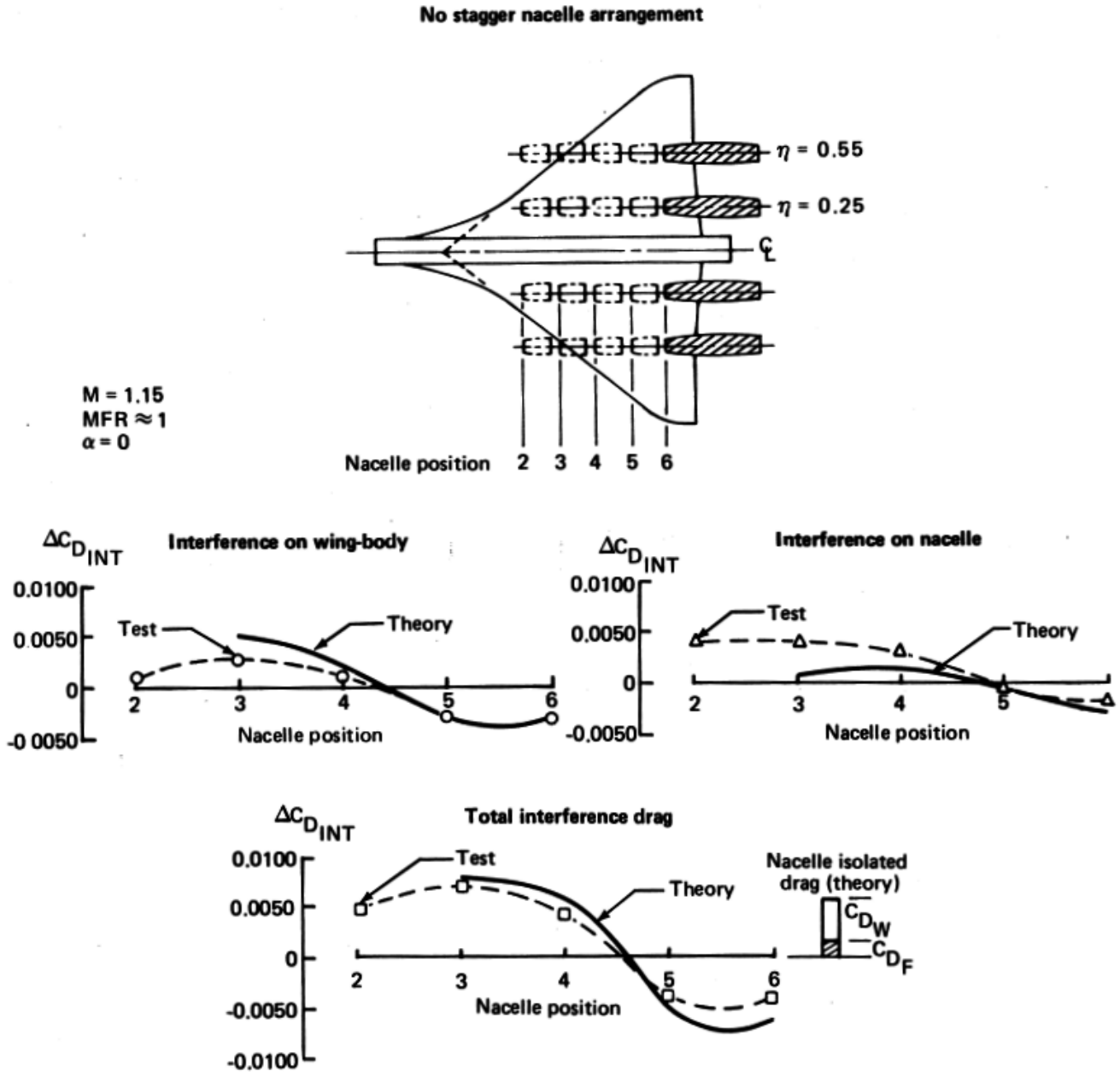

Figure 4-39. Effect of Nacelle Location on Interference Drag, No Stagger, M = 1.15

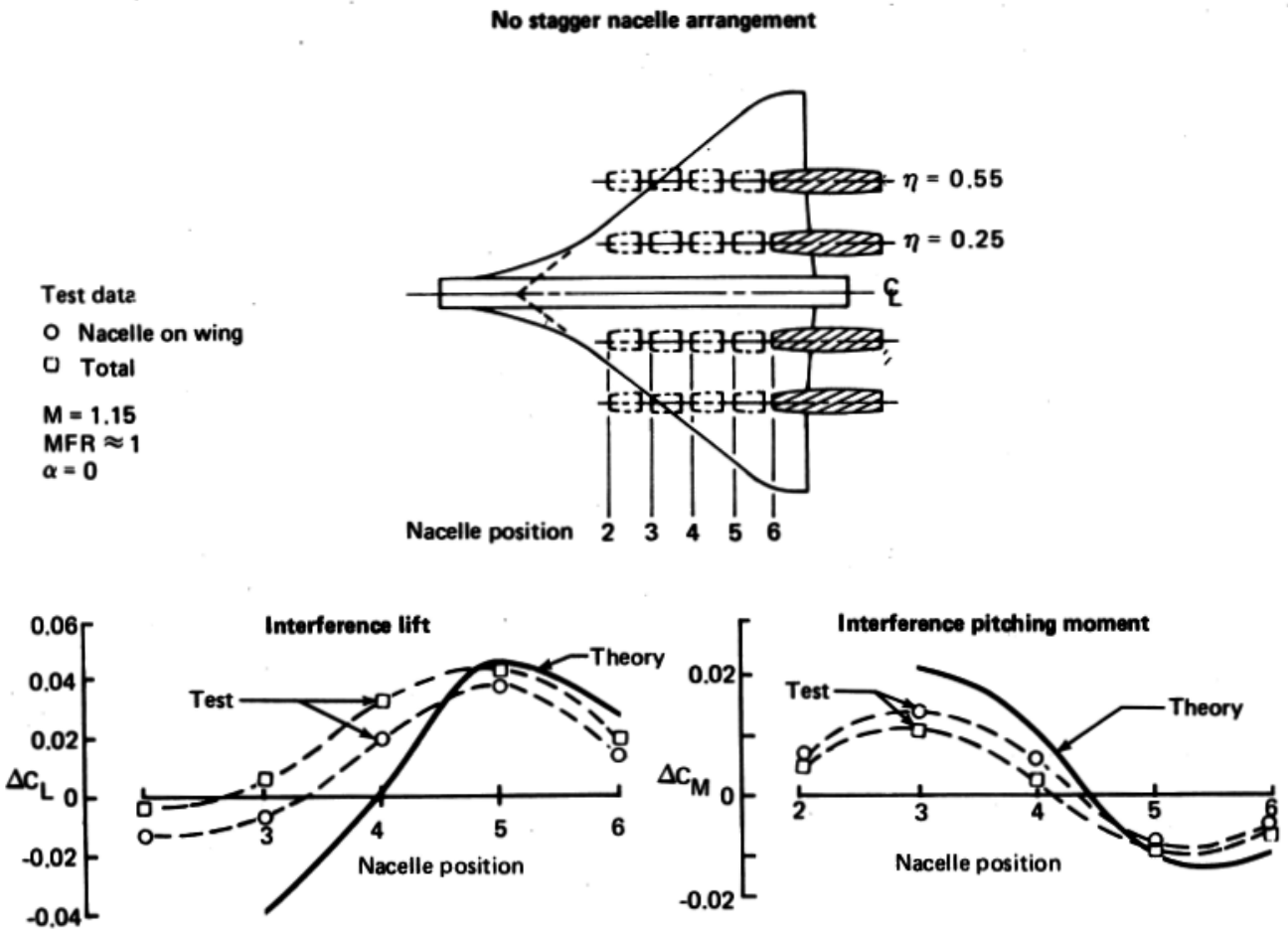

Figure 4-40. Effect of Nacelle Location on Interference Lift and Pitching Moment, No Stagger, M = 1.15

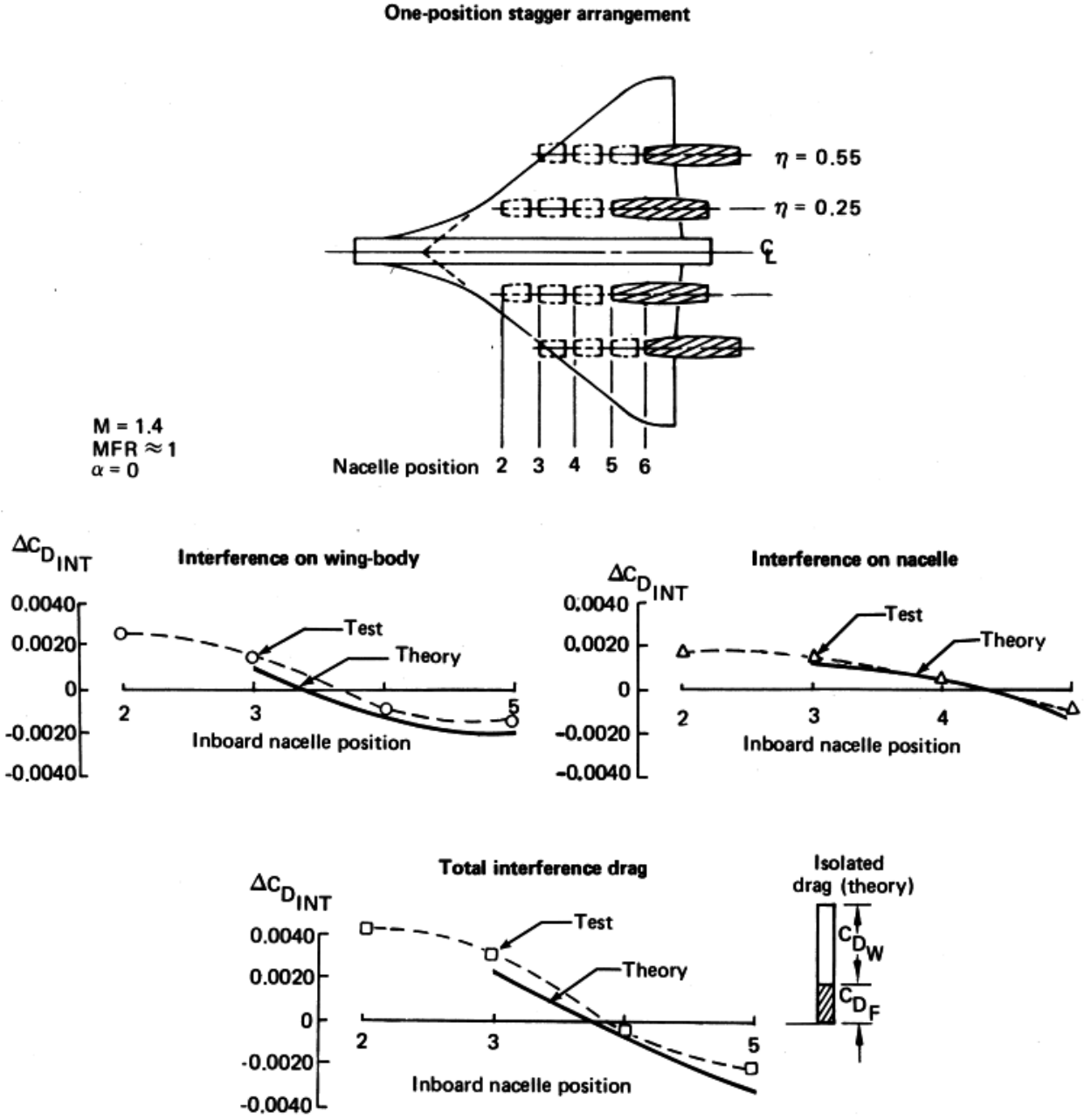

Figure 4-41. Effect of Nacelle Location on Interference Drag, One-Position Stagger, M = 1.4

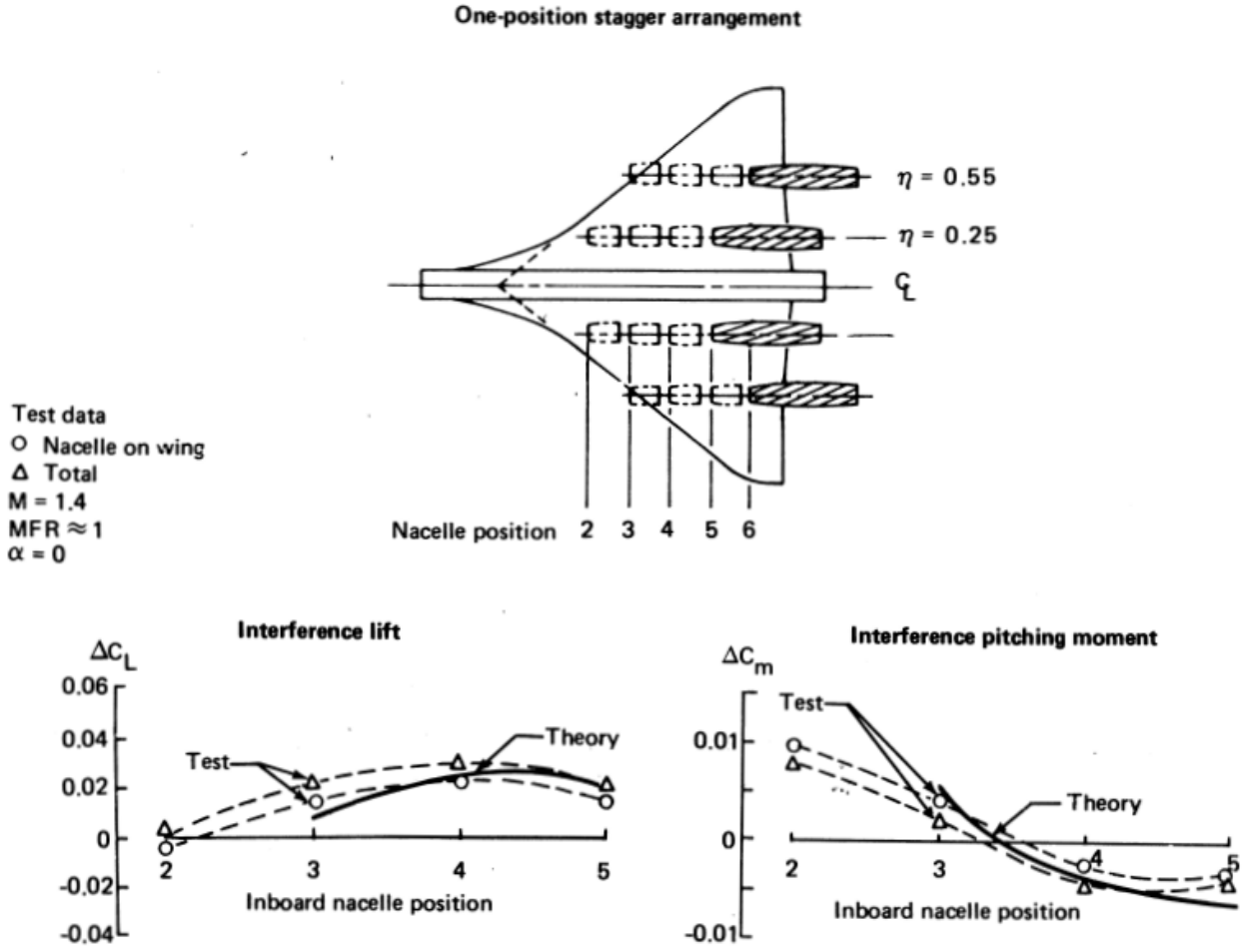

Figure 4-42. Effect of Nacelle Location on Interference Lift and Pitching Moment, One-Position Stagger, M = 1.4

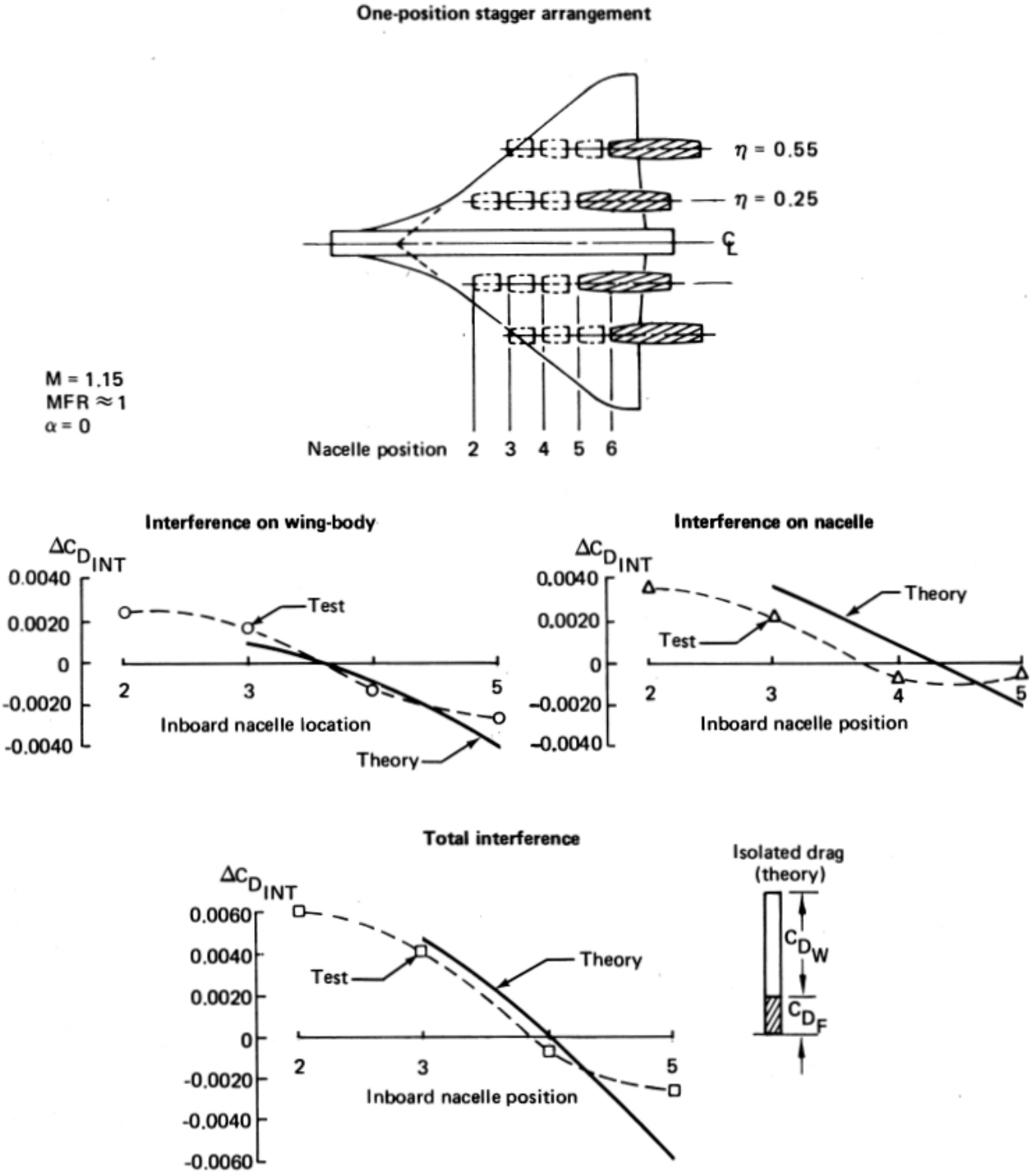

Figure 4-43. Effect of Nacelle Location on Interference Drag, One-Position Stagger, M = 1.15

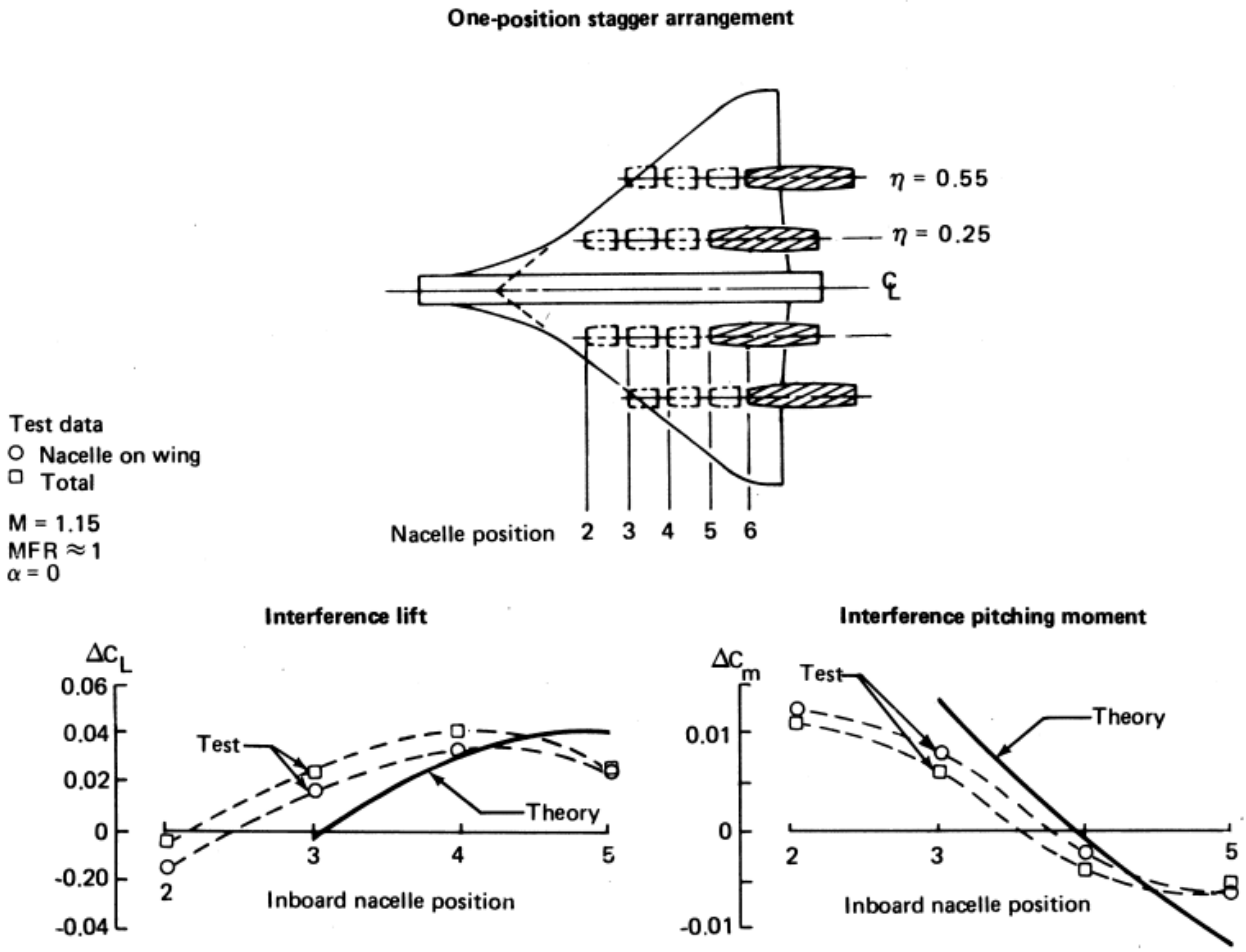

Figure 4-44. Effect of Nacelle Location on Interference Lift and Pitching Moment, One-Position Stagger, M = 1.15

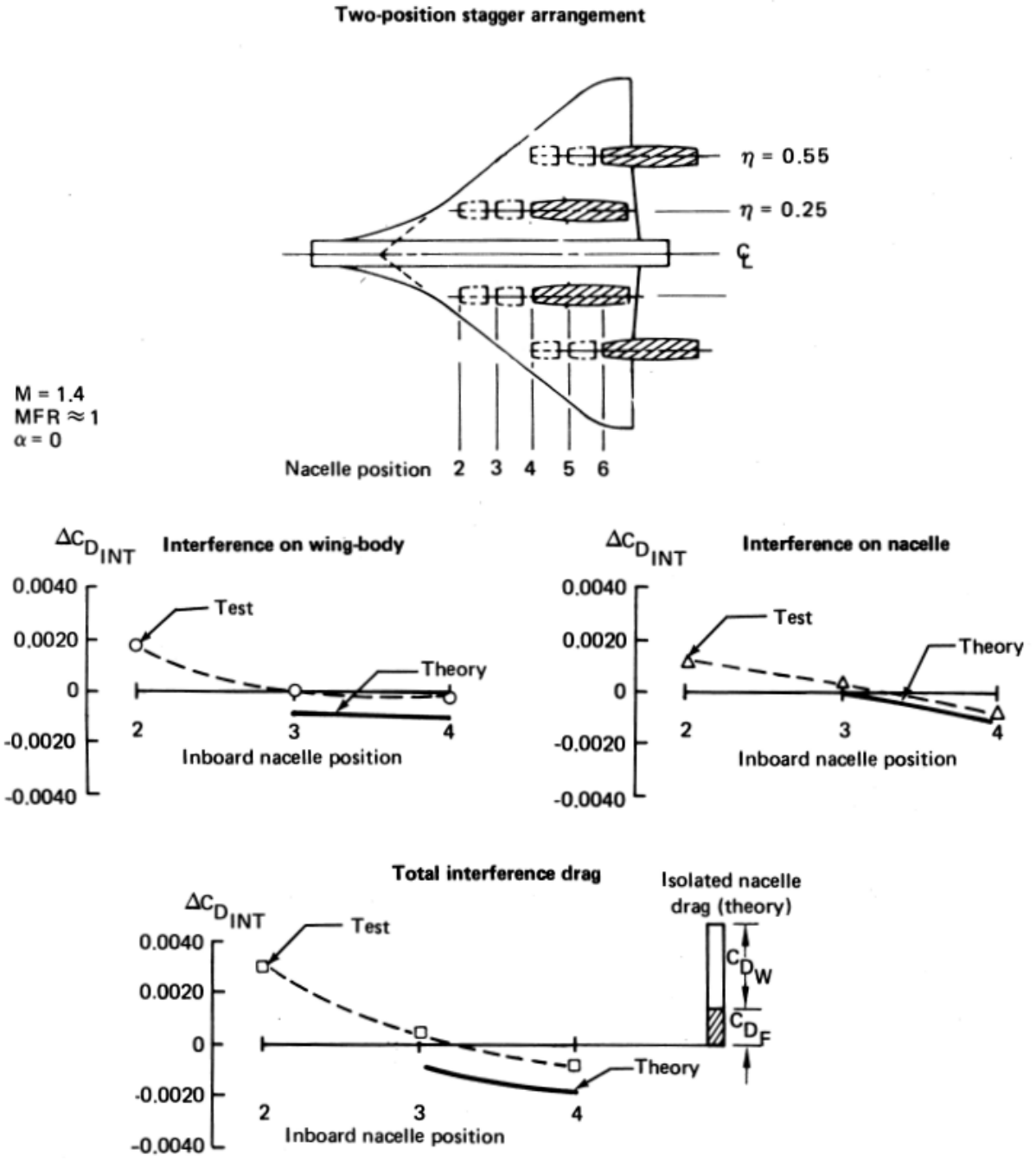

Figure 4-45. Effect of Nacelle Location on Interference Drag, Two-Position Stagger. M = 1.4

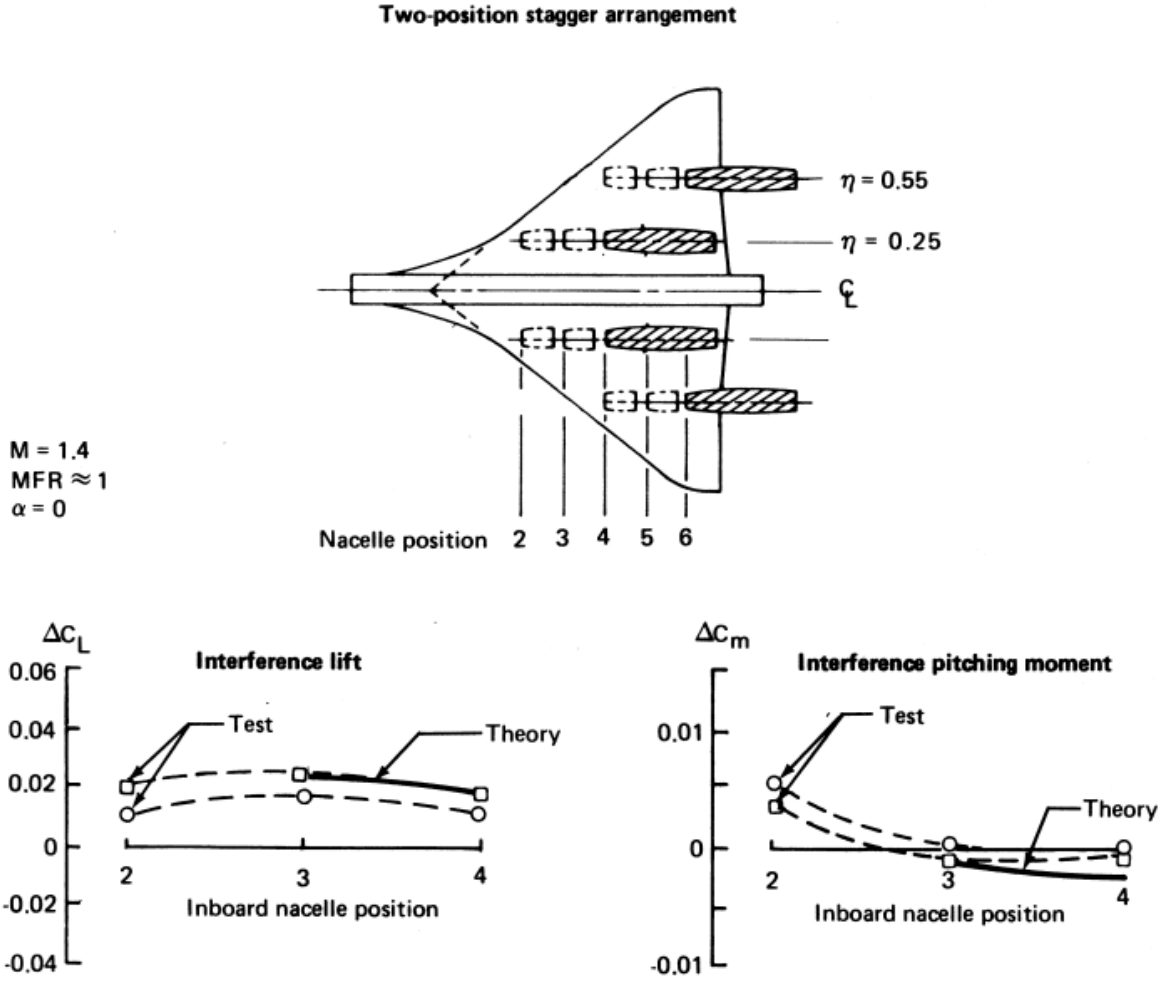

Figure 4-46. Effect of Nacelle Location on Interference Lift and Pitching Moment, Two-Position Stagger, M = 1.4

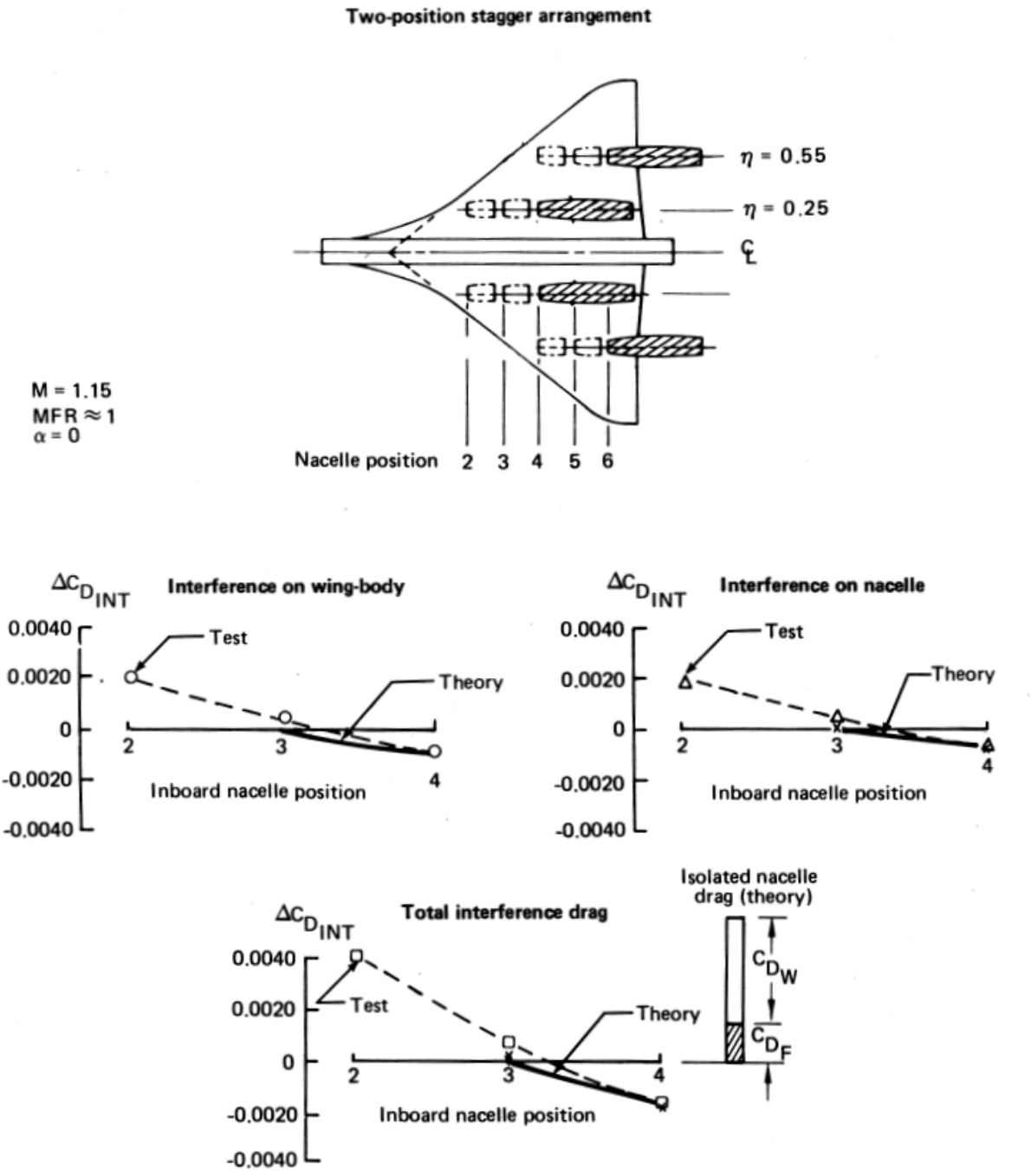

Figure 4-47. Effect of Nacelle Location on Interference Drag, Two-Position Stagger, M = 1.15

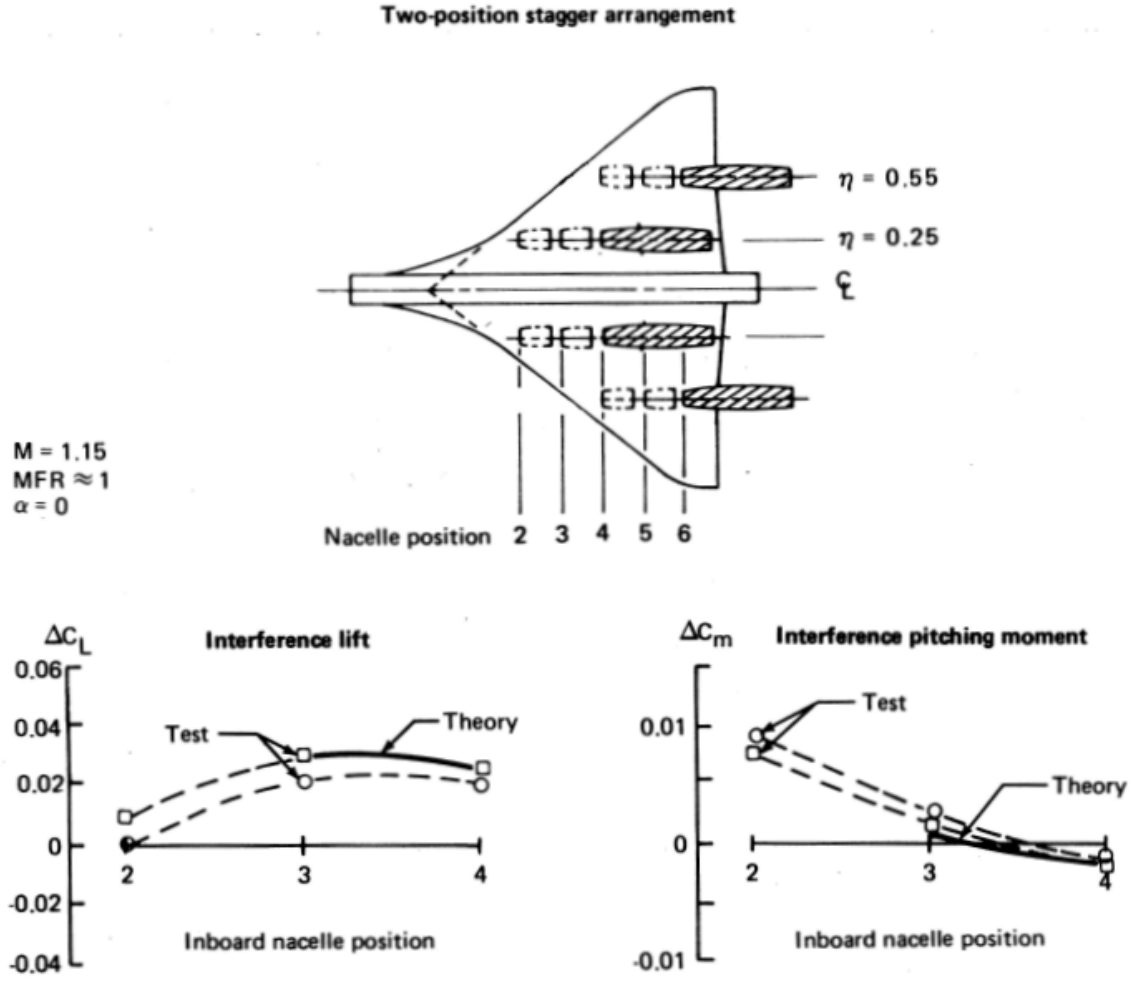

Figure 4-48. Effect of Nacelle Location on Interference Lift and Pitching Moment, Two-Position Stagger, M = 1.15

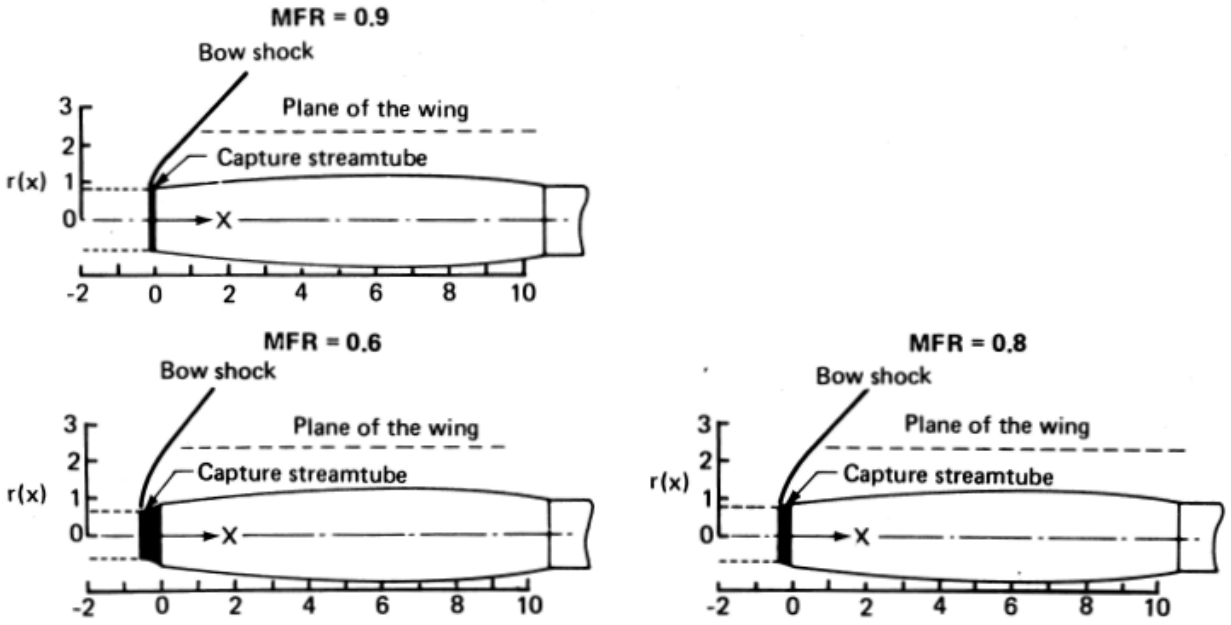

Figure 4-49. Calculated Streamtube Shapes, M = 1.4

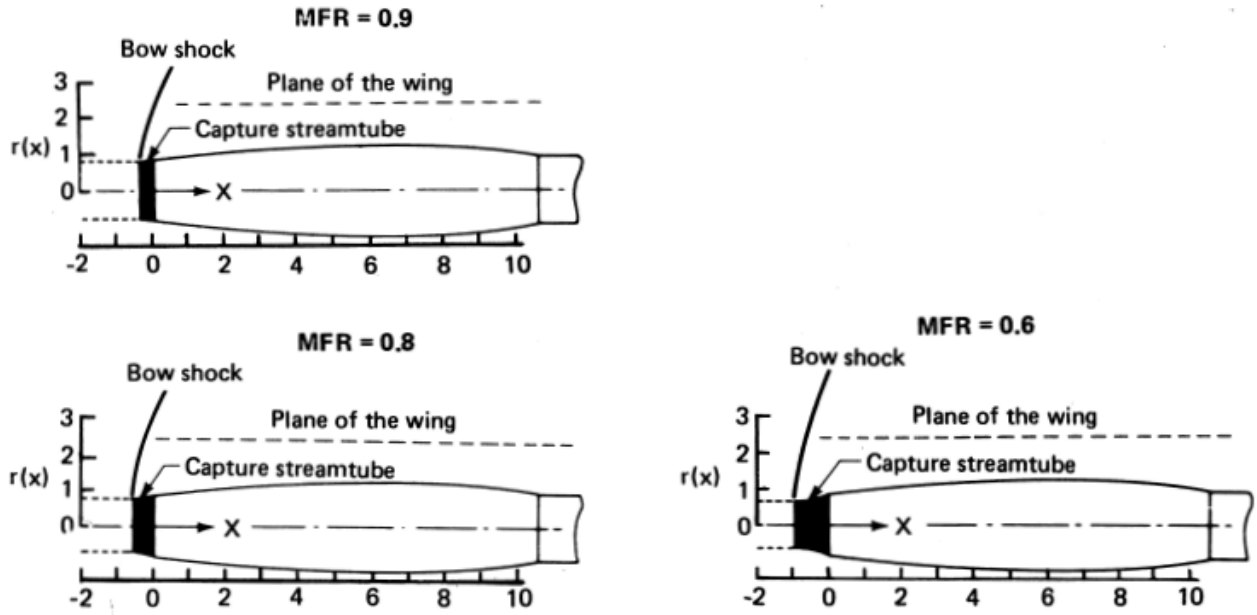

Figure 4-50. Calculated Streamtube Shapes, M = 1.15

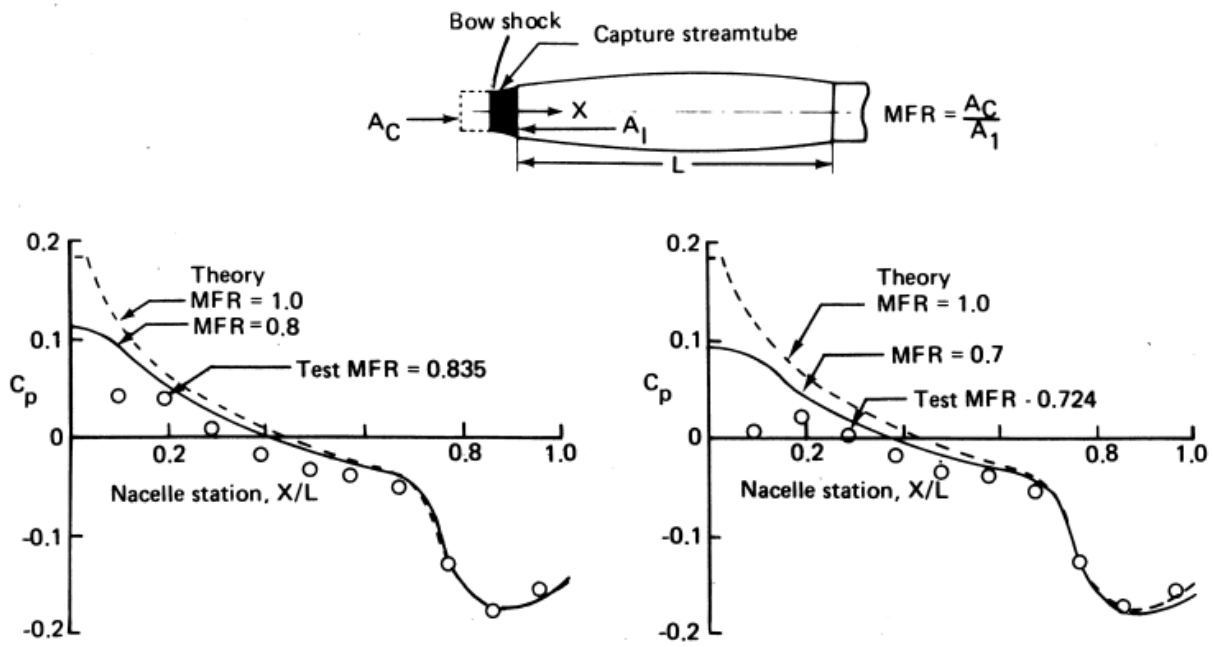

Figure 4-51. Effect of Spillage on Isolated Nacelle Pressures, M = 1.4

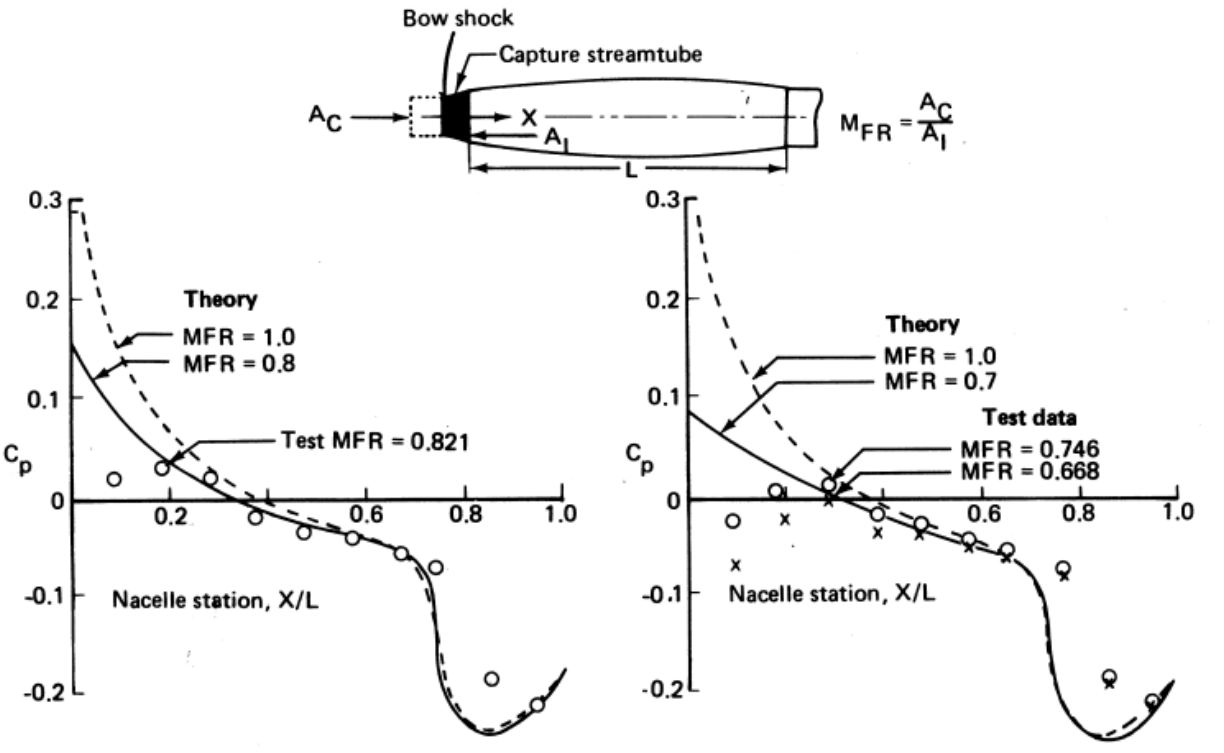

Figure 4-52. Effect of Spillage on Isolated Nacelle Pressures, M = 1.15

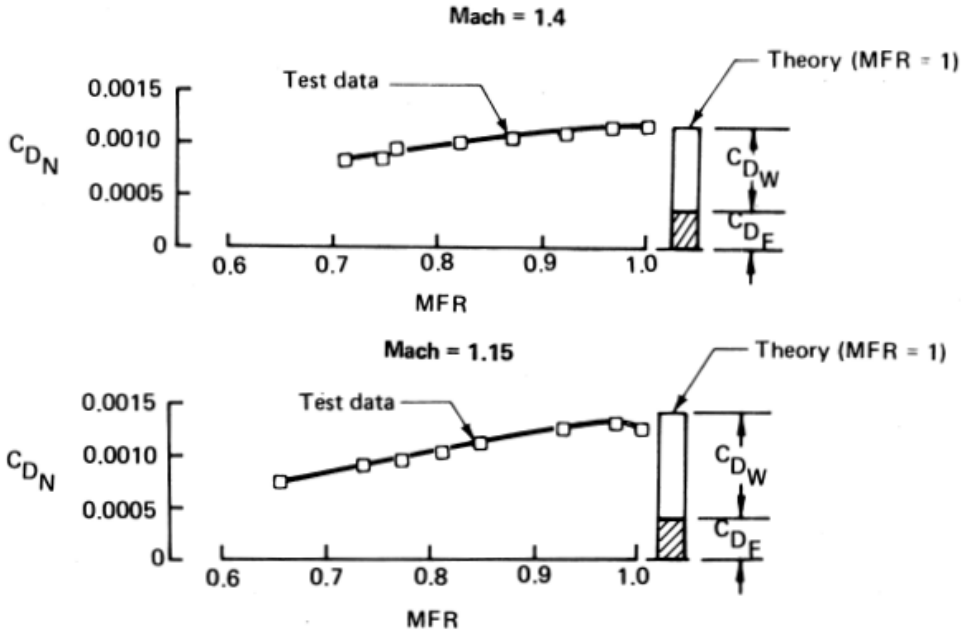

Figure 4-53. Effect of Spillage on Isolated Nacelle Drag

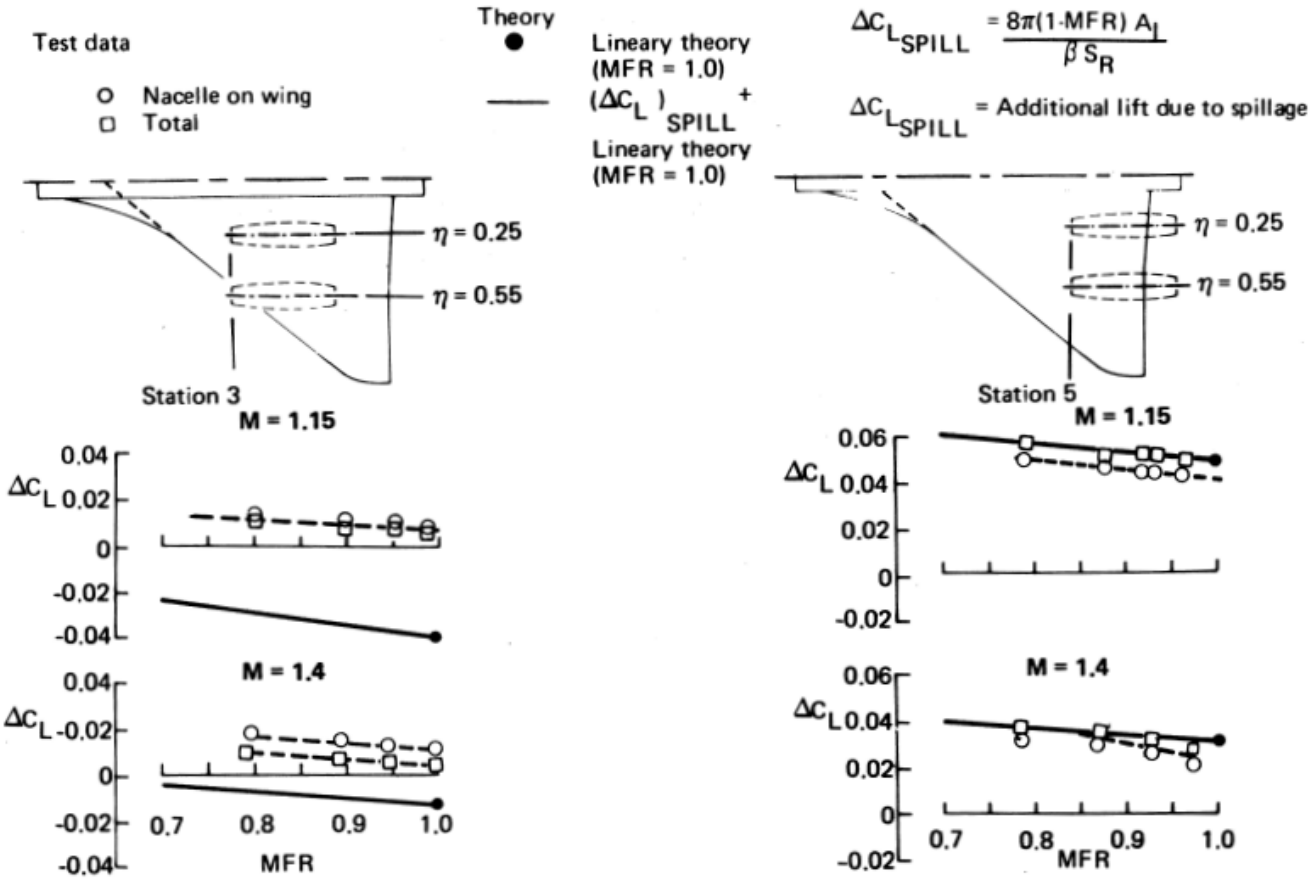

Figure 4-54. Slender-Body Theory Estimates of Spillage Interference Lift

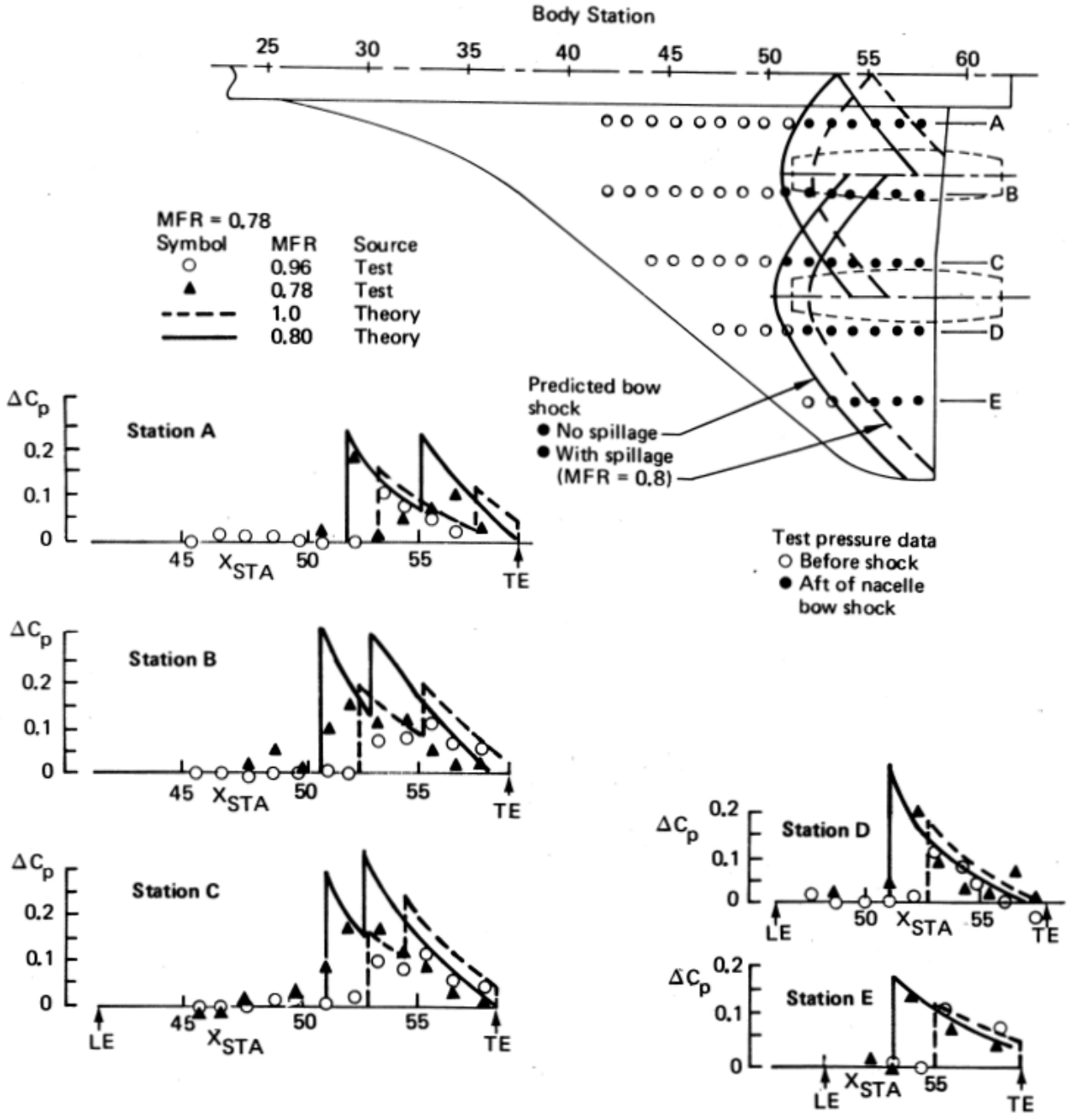

Figure 4-55. Effect of Nacelle Spillage on Interference Pressures, M = 1.4

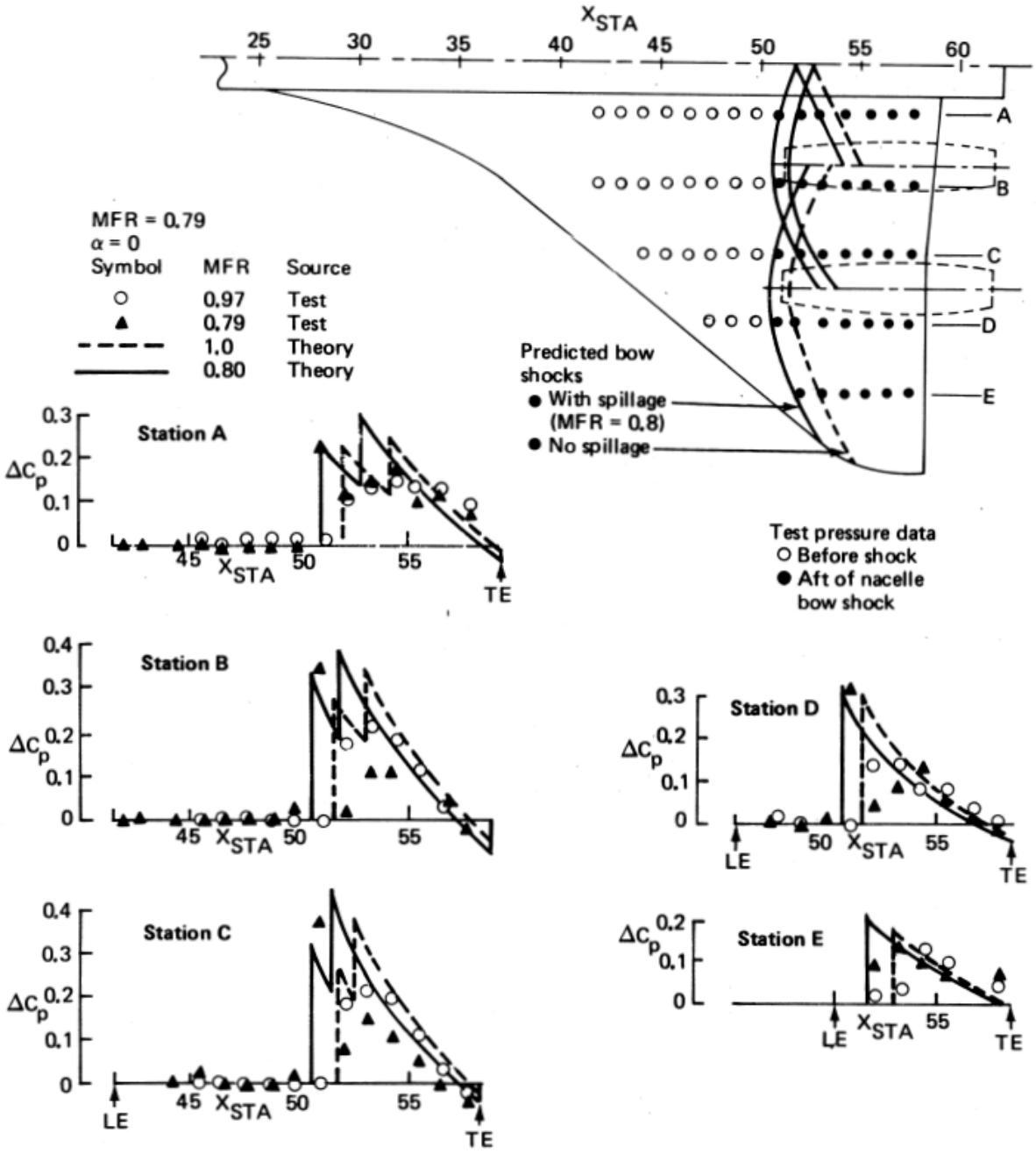

Figure 4-56. Effect of Nacelle Spillage on Interference Pressures, M = 1.15

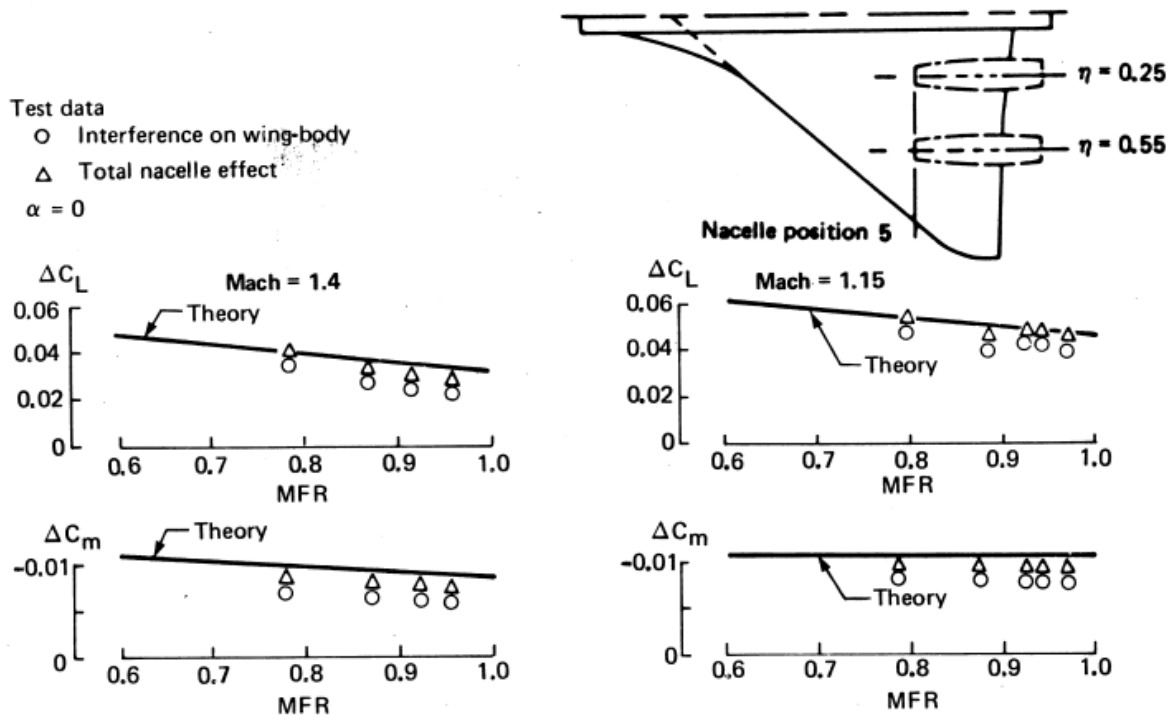

Figure 4-57. Effect of Spillage on Lift and Pitching Moment

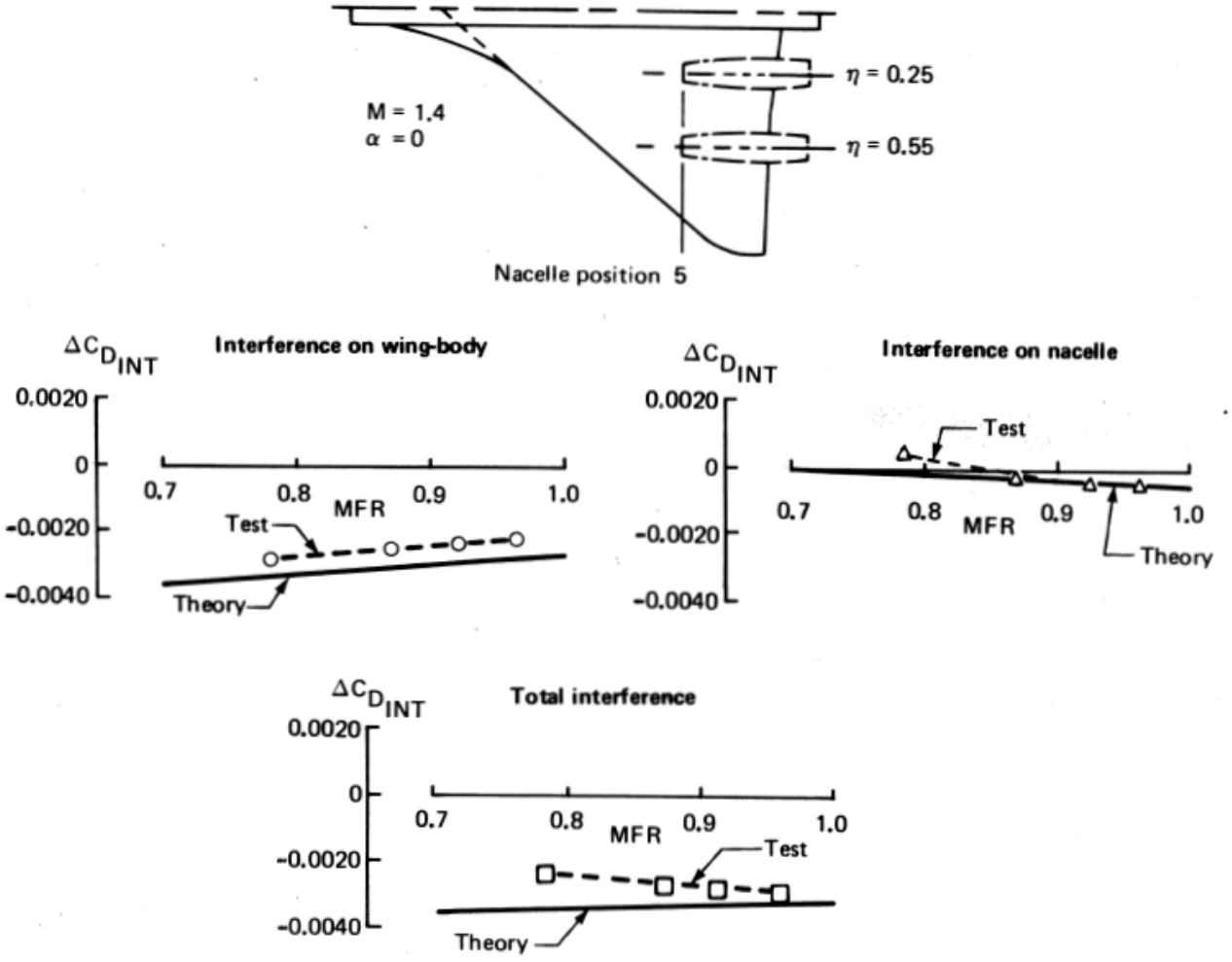

Figure 4-58. Effect of Nacelle Spillage on Interference Drag, M = 1.4

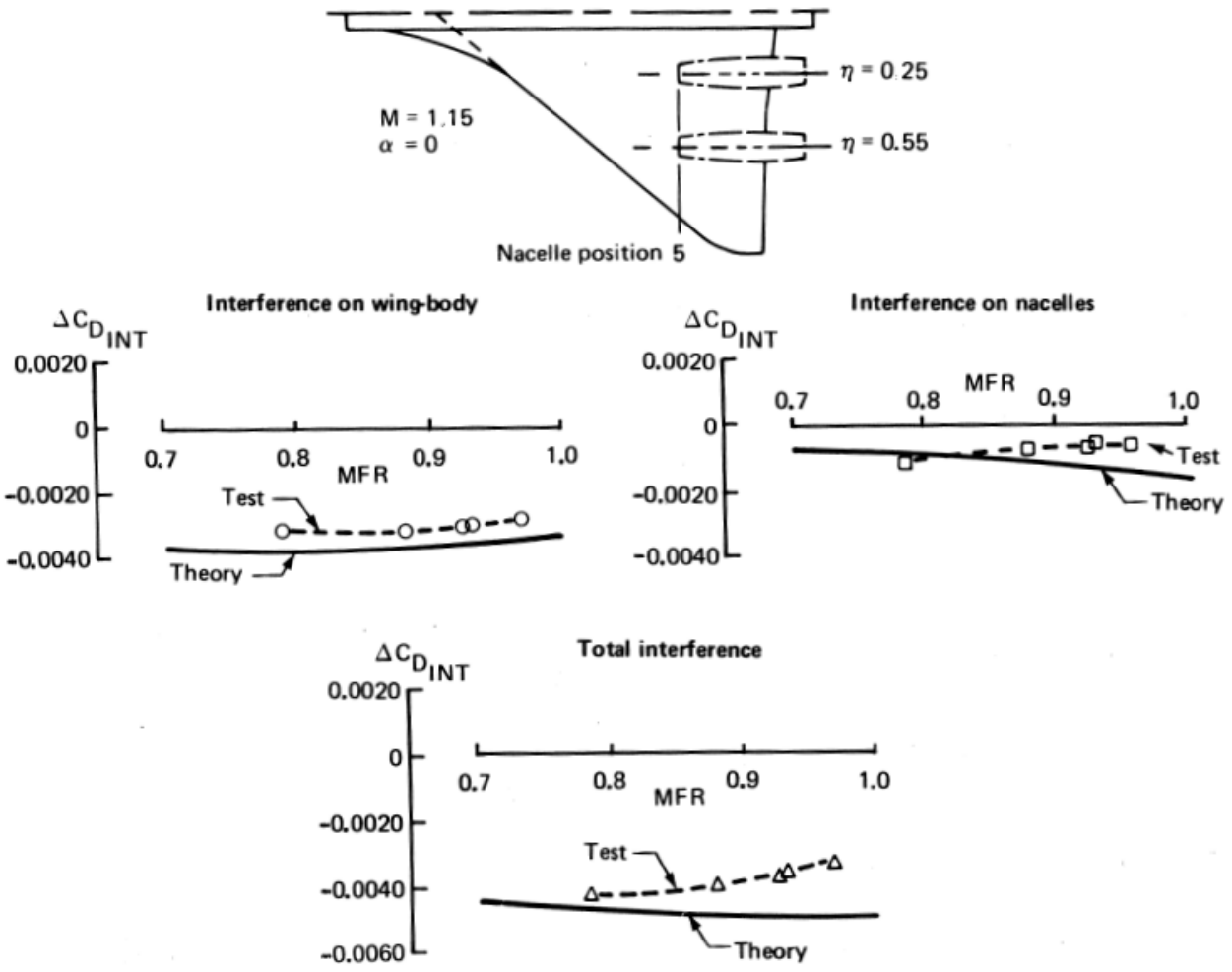

Figure 4-59. Effect of Nacelle Spillage on Interference Drag, M = 1.15